MARCH 1961

VOLUME 10 (1961) No. 3

GREGG M. SINCLAIR LIBRARY
UNIVERSITY OF HAWAII
8-7-63

NUCLEAR INSTRUMENTS & METHODS

A JOURNAL ON ACCELERATORS, INSTRUMENTATION AND TECHNIQUES IN NUCLEAR PHYSICS

EDITOR: K. SIEGBAHN - UPPSALA

CONTENTS

TOBJÖRN WESTERMARK, Measuring techniques for energy loss studies of 2.8 MeV betatron electrons in matter 169

D. FEHRENTZ und H. DANIEL, Einfluss der Quellendicke auf die gemessene Form eines Beta-Spektrums 185

F. LACOSTE and J. LEISS, A fast scaler for pulsed accelerators 189

L. KESZTHELYI, I. BERKES, I. DEMETER and I. FODOR, Detection of high energy γ-rays by plastic phosphors 193

A. SARAZIN, J. SAMUELI and G. BOUGNOT, Discriminateur d'amplitude rapide 202

J. SEGUINOT, J. TEIGER et L. VAN ROSSUM, Selection de mesons K^+ dans un faisceau secondaire de "Saturne" 205

D. M. BINNIE, Photons from positron beams in the GeV range 212

C. SCHUHL et C. TZARA, Monochromateur de positrons en secteur d'orange 217

G. GOETZE and H. KANTER, A high gain image intensifier system with fast shutter action for application in high energy physics . . . 224

Y. HAZONI, Circuit a plusieurs états stables utilisant des diodes tunnel 229

Y. HAZONI, A tunnel diode univibrator and pulse height discriminator 231

F. P. G. VALCKX, Direct current stabilization of scintillation counters used with pulsed accelerators 234

Letters to the Editor

E. BALDINGER and W. CZAJA, On the energy expended per electron-hole-pair produced in p-n-junction-detectors 237

J. RETHMEIER, H. J. BOERSMA and C. C. JONKER, An improved circuit for pulse shape discrimination between neutrons and gamma rays . 240

L. CRANBERG, Time-to-pulse-height converter as coincidence and anti-coincidence indicator 243

JOACHIM KESSLER, Doppelstreuexperimente mit Azimutwinkel integration 245

Book Reviews 247

NORTH-HOLLAND PUBLISHING COMPANY — AMSTERDAM

NUCLEAR INSTRUMENTS AND METHODS

A journal on accelerators, instrumentation and techniques in nuclear physics

EDITOR: K. SIEGBAHN, UPPSALA

EDITORIAL BOARD:

J. B. ADAMS (CERN)
F. A. ALSINA (Buenos Aires)
E. AMALDI (Rome)
H. L. ANDERSON (Chicago)
K. T. BAINBRIDGE (Cambridge Mass.)
P. R. BELL (Oak Ridge)
R. E. BELL (Montreal)
A. BERTHELOT (Saclay)
H. BRINKMAN (Groningen)
E. H. COOKE-YARBOROUGH (Harwell)
S. DE BENEDETTI (Pittsburgh)
M. DE HEMPTINNE (Louvain)
A. DE-SHALIT (Rehovoth)
M. DEUTSCH (Cambridge Mass.)
S. DU TOIT (Pretoria)
B. S. DŽELEPOV (Leningrad)
W. GENTNER (Heidelberg)
P. C. GUGELOT (Amsterdam)
H. HALBAN (Paris)
O. HAXEL (Heidelberg)
P. HUBER (Basel)
S. KIKUCHI (Tokyo)
J. KOCH (Copenhagen)
M. S. KOZODAEV (Moscow)
S. LIVINGSTON (Cambridge Mass.)
E. M. MCMILLAN (Berkeley)
M. G. MEŠČERJAKOW (Moscow)
P. B. MOON (Birmingham)
M. L. OLIPHANT (Canberra)
W. PAUL (Bonn)
A. S. RAO (Bombay)
G. SALVINI (Rome)
P. SAVIĆ (Belgrade)
P. SCHERRER (Zürich)
CH. SCHMELZER (CERN)
R. TANGEN (Oslo)
D. TAYLOR (Northampton)
V. I. VEKSLER (Moscow)
G. VON DARDEL (CERN)
O. WERNHOLM (Stockholm)
R. R. WILSON (Cornell)
S. D. WINTER (Saclay)

INSTRUCTIONS FOR CONTRIBUTORS

Contributions may be sent to the Editor, Professor K. Siegbahn, Institute of Physics, University of Uppsala, Sweden, either directly or through the intermediation of one of the members of the Editorial Board. Contributions may be written in English, French or German but should always, except for very short papers, be supplied with a brief abstract in English. Figures should be in inked original drawings or glossy prints and they should be sufficiently large. Contributors should make sure that important details in drawings and photographs will show up clearly in the diminished copy used by the publisher.

Books for review should be sent to Professor Siegbahn.

Objective and descriptive material on endeavours and product developments from the industry for the section "Spotlight on Industry" should be sent directly to the publishers, North-Holland Publishing Company, P.O. Box 103, Amsterdam.

Nuclear Instruments and Methods is published monthly. The subscription price of a volume of 360 pages is $ 17.00 (130 s), postage free.

Subscriptions should be sent to the publishers, North-Holland Publishing Company, P.O. Box 103, Amsterdam, or to any subscription-agent.

No part of this issue may be reproduced in any form, by print, photoprint, microfilm or any other means without written permission from the publisher.

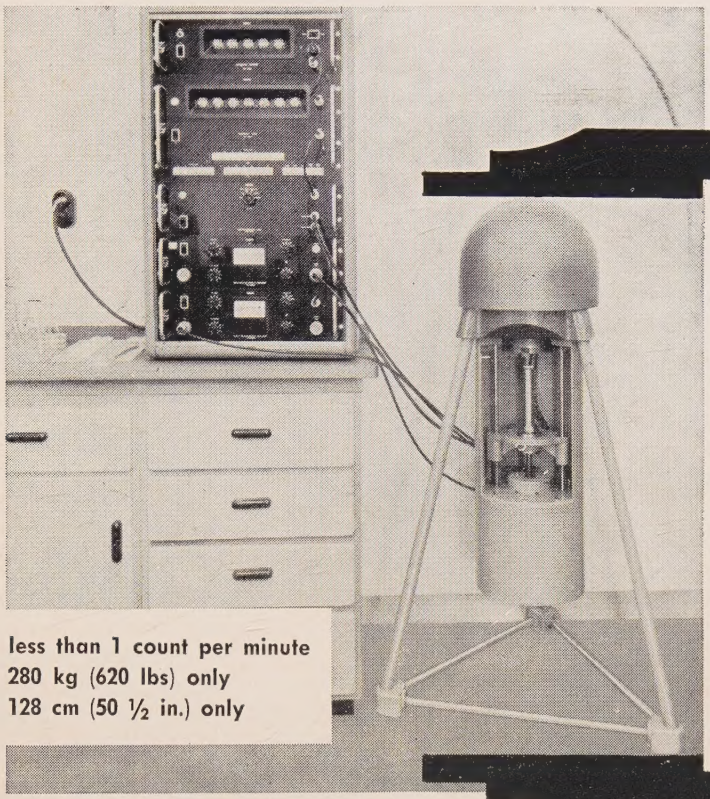

Background	:	**less than 1 count per minute**
Weight	:	**280 kg (620 lbs) only**
Height	:	**128 cm (50 ½ in.) only**

128 cm

low-level beta counting

Low-level beta counting is brought to an elegant and simple solution by the novel Philips anti-coincidence assembly, type PW 4127, together with its associated electronic equipment.
The assembly comprises two radiation-sensitive elements only, viz. a low-level beta counting tube*), and a single guard tube which replaces the conventional array of dozens of guard tubes hitherto required for low-level work.
By virtue of this unique design tons of shielding material are eliminated; the electronic circuitry is considerably simplified, and hence overall reliability is greatly improved. Reproducibility is guaranteed by the fixed geometry of the sample with respect to the counting tube.
With a background of less than 1 count per minute, it is now possible to measure in a 300 mg sample a beta activity (e.g. Sr^{90} or Tl^{204}) of $(5 \pm 0.5) \times 10^{-12}$ Curie in only one hour.

***) Two types available:**

type 18515 for measuring low-energy beta radiation, with a 1.5 mg/cm² mica window;

type 18516 for general low-level beta work, with a 10 mg/cm² Cr-Fe window.

PHILIPS

nuclear equipment

N.V. PHILIPS' GLOEILAMPENFABRIEKEN - EINDHOVEN - HOLLAND

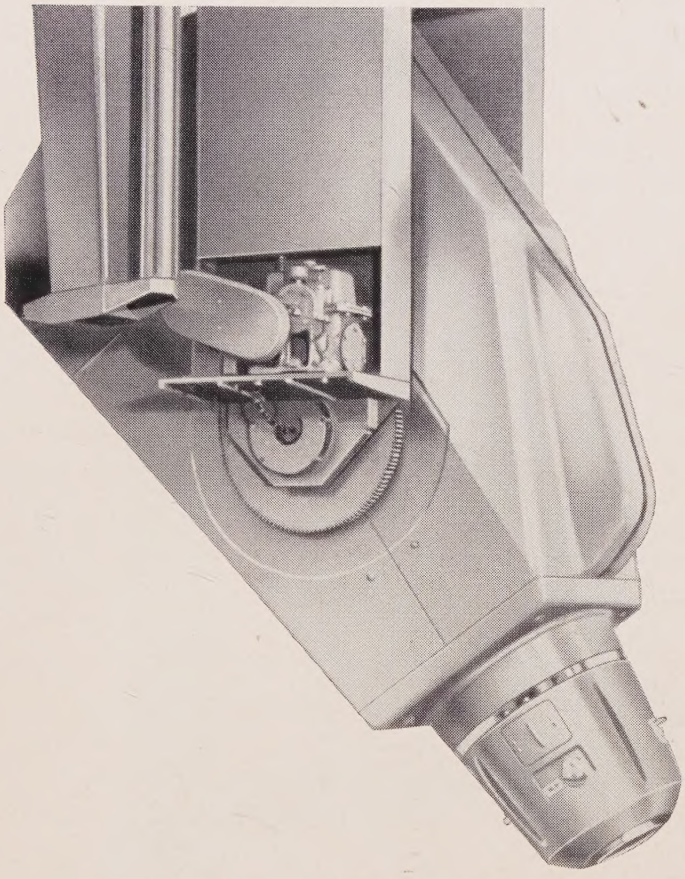

electron linear accelerators for research industry and medicine

by Mullard Equipment Limited

Electron Linear Accelerators manufactured by Mullard Equipment Ltd. are the logical result of wide and detailed experience in this field. Machines for all types of applications are available, from the standard 4.3 MeV model to equipments specially built to meet individual requirements with electron beam energies up to 50 MeV.
The units are designed for continuous operation, ease of control and high reliability.

STANDARD MACHINE OPERATING AT 4.3 MeV

Mean power output at 500 pulses per second	850 W (electrons)
Maximum pulse repetition frequency.....	500 p.p.s.
Electron pulse length.....	1.65 microseconds
When used as an X-Ray source maximum X-Ray output is approximately.....	600 röntgens per minute at 1 metre

MULLARD EQUIPMENT LIMITED

Mullard House · Torrington Place
London W.C.1 · Tel: LANgham 6633

RESEARCH Now regarded as indispensable in ma research laboratories Linear Accelerators can be fitt with supplementary heads to provide X-Rays neutrons. Present day applications include investigati of properties of irradiated materials; preservation food; basic studies on structure of organic molecul modification of the properties of plastics.

INDUSTRIAL RADIOGRAPHY The compact accel ator design with wide range of movements and pre sion positioning enables radiographs of complicat heavy metal sections to be taken with minimum settir up times. The high X-Ray output gives short exposu time and the extremely small (2mm) focal spot giv the highest possible definition. Penetration is sufficie to radiograph steel sections up to 12 inches thick.

MEDICAL THERAPY The use of Linear Accelerat for X-Ray and Electron Medical Therapy is well esta lished. These machines give rapid treatment times w precisely defined fields and negligible 'penumb effects. Skin and exit dosages are minimised.

ME

the first portable, "desk-top" 400-channel pulse height analyzer

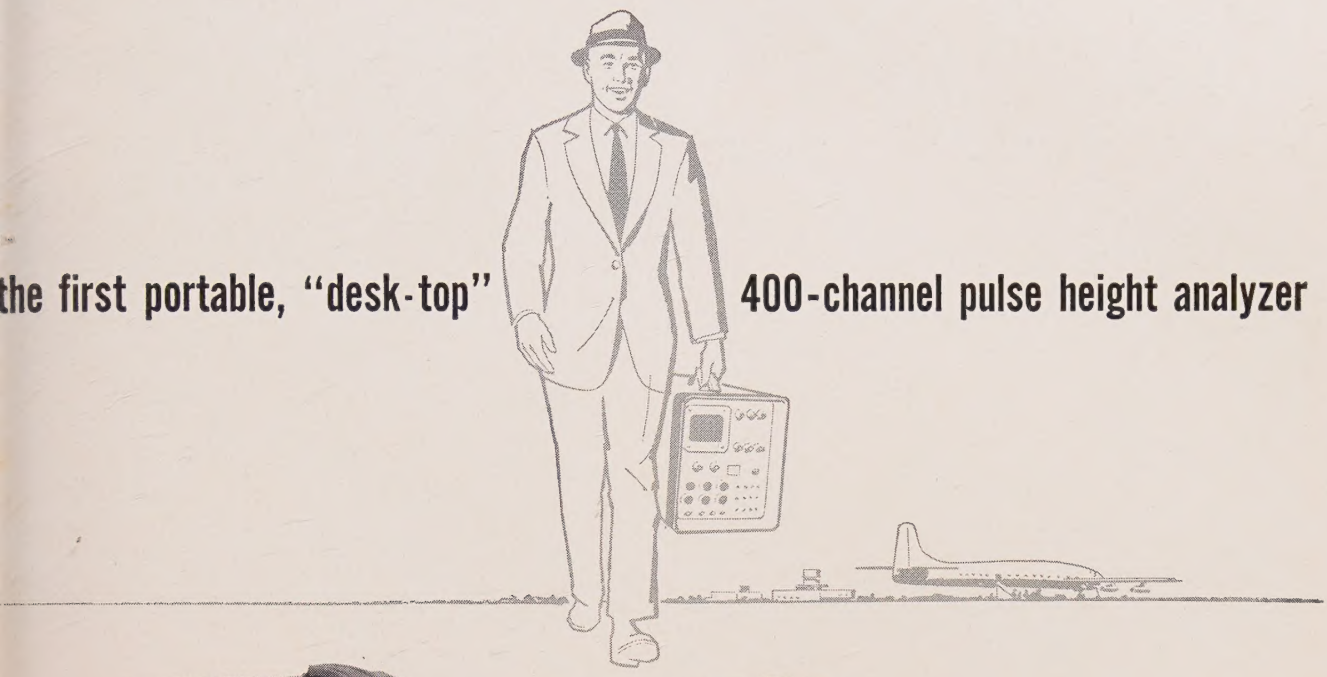

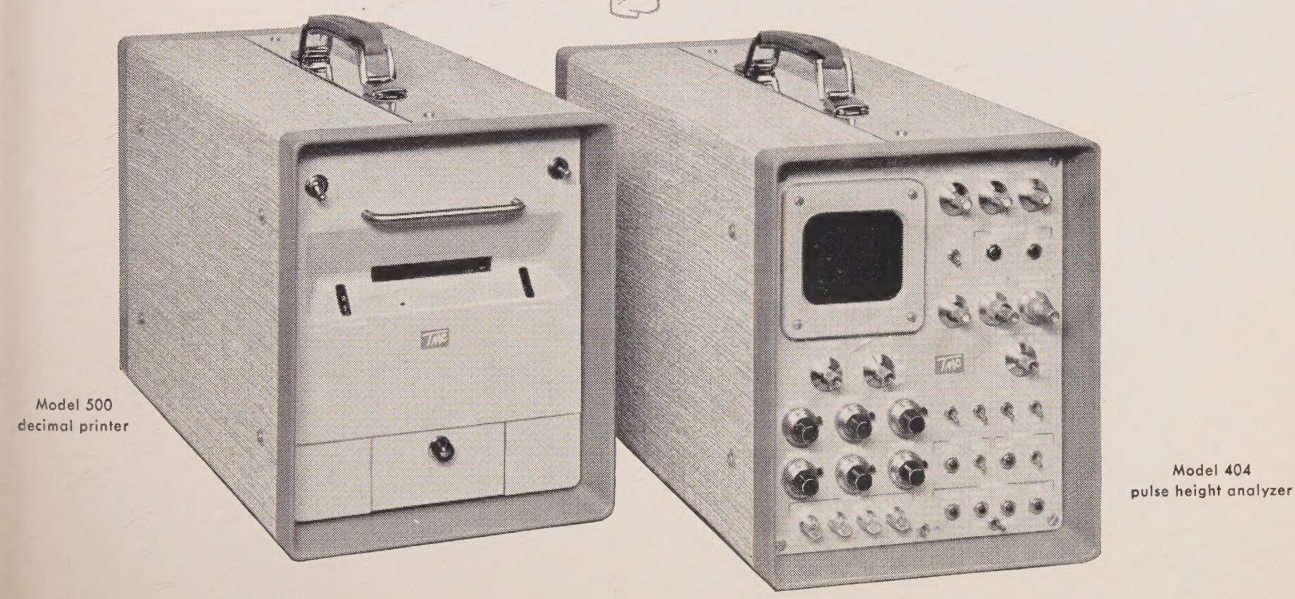

Model 500
decimal printer

Model 404
pulse height analyzer

— the TMC Model 404

The new TMC Model 404 is the most portable pulse height analyzer you can own. Take it and use it anywhere. With its all-transistor, printed circuitry and 400-channel memory in a package just over a cubic foot, this analyzer is small enough to operate on your desk. *All* the instruments needed for an experiment can be carried easily by one person.

The Model 404 has a magnetic core memory that can be used in sub-groups of two or four; four separate inputs and associated amplifiers; internal pulse routing circuitry; pushbutton data transfer and display overlap; very low power requirements and many "system" advantages. And it can be used with the new solid state detectors.

For readout, use its companion unit, the Model 500 Decimal Printer; a high speed paper tape punch; strip chart or X-Y recorders; or an IBM electric typewriter.

LITERATURE ON REQUEST

TECHNICAL MEASUREMENT CORPORATION

441 WASHINGTON AVENUE NORTH HAVEN, CONNECTICUT

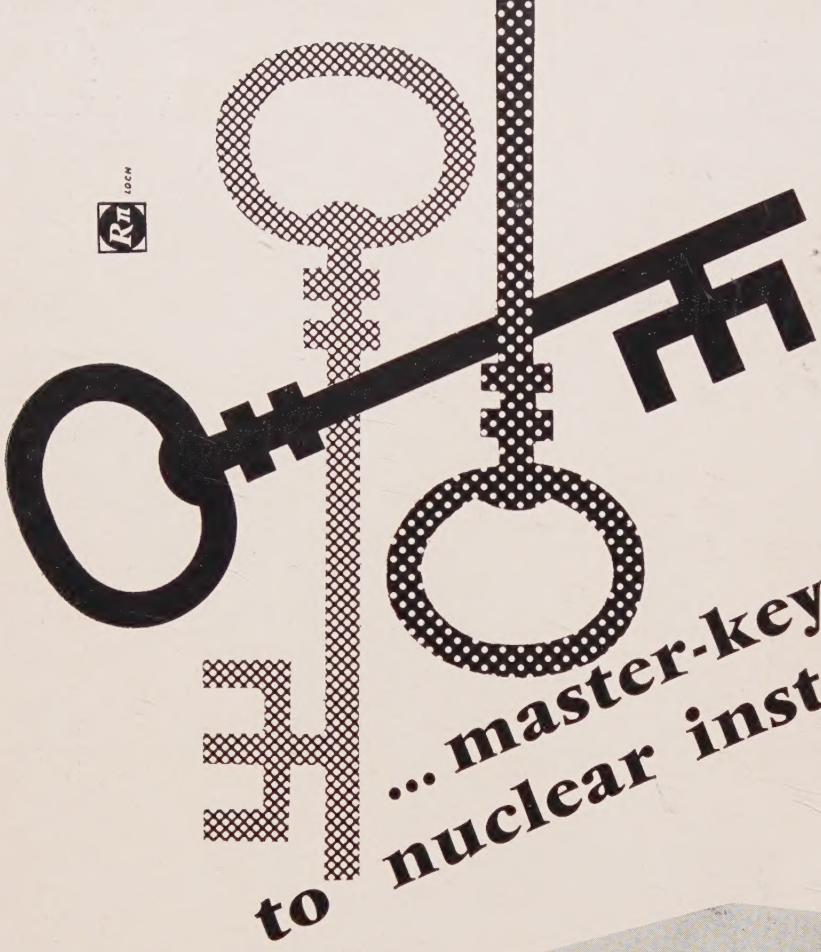

STANDARD FUNCTIONNAL UNITS . . .

FRENCH ATOMIC ENERGY COMMISSION SYSTEM

. . . master-key to nuclear instrumentation

Standard functional units are assembled in cabin... in order to be used as complete assemblies : scales for counting, amplitude selectors, ratemeters, etc...

REGISTER UNIT TYPE TN...
Function :
counting (registering)
Dekatron divider

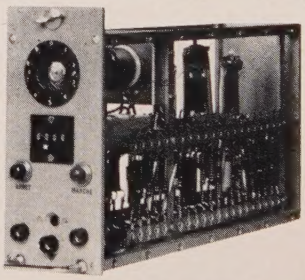

TIMER UNIT (SLOW RESPONSE)
TYPE TAL.2

Intended for automatic pre-set counting

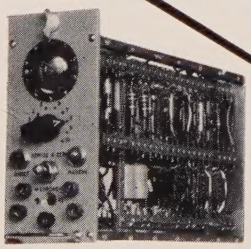

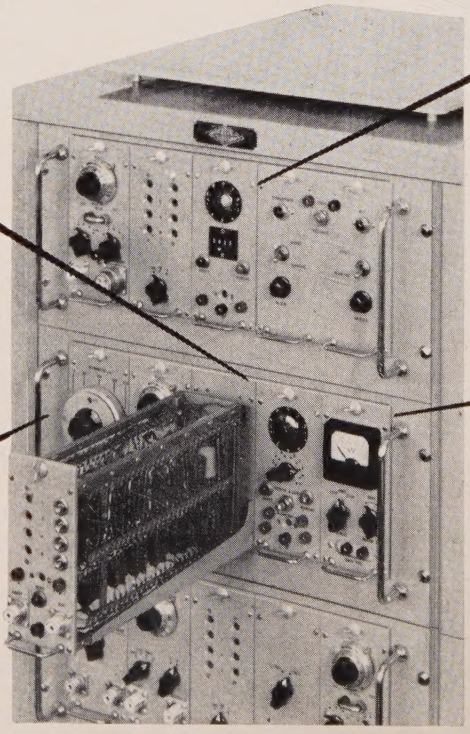

VERY HIGH TENSION U...

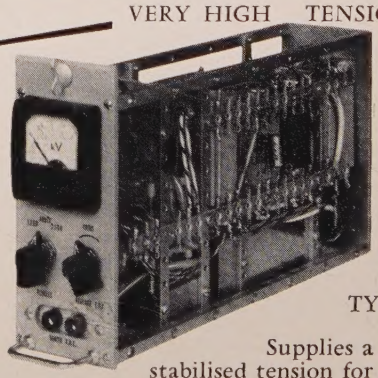

RATEMETER TYPE TIS.1
supplies a tension or a current proportionnal to the number of counts received

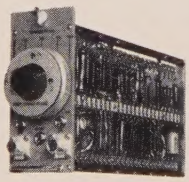

TYPE T...

Supplies a very ... stabilised tension for detec... pre-ampl...

L'ÉLECTRONIQUE APPLIQUÉE

96/100, rue Maurice Arnoux • MONTROUGE • ALE 45-20, 83-20
25, rue du Docteur Finlay • PARIS 15e • TÉL. SÉGUR 14-75

E-H PRESENTS 4 PULSER THOROUGHBREDS

Which one of these advanced, quality-built instruments is right for your requirements?

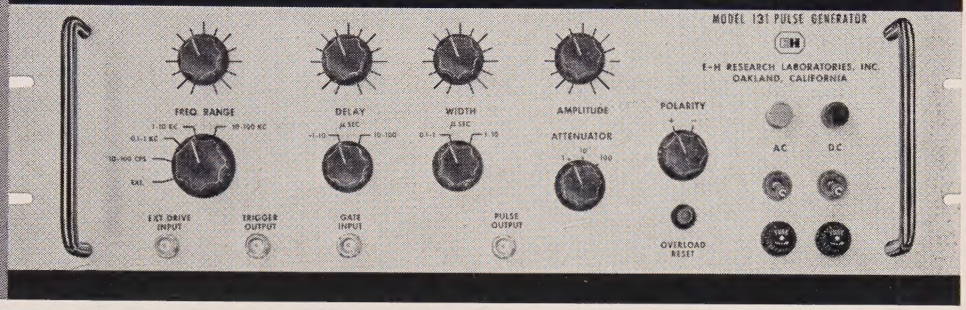

NEW! MODEL 131

Low cost pulse generator with rise time of 10 nanoseconds!

$575 f.o.b. Oakland, California

If you've been looking for a high-quality pulser with excellent performance characteristics — but **without a high price tag** — the new E-H 131 was designed for you. The 131's fast rise time and high-power output pulses make it an ideal pulser for laboratory and research applications as well as production line testing of components and solid state devices. Check the 131's specifications. You'll agree it is the outstanding instrument in its price range.

SPECIFICATIONS

REPETITION RATE: 10 cps to 100 kc, internally controlled, zero to 100 kc externally driven.
RISE TIME: 10 nanoseconds.
PULSE DELAY: Zero to 100 microseconds with respect to the trigger.
TRIGGER (for sync. purposes): Positive 10 volt pulse.
EXTERNAL DRIVE: 5 volts RMS or equivalent positive pulse required.
ELECTRONIC GATE: Negative 20 volts required to block the pulse train.
PULSE OUTPUT: 50 volts into a 50 ohm load.
PULSE WIDTH: 100 nanoseconds to 100 microseconds, continuously variable.
POLARITY: Positive or Negative pulses available.
DUTY FACTOR: 10 percent. An automatic limiter prevents overload.
OUTPUT ATTENUATOR: 100:1 coarse selector, 10:1 vernier control.
DIMENSIONS: Standard 19" rack panel, 5¼" high.

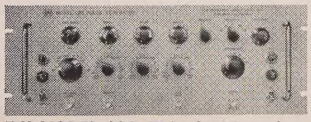

E-H MODEL 130 This **double** pulser has repetition rates to 4 mc, rise and fall time of 10 nanoseconds, pulse widths and delay variable from 100 nsec to 50 milliseconds, and delivers 50 volts at 500 ma at 50% duty cycle. Either pulse polarity, output attenuator, and provisions for external drive and electronic gating. Especially suited for fast circuit applications in transistor testing, computer and missile fields. $1175 f.o.b., Factory.

E-H MODEL 121 A high-current pulser delivering a 50 volt pulse into 50 ohms. Rise and fall times 4 nanoseconds. Width variable from 20 nsec to 1μsec. Repetition rate from 10 cps to 10 mc. Either positive or negative pulses may be selected on the front panel. Ideal for ferrite and magnetic switching studies, applications in high speed transistor and diode switching, and design of logic and memory circuits. $1675 f.o.b., Factory.

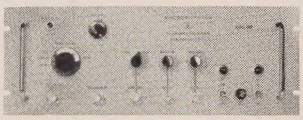

E-H MODEL 120B Rise time — 2 nanoseconds—is ahead of the field and offers new tool for fast, high-resolution work. Two outputs independently variable in amplitude (—8 volts into 93 ohms) and widths (2.5 to 25 nsec). Inverting and impedance matching transformer available. Repetition rate 10 cps to 10 mc. Advanced trigger pulse and a fast, flexible gate for complex pulse-time and pulse-amplitude selection. $1275 f.o.b., Factory.

WRITE, WIRE OR TELEPHONE TODAY FOR MORE INFORMATION — REPRESENTATIVES IN ALL MAJOR CITIES

E-H RESEARCH LABORATORIES, INC.
163 ADELINE STREET • TEMPLEBAR 4-3030 • OAKLAND 20, CALIFORNIA

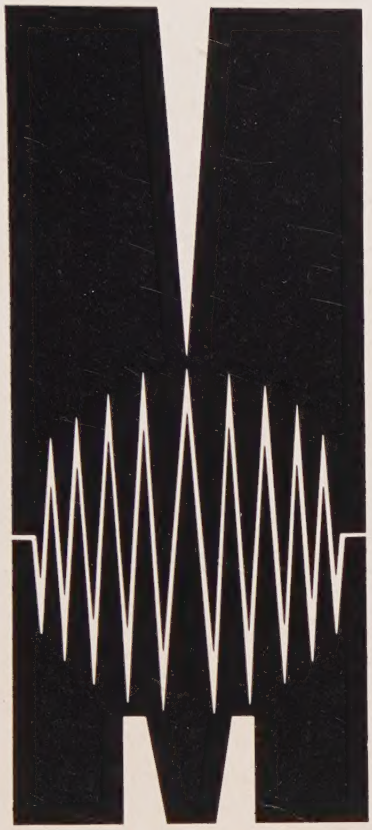

PARIS FROM MAY 9TH TO MAY 17TH 1961

MESUCORA

INTERNATIONAL EXHIBITION
MEASUREMENT - CONTROL - REGULATION - AUTOMATION
AND 58TH EXHIBITION OF THE
"SOCIÉTÉ FRANÇAISE DE PHYSIQUE"

- First French Exhibition exclusively devoted to these techniques, the most important and the most international one realized in Europe.
- International Congress, the subject of which will be "Recent progress in the fields of Measurement Control and automatic Regulation, resulting from the cooperation of the Techniques (electric, electronic, mechanical)".
- 700 Exhibitors - 14 nations - 35.000 square meters.
- The most recent discoveries and appliances of the theoretic and experimental research.
- Most refined measurement and control equipments, materials and methods for their applications to regulation and automation in the fields of the industry and of the public services.
- An unprecedented gathering, an international confrontation of the highest technical value which

ALL the responsible persons in industry and the public services
ALL engineers and research workers
ALL teachers and students of the technical and scientific Upper Teaching

MUST VISIT

centre national des industries et des techniques

Call on: MESUCORA - Service Propagande - 40, rue du Colisée - Paris 8e - Tél. BALZAC 77-

FRANCE for the complete documentation, stating if you want it in French, German or English

SCINTILLATION

Scintillation Phosphors, Liquids & Crystals (Bulletins 9, 11, 12, 13, 23 and 25) The NaI(Tl) crystals, (illustrated above) form part of the extensive range of mounted crystals offered by Nuclear Enterprises. CsI(Tl) and LiI(Eu) crystals are also available in mounted form. All three are featured in the crystal-photomultiplier assemblies which afford improved resolution and offer special facilities for counting low level activities. Full details of NE 102 plastic phosphor scintillators, liquid scintillators, loaded liquid scintillators, neutron detectors, scintillation chemicals, crystals and crystal-photomultiplier assemblies will gladly be sent on request.

Complete Assemblies: Scanning Scintillation Spectrometer of high performance. Also Liquid Scintillation Spectrometer providing greatly simplified technique for measurement of C14, H3 and Fe55 (with efficiences of 90%, 30% and 20% respectively).

Probe Units: Compact probe units for study of gamma rays, low energy X-rays, slow neutrons, fast neutrons and alpha particles. Also special transistorised head units for pulse shape discrimination investigations.

Special Transistorised Units for Field Investigations: Four channel Scintillometer for geological and geophysical surveys; Moisture & Density Gauge; Beryllometer. etc.

Shielded Scintillation Head Units: To accommodate photomultipliers, phosphors, and samples. Special units for C14, & H3 analyses.

Precision Laboratory Instruments: Non-overloading linear amplifiers, pulse height selectors, EHT units, ratemeters, etc. Also a new range of transistorised instruments of unitised construction.

Low Level Counting Facilities: Wide range of human body radiation monitors. Also installations for measuring lean:fat ratios in carcases and live animals.

NUCLEONIC INSTRUMENTS

Nuclear Enterprises (G.B.) Ltd. offers a complete range of precision nucleonic instruments and a special design and development service to meet individual customer requirements.

NEW NE 5550 and NE 5560 series probe units employing pulse shape discrimination techniques for detecting neutrons in a high gamma background.

For full details write for Technical Bulletins (No's 14, 15. 16, 18, 21, 22, 24.) & Catalogue to the Sales Division, Edinburgh.

Nuclear Enterprises (G.B.) Ltd.

Sighthill, Edinburgh 11, Scotland.—Tel.: Craiglockhart 5262

Associate Company: Nuclear Enterprises Ltd.
550. Berry Street, Winnipeg 21. Canada.

8212

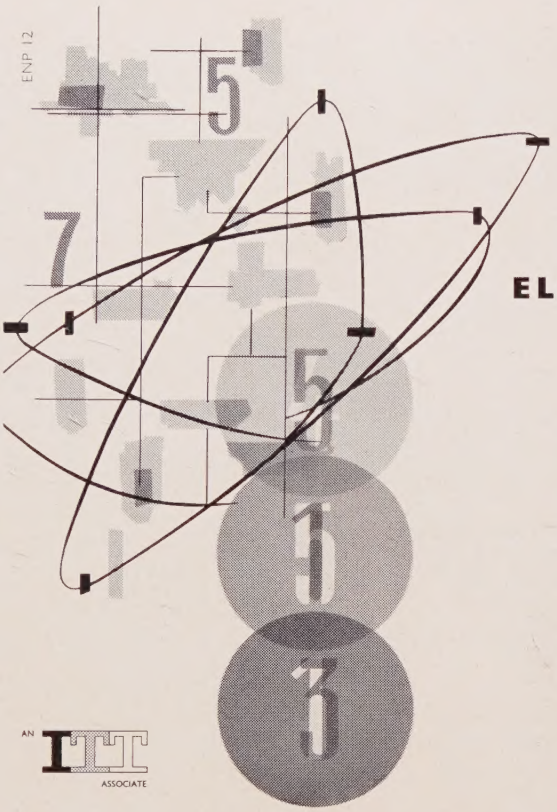

ELECTRONICS FOR NUCLEONICS

SCALER CHRONOSCOPE

Bell Telephone scaler chronoscope gives you top quality reproduction of automatic counting and printing.
It is so constructed that from a small stock of basic modules a wide scope of performances can be covered. This type normally supplied in a metal case is also available for rack mounting

- preset time
- preset count
- result printing facilities
- interchangeable modules
- in line read out
- fully transistorized

Our staff is always available to answer your inquiries.

Bell Telephone Mfg Co

"Nuclear Energy division"
33, Berkenrodelei
HOBOKEN-Antwerp-BELGIUM

MODEL 412 MERCURY RELAY

PRECISION SLIDING PULSER

for Precise Calibration of Single & Multi-Channel Pulse Height Analyzers

Determines Window Widths Using Principle of *Constant Angular Velocity*

AUTOMATICALLY
10 × more accurately
40 × faster than conventional pulsers

Incorporates Both Manual Control and Precision Motor Drive

Simulates Pulses from Scintillation, Proportional or Geiger Counters

MERCURY PULSER, Model 401

Featuring Versatility and Precision

Specifically designed for the Nuclear Physics Laboratory

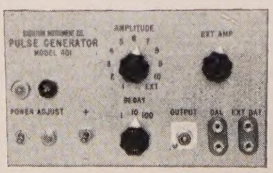

Fast rise and exponential decay simulates scintillation, proportional or geiger counter pulses for test and calibration of amplifiers, pulse height analyzers, scalers, etc.

MODEL 412 . . . $ 450.00 — MODEL 401 . . . $ 125.00

RADIATION INSTRUMENT CO.

P. O. BOX 733, SILVER SPRING, MARYLAND, U.S.A.

NORTH-HOLLAND BOOKS

Paul Ehrenfest

COLLECTED SCIENTIFIC PAPERS

XII + 632 pages

Guilders 45,00 (90s.)

This volume makes widely scattered publications readily available. All Dutch articles appear here in English; the German publications are in the original language.

Sole Agency for U.S.A.:

Interscience Publishers Inc. — New York

NORTH-HOLLAND PUBLISHING COMPANY - AMSTERDAM

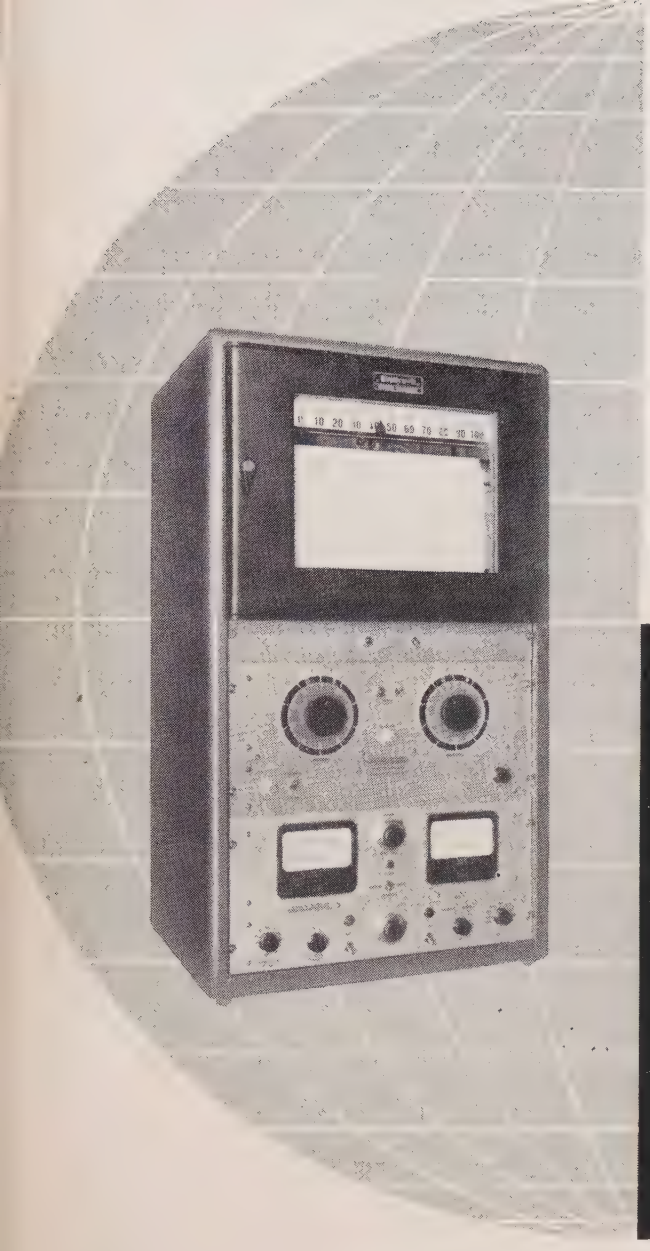

RAPID RADIATION ANALYSIS

with RIDL Model 50-1 AUTOMATIC SCINTILLATION SPECTROMETER

.scans whole or any part of spectrum
...automatically prints out data and resets

y much stability can one expect in an instrument? Surpris-y, a great deal . . . as found in the RIDL Model 50-1 omatic Scintillation Spectrometer. This fine spectrometer is as useful today as it was when first introduced. Actually s have increased each year. This obviously indicates good c design, the utmost in reliability and wide versatility.

he Model 50-1 is a completely automatic integral and dif-ntial **single-channel pulse height analyzer.** It is used identification of isotopes, for gross counting studies, com-ative measurements, luminescence studies and half-life deter-ations. It is ideal for use with automatic sample changers, tting with each new sample. Due to the use of an **elec-tronic sweep,** there is no mirror effect.

For beta and gamma spectroscopy or spectrometry, the Model 50-1 offers small laboratories an instrument adaptable to a variety of detectors and experiments. Its separate components find multiple uses in large laboratories. It provides a choice of full-scale ranges and time constants, various scanning speeds, and a stable HV supply. **The two-second Brown recorder** included in the system provides various chart lengths.

For a quality line of beta, gamma and X-ray spectrometers consult the RIDL General Catalog 61. For all detection and measuring instruments used in the radiation field, write today to Department K.

RIDL INC.

Radiation Instrument Development Laboratory, Inc.

61 EAST NORTH AVENUE • NORTHLAKE, ILLINOIS
PHONE: MUrray 1-2323 • Cable Address: RADILAB

"CHARGED PARTICLES"

Nanosecond Pulsing

The timing of nuclear events and the discrimination between them continues to be a major hurdle for the experimental physicist.

We don't need a market research program to reveal the need for apparatus which will assist the experimenter to do accurate neutron time-of-flight work or to determine excited state lifetimes in the milli-u-sec. region. Ultra-short high-intensity pulses of charged particles, and the resulting neutron bursts, provide one of the most promising techniques in these experimental areas.

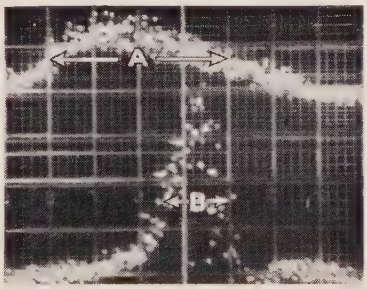

Lumatron scope presentation of 8-nanosecond terminal-pulsed beam (A) and compression to 2-nanosecond post acceleration pulse (B).

We have completed the development of a system for producing and measuring *pulsed proton beams with an intensity of several milliamperes and a pulse duration of less than one nanosecond (10^{-9} seconds).* The first research results from this apparatus are soon to be reported.[1]

The beam is accelerated to 3-Mev by a Van de Graaff fitted with a terminal pulser of the deflection type, delivering ion pulses of 10 ns duration every 1000 ns at the input end of the acceleration tube. After acceleration, the pulse is compressed by a 90° double-focusing Mobley[2] magnet whose radius of curvature is 30 inches. The deflection electrodes at the entrance of the magnet are driven by a 10 Mc sinusoidal voltage which is synchronized with the pulse from the accelerator. Observations were made with a time-to-pulse-height-conversion measurement system checked by nuclear methods.

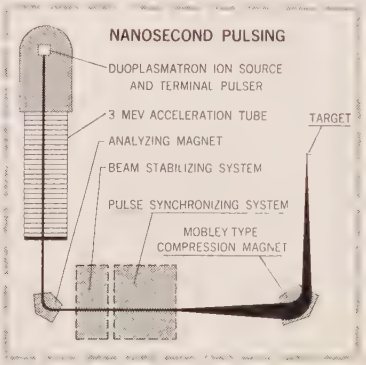

Isotopes of Rare Purity

The need for pure isotopes in work concerned with nuclear structure and particle reactions has led us to develop a new, broad-range electromagnetic isotope separator that is faster, simpler to use and provides purer samples than any comparable equipment we've seen.

This instrument is designed to produce up to 10 microamperes of individual particle beams — *with a mass resolving power better than 400.* Separation is achieved in a 5000-gauss, 160 cm radius magnetic field. Time for recovery of samples after collection is less than two minutes. Those who have had their decay schemes disappear before their eyes will appreciate this bit of engineering in working with short-lived isotopes.

The instrument can also be used to produce nuclear targets for studies of energy level, scattering, neutron cross-section or other phenomena, as well as pure radioactive tracers. Two of these instruments are now being built for U.S. atomic energy program. Specifications for the machine are presented herewith.

160 CM ELECTROMAGNETIC ISOTOPE SEPARATOR

Range:	Atomic mass 1 to 400
Current:	$10\mu a$ of most abundant isotope ($100\ \mu$ achievable with some loss in resolving power)
Voltage:	80 kv
Magnetic Field:	5000 gauss
Field Stability:	Better than .01 per cent
Ion Sources:	Modified Arc
Operation:	Time for removal of collector after full operation — 2 minutes
Vacuum System:	All metal bakeable gasketing

Accelerator Conference

The 2nd Accelerator Conference held recently in Amsterdam was a rewarding occasion for High Voltage and its Dutch affiliate, High Voltage Engineering (Europa) N.V. Three hundred participants from 24 countries joined in this exchange of information on accelerators and experimental techniques. There was some healthy give and take between the "ideal" machine described by physicists and the "present state of the art," reported by our engineers. If there were no gap between what is wanted and what is commercially available, most of us could pack up and go home.

As things stand, High Voltage continues to push its development to the limit and is glad to share a challenge with its insatiable customers in research.

The Conference Proceedings were published in a January special issue of *Nuclear Instruments and Methods.* Check with your librarian, or write us for a complimentary copy.

HIGH VOLTAGE ENGINEERING CORPORATION
BURLINGTON, MASSACHUSETTS, U.S.A.
•
APPLIED RADIATION CORPORATION
•
HIGH VOLTAGE ENGINEERING (EUROPA)

1 *L. Cranberg, et. al., to be presented at Am. Phys. Soc. Meeting, New York (February 1961)*

2 *R. C. Mobley, Phys. Rev. 88, 360 (1952)*

NUCLEAR INSTRUMENTS AND METHODS **10** (1961) 169–184; NORTH-HOLLAND PUBLISHING CO.

MEASURING TECHNIQUES FOR ENERGY LOSS STUDIES OF 2.8 MeV BETATRON ELECTRONS IN MATTER

TORBJÖRN WESTERMARK

Division of Physical Chemistry, The Royal Institute of Technology, Stockholm 70, Sweden

Received 10 September 1960

Methods for the accurate recording of energy loss spectra for electrons at a few MeV are discussed. Some experience with an electrostatic method is described. The method selected involves the variation of a portion of the current of the spectrometer magnet and recording of the spectrum with an XY-recorder. (Some experiences with Hall generators for steering the X-axis are given). The record includes the primary line as well as two or even three energy loss spectra. One of the latter is due to a standard absorber. Various detailed problems are discussed including evaluation of energy loss properties.

1. Introduction

The energy loss of fast electrons has been studied by several authors since 1950 (ref.[1,12–15]). The aim has been mainly to test the Bethe-Bloch theory and the so-called density or polarization effect for which this theory must be corrected. The objects of study were metallic absorbers in most cases but one or two chemical compounds were also studied. The present investigation will emphasize the study of chemical compounds to reveal any possible valence effects, particularly for light elements.

In this paper, the methods adopted will be described. Two earlier papers[1,2]) describe a magnetic spectrometer and investigations of a betatron as the electron source used. The first results of energy loss studies for about 15 substances are given elsewhere[10]).

2. Selection of Experimental Method

2.1. GENERAL OUTLINE

The present investigation uses a 5 MeV betatron as the electron source and a double-focusing magnetic spectrometer as energy measuring device. The spectrometer has been described in a previous paper. The betatron will be described by Smårs and Wernholm[3]). The energy stability has been found to be very good (better than $\pm 0.3^0/_{00}$ over 2–3 hours) and the half-width of the primary line was found to be $2.8^0/_{00}$ (momentum scale) using appropriate slits and unavoidable windows. Of this, $0.3^0/_{00}$ or less (corresponding to $\sim$ 1 keV) is attributed to the betatron itself. These betatron properties are favourable and should allow accurate energy loss studies to be made.

A few alternative methods of energy loss measuring technique existed and will be briefly outlined.

2.2. ELECTROSTATIC METHOD

In a previous paper[1]), the author described a method for measuring electron line-widths electrostatically. The method was first applied by Rutherford and some of his collaborators and was re-emphasized again by K. Siegbahn[4]) for the case of determination of h/e. The method has also been used by Russian workers (ref. 14 of [1])).

The electrostatic method has thus proved valuable for the measurement, directly in

[1]) T. Westermark, A double focusing magnetic spectrometer for studies of energy losses in matter of electrons from a 5 MeV betatron, Nucl. Instr. and Meth. (to be published).

[2]) T. Westermark, Energy distribution and energy stability of the electron beam from a 5 MeV betatron, Nucl. Instr. and Meth. (to be published).

[3]) E. Smårs and O. Wernholm, A 5 MeV betatron, Nucl. Instr. and Meth. (to be published).

[4]) K. Siegbahn, Appl. Sci. Res. B4 (1954) 25.

electron-volts, of energy differences in alpha and beta spectroscopy (including gamma) and of line widths. No knowledge of elementary constants and no calibration of, for instance, magnetic fields are necessary. What is required is an accurate voltage measurement but this technique is already far developed and can in principle be based experimentally on the Weston cell or other accurate reference voltage. Some experimental limitations exist however.

The use of the electrostatic technique for the measurement of energy loss spectra should in principle be quite feasible and possess important merits. (For low electron energy work, the method is well-known.) All results would be absolute and all particle transmission through the magnetic spectrometer (in our case) would occur at a single electron energy. The latter point means that the instrumental transmission properties are exactly the same and, moreover, the detector always receives particles of a fixed

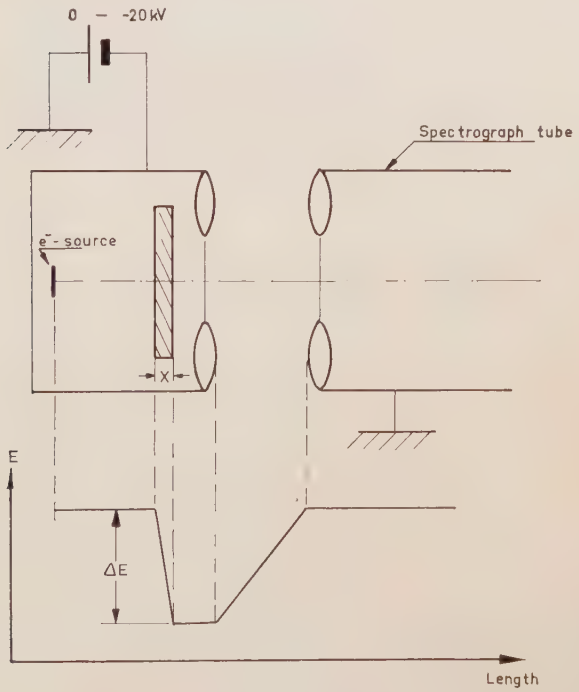

Fig. 1. Principle ofl eectrostatic method for energy loss measurements of internal conversion electrons. The lower sketch illustrates the changes in kinetic energy of the particle. By using a reversible voltage generator it is possible to double the voltage range permitted by breakdown limits.—It is seen that the spectrometer detects particles at a fixed energy.

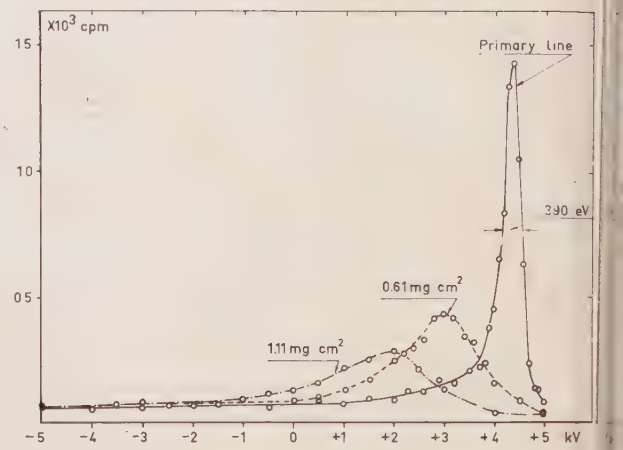

Fig. 2. Application of the electrostatic method for measurements of electron energy losses for ThF electrons in thin absorbers of pliofilm (roughly C_5H_8Cl).

energy. The annoying magnetic hysteresis phenomenon is wholly avoided etc.

We have made some studies in order to investigate the possibilities of applying the method to electron energy loss studies. Fig. 1 shows the application to internal conversion electrons. The loss of energy is compensated by a known amount of acceleration voltage applied before the entrance of the spectrometer. Fig. 2 shows some results for energy loss spectra of ThF electrons (from the ThB deposit) in "Pliofilm" (hydrochlorinated rubber). It has been shown in one of the previous papers[1]) that the narrow geometry is very insensitive to changes in the optical source point. Such changes are expected as soon as curved lines of force are present[4]). The energy loss spectra of fig. 2 can obviously be employed, in addition, to give various energy loss properties after appropriate corrections.

The application of the electrostatic technique to electrons ejected from an accelerator such as a betatron is very difficult. The potentials of the different parts of the accelerator are well grounded and so the only possibility is to put the whole spectrometer tube on a high voltage. To this end, the spectrometer tube can be constructed using glass coated on the inside with a conducting layer. The joint to the absorber section near the entrance slit of the spectrometer can be made by electrostatic lenses (c

g. 1). The same arrangement is appropriate for he exit side to decelerate the electrons so that he detector can be put at ground potential. Our xperience showed that at least 50 kV can be pplied in practice using such arrangements ithout sparking. The polarity can be reversed nd thus 100 kV energy losses can be covered.

This requires the energy loss itself to be large. Moreover, the energy loss spectrum (Landau distribution) has a long tail at the low energy side and it is absolutely necessary to record this part if average energy loss studies are intended. This property is of more fundamental interest than the most probable energy loss (refs. [1,29]).

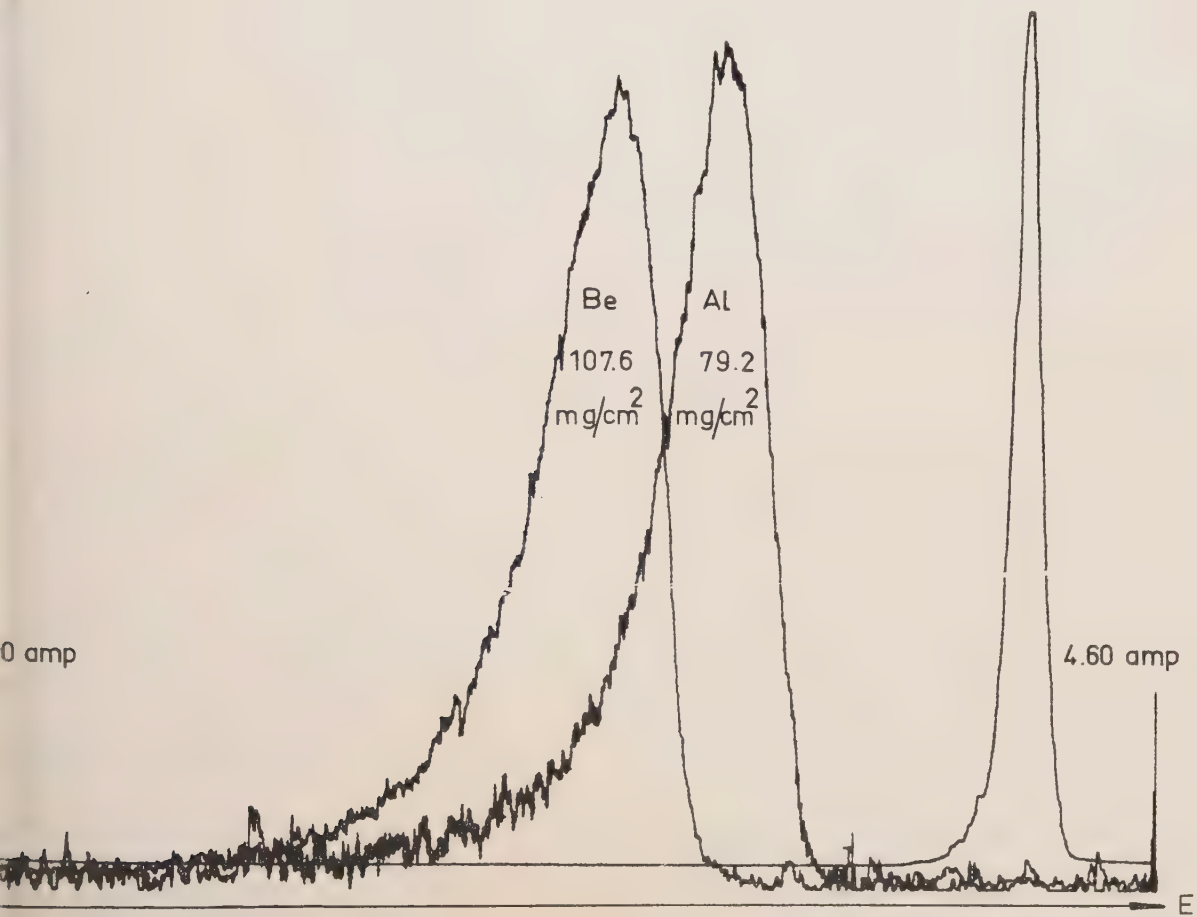

g. 3. *XY*-record of primary line and energy loss spectra in a beryllium absorber and an aluminium one. *X*-axis steered r current change of spectrometer (closely proportional to particle momentum). *Y*-axis fed from electron beam trans- itted through spectrometer as detected by an ionization chamber and a vibrating-reed electrometer.—Record taken an early stage of development and should be compared with fig. 14 which represents a stage of considerable improvements.

urther improvements are no doubt possible and nce it might be possible to cover larger energy sses.

The requirements for the energy loss meas- rements are, however, very stringent. It is ecessary that the half-width of the energy loss ectrum is several times (ideally more than ten nes) broader than the primary line half-width.

Further studies showed that a least 500 kV had to be covered in the present case, among other things because the half-width could not be reduced further than a certain figure (see above). It is obvious that it is much more practical at present to vary the magnetic field strength of the spectrometer than to meet these electrostatic requirements. For these reasons, the electrostatic

method was abandoned and the current variation method had to be selected despite its inherent difficulties.

The method and the introductory studies made have been described here with the thought that it may inspire other workers in a more favourable position to use it.

2.3. MAGNETIC FLUX DENSITY VARIATION

The procedure adopted for making an energy loss experiment was to vary the magnetic flux density according to the preceding discussion. A certain fraction of the magnet current was varied mechanically and was used to steer the X-axis of an XY-recorder. The signal from the detector situated outside the exit slit of the spectrometer was fed to the Y-axis.

Scanning back and forth with two different absorbers one at a time in the electron beam and a third run without any absorber yield on the XY-graph the primary line as well as the two energy loss spectra. Fig. 3 gives a typical example from the earlier phase of the work.

2.4. DISCUSSION

The current variation method is no doubt very practical. Another alternative might be the movement of the detector slit in a radial direction at the exit end of the spectrometer. The deciding factor here is the dispersion (see ref. [1])). This property is about 4% momentum change per cm. The spectrometer tube is 45 mm and so the maximum momentum band available is less than 5%. (Of course it has to be exactly proved that the dispersion is linear in the range and that peripheric regions are free of disturbances.) This range is too small for our studies and so this alternative is not suitable without large instrumental changes.

The current variation method selected will be closer described in the following.

3. Recording Energy Loss Spectra by an XY-Recorder

3.1. OUTLINE

The procedure for recording the energy loss spectra of some predetermined electron energy has already been briefly described (cf. fig. 3). In this section we shall therefore describe certain details pertinent to achieving as precise records as possible.

3.2. THE BETATRON

The energy region that can be covered with the betatron is not exactly known but a useful beam has been obtained from 0.5 to 4 MeV. The energy for which the instrument was designed is slightly more than 5 MeV and so the range might be somewhat larger than indicated. Most studies hitherto have been made at 2.8 MeV.

A knowledge of the exact energy was obtained by calibration using gamma radiations of known energy (see section 4).

The energy stability and energy distribution of the betatron electrons have been described in detail in the preceding paper[2]). Most of these studies also apply to 2.8 MeV.

The betatron cannot be operated for too many hours and so the time available for each experiment is limited. Thus fast procedures had to be selected.

Whereas energy stability and energy width are rather satisfactory, (after introducing the improvements reported[2])), the *intensity variations* have caused much trouble. Several circuits suspected to cause such variations were inspected and stabilized further without any effect. The electron gun can, no doubt, cause serious intensity variations and different guns behave quite individually. The introduction of the long shafted guns of Mr. G. Hansson's design (see[2])) was apparently an improvement as far as the intensity variations were concerned. Another point, mentioned in[2]), is that the injection voltage has been reduced to a safe level so that sparking very seldom occurs. After sparking, the intensity is unstable for some time.

Some observations made by the operator indicated that the resistance of the conducting layer on the inside of the glass doughnut tube plays an important part in the intensity variations. A special type of failure, viz. a gradual deterioriating contact between the conducting layer (tin dioxide) and the connection pin

arth (via emission current indicator), showed hat, before complete breakdown, the intensity ariations get worse. It is reasonable to suppose hat a too high resistance leads to small isolated harged areas which change their voltage and hus cause intensity variations. It was confirmed rom the Siemens Reiniger Company in Germany hat reducing the resistance decreases the va- iations in a certain type of machine. The iemens betatron has, moreover, a continuous njection system (guided by lenses) and so the nal intensity variation is $\pm$ 1% (maximum eviations), a very good figure indeed[5]).

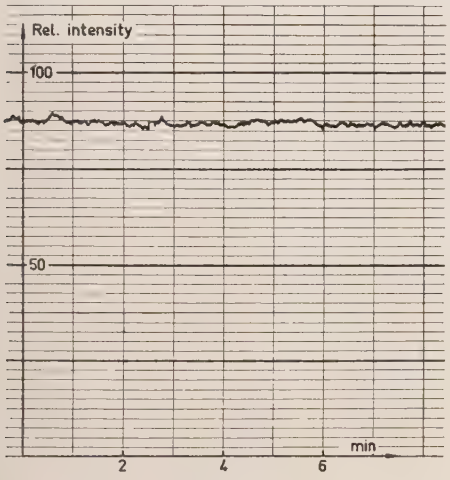

ig. 4. Example of our best intensity records. Maximum ariations during 8 minutes is $\pm$ 2.3% (From record 58:60).

The doughnut was therefore demounted and he tin dioxide layer removed using alkali and a latinum layer applied. (Thanks are due to Dr. . Wernholm for kind advice on this point.) A olloidal platinum suspension (Liquid Bright latinum F 104) procured from Johnson, Mat- hey Ltd., London was applied and the doughnut ube thereafter heated to 550°C for some hours nd then slowly cooled. The D.C. resistance easured between two diametrically opposite oints was now ~ 400 ohms instead of the revious 2000 ohms. (The layer was now non-

[5]) Drs. Berger and Malch, Siemens Reiniger Werke, Er- ngen, Germany. (Kind private communication); Their tatron is well described in Atomwirtschaft, (July-Aug.) 959) p. 349.

transparent but this was no drawback in the present case). The intensity variations were much improved. With the tin dioxide layer, they amounted to $\pm$ 10% or in the best runs $\pm$ 5%. They were now steadily within $\pm$ 5% (although not always) and some were even within $\pm$ 2%. Fig. 4 shows one of our best performances. These variations were generally symmetrical but sometimes a drift was present.

This improvement has reduced the number of records that have to be rejected and thus decreased the need for corrections. The precision of both the average energy loss and the most probable energy loss were improved. (As is well known the resistance of the conducting layer should not be too low because of the induction of eddy currents. As Dr. Wernholm has pointed out, the resistance might be reduced even further perhaps to some tens of ohms.)

3.3. THE SPECTROMETER

The design and construction of the spectrometer has been described previously in detail[1]). It was also described how the spectrometer was accurately aligned to the betatron output. The whole equipment was fixed in this position during the energy loss studies and only minor changes were made. For instance, the entrance slit has been replaced to give the best compromise between resolution and transmission. 1 $\times$ 6 mm lead slits have often been used. The entrance aperture slit has also been replaced (normally it is 7.5 $\times$ 7.5 mm). The exit aperture slit, which was found necessary to reduce ghost lines[1,2]), has never been removed (it is 10 (radial) $\times$ 30 mm).

The betatron tube and the spectrometer tube have formed two separate vacuum systems mainly because the absorber position (see below) had to hold liquids. The entrance window has been 0.9 mg/cm^2 pliofilm covering an area of 10 mm diameter. (The author is indebted to Lic. Hagström, Physics Institute, Uppsala University and Mr. Å. Svanheden of Gustaf Werners Institute for Nuclear Research for kind advice on thin windows in radiation fields.) The exit window was also made from the same material. No difficulties were met with these windows.

3.4. THE DETECTOR FOR THE SPECTROMETER

The twin ionization chambers described before contained air from the beginning. They were later on filled with pure sulphur hexafluoride in order to produce a gain in signal level. SF_6 has, in addition to Xe, apparently the highest gas density of all non-condensable gases at ordinary temperatures. It was procured from the Matheson company, Newark, USA and was filled to atmospheric pressure into the twin chambers after evacuation. No difficulties at all occurred and the gain in ionization current was about five times.

Since it was decided to increase the signal further, the high-ohm resistor has been replaced a few times with higher resistors. The final choice was 5×10^{10} ohms. Experiments were made to ensure that the scanning speed is low enough not to disturb the peaked curves (see fig. 10 of[2]).

In some cases it was observed that the intensity as recorded by the vibrating-reed electrometer and the XY-recorder showed memory effects, viz. the intensity did not fall exactly to zero after a high intensity. This effect, which was supposed to be partly caused by after-effects in the insulators, perhaps in connection with irradiation, was reduced by using further lead shielding not only for the ionization chambers but also for the vibrator unit and its connection. Moreover, the intensity of the primary line was reduced to the same order as that of the energy loss spectra. This was done using a special slit with reduced height. With these precautions, the effect is seldom seen.

3.5. THE X-AXIS

The X-axis of the XY-recorder shows the momentum scale. Several possibilities exist for feeding it with a signal related to the magnetic flux density. The easiest is simply to feed it with part of the current passing through the exciting coils of the spectrometer magnet as is shown in the previous paper[2]) for the recording of the primary line. The method rests on a knowledge of the dependence of flux density on magnetic current. As will be shown in the next section, this relationship is close to linear at least within the ranges considered. For high precision, it is necessary to consider the hysteresis effect (see below). In the present case, it is possible to feed the X-axis of the recorder directly with part of the voltage produced by the spectrometer current across a precision manganin resistor. No amplification of the signal is required.

A second alternative was tried (at the suggestion of Prof. K. Siegbahn after presentation of this work before the Conference of Swedish National Committee of Physics, Uppsala June 4 1957), namely the use of a *Hall generator*. An InAs Hall generator (type FA 23) produced by Siemens-Halske, Germany was procured. The unit requires 300 mA transverse current and yields approximately 1 mV/100 gauss. The unit was mounted within the spectrometer magnet symmetrically between the pole shoes. It had to be mounted at a larger radius than the spectrometer tube and thus receives a lower magnetic flux density than that for the central orbit. It is fed with exactly 300 mA from a special transistorized current stabilizer (design Oltroni Company, Vällingby, Sweden). The feeding of the X-axis of the XY-recorder by a part of the

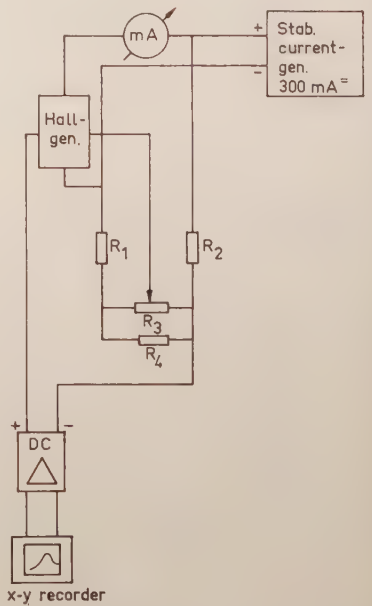

Fig. 5. Circuit for use of Hall-generator for feeding X-axis recorder. Hall-generator is placed just outside spectrometer tube centrally within the magnet. It is fed with exactly 300 mA which has to be well stabilized.

Hall voltage had to proceed via a DC-amplifier (Leeds & Northrup's Stabilized D-C microvolt amplifier No 9835 A). The latter is stated to have an accuracy of 0.4% with external recording.

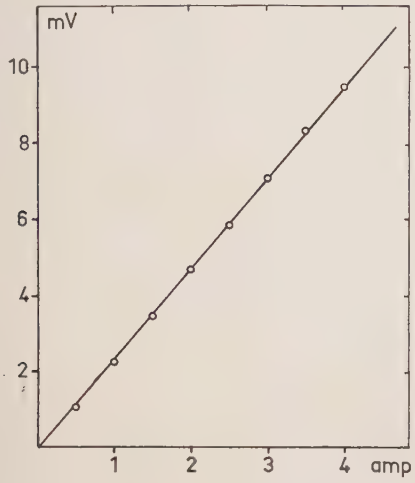

Fig. 6. Hall generator output as a function of spectrometer magnet current. It is seen that the region of interest is close to linear.

The final choice was the simple current feeding alternative. The Hall method has the important merit that hysteresis is of no concern but, on the other hand, it adds to the complexity of the whole apparatus, requiring a DC amplifier and a very stable current source and the generator has to be kept at a constant temperature. Moreover, it remains to be found out if it is reproducible enough down to changes corresponding to $1.5^0/_{00}$ or better, a precision of interest here. The point about the amplification and also the other points mentioned above were the deciding factors since it was judged that they might introduce a source of error which might have more influence on the final error than the hysteresis effect.

Nevertheless the Hall generator unit has been used in several experiments—particularly for the recording of hysteresis effects (see below). The scheme used is shown in fig. 5 and the connection between Hall generator output and spectrometer magnet current in fig. 6.

3. ABSORBERS AND ABSORBER POSITION

The absorbers are plane parallel sheets of matter of various kinds. The metallic ones have been stamped or machined from larger pieces which were bought from well-known international sources in as pure form as possible.

A special class of absorbers is very sensitive to air, e.g. the alkali metals and lithium hydride cut out or pressed mechanically with special techniques which will be described in a paper on the first electron energy loss results[10]). These absorbers had to be protected with thin elastic films[10]) (polystyrene or pliofilm).

Liquids were filled into a simple cell constructed according to fig. 7. Many studies were devoted to the problem of the bending produced by the windows. The bending is caused by unavoidable hydrostatic pressure and is for elastic materials dependent on the diameter (fourth power), thickness of the membrane (inversely third power) and pressure (linear[11])). These factors were therefore reduced as much as possible. Moreover, it was found that stressing the membrane before use reduces the bending

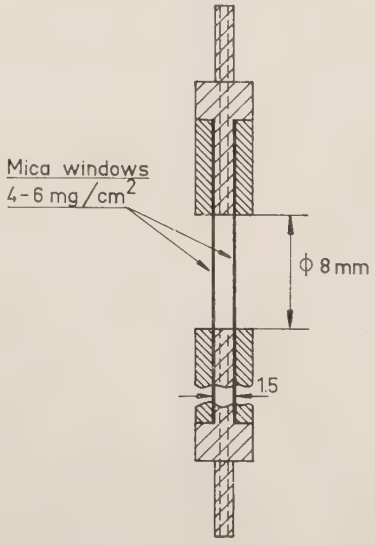

Fig. 7. Cell for holding liquids in the absorber position. It is closed by mica windows of about 4 mg/cm² thickness. They are mounted in a stressed manner described in the text to reduce bending effects.

amplitude. The brass ring and the windows were cooled in a refrigerator to —20°C for some time. They were then mounted by means of screws as fast as possible. Upon reaching room temperature, radial stress is introduced by the larger

coefficient of thermal expansion of brass in comparison with mica. This method often reduces the bending effect by as much as a factor of ten. The bending was followed by observing in a microscope a small glass rod fastened to the mica window. The maximum bending was about 19 μ in the cell shown in fig. 7 and with 16 cm water pressure (both windows). The effective hydrostatic pressure at use was 1 cm water or less and so the bending effect can be neglected in comparison with the total liquid thickness ($\sim$ 1500 μ).

The absorbers are fixed in a wheel providing 8 different positions. The wheel can be operated mechanically from the control-table. The wheel is accurately constructed and care was taken that the electron beam passes the absorbers normally. Enveloped materials as well as liquid cells can be fixed at the absorber position as well as more easily handled solids such as metal sheets, semi-conductor plates etc. One position on the wheel is left free for studies of the primary line or is masked down to reduce the height as described above to reduce the intensity of the primary line to the same level as that of the energy loss spectra.

Sometimes a hole was bored through the absorbers (cf. ref. 20 of [1]). In such a case the record shows the primary line on the same trace as the energy loss spectrum. This technique is very elegant but is, however, not generally applicable (cf. enveloped or liquid absorbers).

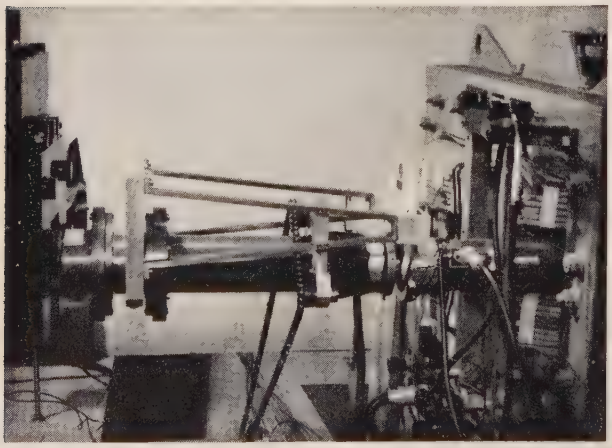

Fig. 8. View of the absorber zone with betatron exit leg to the right. The electron beam passes out through a 3.8 mg/cm² mica window, passes through the output ionization chamber and through the absorber (absorber wheel is seen on fig.). It then enters the 1 × 6 mm slit of the spectrometer (entrance window 0.9 mg/cm² mylar).

The position of the absorbers is shown in fig. 6 of [2]). It is seen that the entering electron beam is confined before the absorber by means of a circular aperture of 10 mm diameter. Since the virtual source point of the beam is at least 30 cm away, the entrance is close to normal. The entrance slit of the spectrometer is situated close to the absorber and is the one defining the beam position and intensity. It is normally 1 × 6 mm. The aperture slit defines the angular spread accepted. It is 0.93° in our experiments (angular deviation from the normal). There is a small difference in source position for the primary beam and the absorber runs but it is clear from [1]) that this does not change the transmission properties of the instrument. Fig. 8 gives a view of the absorber zone.

3.7. HYSTERESIS EFFECT

The hysteresis effects of the magnet are small due to the selection of the soft magnetic material. However, for attainment of the highest possible precision in energy loss measurements this phenomenon has to be considered.

The following experiment gives an idea of the magnitude. The K and L internal conversion lines of $Cs^{137} - Ba^{137}$ were recorded by using the anthracene scintillation detector, a counting rate-meter and the XY-recorder (cf. fig. 9). The peak positions were evaluated for different scanning directions and plotted on a diagram (fig. 10). This diagram, which could be reproduced many times (provided the turning points are the same) with good accuracy, shows the magnitude of the hysteresis effect at the electron momentum ($B\rho \sim$ 3300 gauss·cm). The slope for the first upward record is found to be about 3% larger than that for the downward one. The slopes for the upward and downward scanning on the established hysteresis cycle differ by only 1% or less.

Further experiments were devoted to the energy region selected for energy loss mea-

urements, viz. just below 2.8 MeV. The output from the Hall generator (see above) was connected to the Y-axis and the spectrometer current to the X-axis. (We shall assume that the Hall generator gives a true linear signal for the flux density). The hysteresis trace shows a small but quite clear hysteresis effect. The worst deviation from linearity upon use was found to be 1.7%. By considering the actual position of the energy loss spectrum it could be shown that relative measurements of a substance in relation to the standard cannot be affected with a larger effect than 1%, 0.5–1% being the most probable range. Thus it is seen that the hysteresis effect prevents the precision to be increased beyond these data.

With these and other data on the hysteresis effect, the following routine was introduced. All records were taken on the *upward* part of an

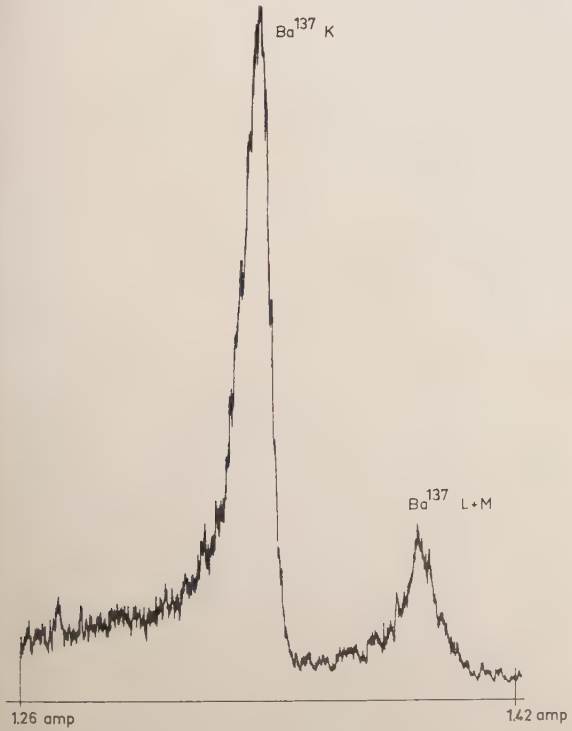

Fig. 9. XY-record of internal conversion electron spectrum of K and L + M peak of Ba^{137} using a Cs^{137} source. Fig. illustrates the technique of recording sections of beta spectra with an XY-recorder with current scanning and scintillation detector and counting-rate-meter. Peak positions are studied to establish knowledge of reproducibility of hysteresis cycles (cf. fig. 10).

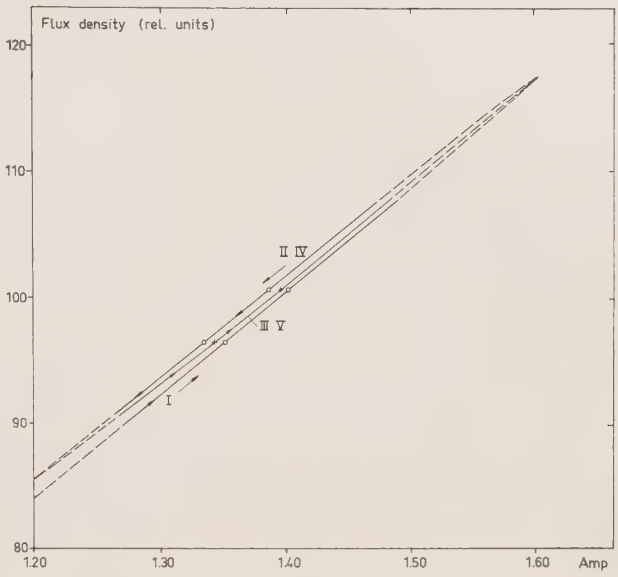

Fig. 10. Construction of hysteresis cycle from studies of Ba^{137} electron energy spectrum (cf. fig. 7). I is record from zero current and upwards. II is taken for downward scanning (1.60 amp–1.20 amp). III upwards the same range, IV downwards and V upwards again. II and IV give identical peak positions within experimental accuracy ($\pm$ 0.001 amp). III and V also give such a result. It is seen that upward traces are reproducible within the accuracy stated. (No demagnetization was made.)

established hysteresis curve, i.e. one obtained by scanning back and forth before records are taken. With this procedure it was found unnecessary to perform any demagnetization.

Hysteresis would not affect *relative* stopping power measurements which are the main intention of the present phase of the work. A few attempts to obtain absolute measurements have been made, however, and will be reported in the next section.

3.8. SUMMARY OF THE REQUIREMENTS FOR A GOOD ENERGY LOSS RECORD

There are several requirements for the different parts of the complex instrumentation which have to be fulfilled in order to obtain a good record that is worthwhile to be evaluated. Some of them have been touched upon but others have not. A brief summary follows:

Betatron

The electron gun has to be well selected and tested. Failure is caused by repeated sparking or

wire breakdown. The conduction layer on the inside of the doughnut tube has to be in good condition. The contact between the layer and the earthing point has been a source of failure. For unknown reasons, contact material sometimes disappeared here despite precautions.

Some electronic components, especially the injection and ejection thyratrons and condensers, are especially liable to cause failures. The main causes of failures are (in order) conducting layer contact, electron gun, trivial vacuum leaks and electronic components. Many other conceivable sources of failure have caused trouble but less so. What has been said about failure also includes bad intensity behaviour. The intensity variation should be at least within $\pm 5\%$ and show no drift.

The spectrometer

The storage batteries have to be well charged. The switching-on of the spectrometer current several hours before normal use reduces drift to almost negligible levels.

The detector system

The vibrating-reed electrometer has behaved as good as claimed by the manufacturer. The only important concern is the small memory effect described above but the cause of this effect might be elsewhere.

The current varying device and XY-recorder

The potentiometer wire of the former has to be cleaned at intervals to give a continuous contact. Drift of the compensating voltage has occurred. The presence of this is indicated by the end markers of the record. The XY-recorder itself has sometimes shown sudden jumps or wholly irregular records and had then to be repaired. Before using it once again, it was appropriately tested and approved. Because the XY-recorder is the central instrument for the studies, it might be added that drift may be suspected to occur in the adjustment potentiometric circuit resulting in a movement of the zero point and in the response itself.

4. Calibration of the Spectrometer for the Determination of Betatron Electron Energy and for Attempts towards Absolute Energy Loss Measurements

The spectrometer was calibrated in the ordinary fixed and adjusted position by the methods of beta-spectroscopy. Au^{198}, Na^{24}, La^{140}, Cs^{137} and the thorium deposit were used. The first three were produced by activation of appropriate samples in the reactor R1 in Stockholm (flux 10^{12} n/cm^2 sec).

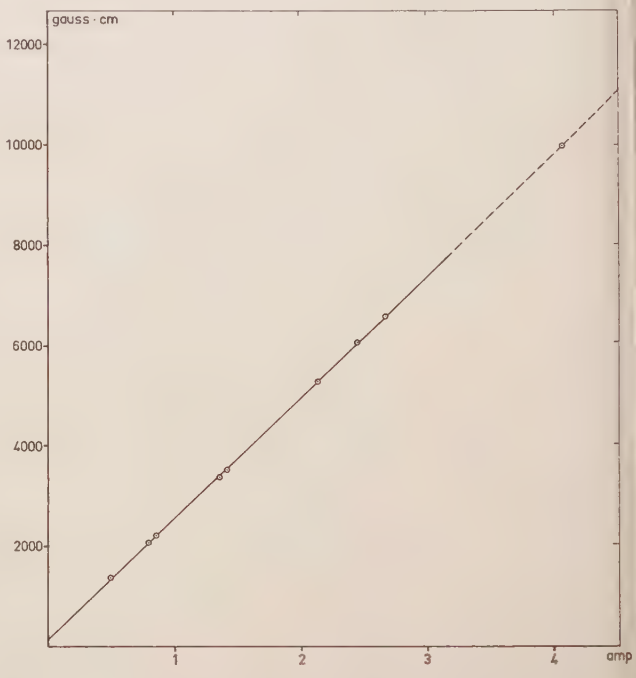

Fig. 11. Calibration of spectrometer with some of standards of beta-spectroscopy. $B\rho$ in gauss-cm as a function of current in amps. Points correspond to the known $B\rho$-figures (corrected for energy loss in covers and windows) found at a certain current by extrapolation of high-energy sides of peaks or Compton continua. A certain remanence of 6–8 gauss gives a certain threshold. The curve is dashed in the upper region since it relies on a single point (Na^{24} Compton limit). It is known that a curvature upwards takes place here.

Despite the use of about 200 mc of Na^{24} and the same amount of La^{140}, no photolines could be found either using a 25 mg/cm^2 Au foil or a 4 mg/cm^2 U foil. This was apparently due to the low cross-section for the photoelectric effect and the background. Instead, the Compton limits were used. In all cases, the steep high energy side of the photoline or Compton continua were

TABLE 1

Calibration of spectrometer with standards from beta-spectroscopy

Line	E_{keV}	E_{keV}-corrected for covers (keV)	B_{corr} (gauss cm)	I (amps)
ThF	148.08	148.08	1388.4	0.49
Au^{198}-U_K	296.73	291.5	2063.9	0.791
Au^{198}-Au_K	331.10	326.0	2211.2	0.856
Cs^{137}-K	624.2	622.1	3373.5	1.355
Cs^{137} LM	660.6	658.5	3508.9	1.408
Na^{24}-Compton max.	1152.7	1151.6	5277.4	2.13
La^{140}-Compton max.	1375.8	1374.9	6055.4	2.445
La^{140}-Ta_K	1528.5	1527.6	6582.7	2.67
Na^{24}-Compton max.	2520.2	2519.3	9963.3	4.08

Data including numerical conversions have been taken from Gerholm[16]) and Mitchell[17]). Compton limit is calculated from $T_{max} = \frac{E_\gamma}{1 + \frac{1}{2\alpha}}$ where T_{max} is maximum Compton electron energy and $\alpha = \frac{E_\gamma}{m_0 c^2}$ (Evans[17]). Energy losses in covers and windows were calculated in the same manner as discussed in[1]).

extrapolated to the background. Fig. 11 shows the results obtained. Table 1 summarizes the details.

Fig. 13 shows the apparent spectrometer constant $B\rho/I$ (cf. Arbman-Svartholm ref. 51 in [1]) corrected for a remanence effect of 200 gauss·cm ($\sim$ 8 gauss remanence, found to be rather independent of current used). The trend upwards is clear and is in accordance with direct measurements of flux density presented before (ref. [1]), fig. 7). Actually the curve bends slightly upwards in the region 3–5 amps. The spectrometer constant (s) relevant to the region of the energy loss records is therefore certainly larger than 2400 gauss·cm/amps, but the actual figure is not known. Records with the Hall generator (cf. above) show the curvature clearly. Energy loss studies of absorbers supposed to be known

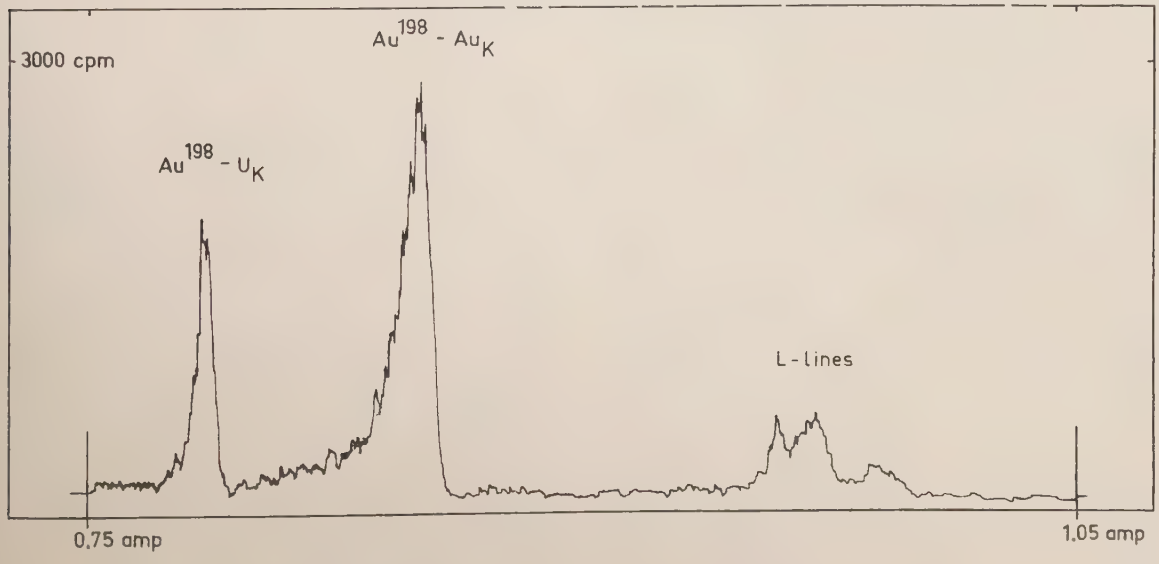

Fig. 12. External conversion electron spectrum of Au^{198} gamma radiation. Two converters, one 4 mg/cm² U foil and one 7.5 mg/cm² Au foil, were used covering one half of entrance slit (placed above one another). Accordingly two peaks are got on the XY-record, the difference being the difference in K-binding energies of U and Au (34.37 keV). This method might be used to give absolute calibrations of energy loss data in this region.

TABLE 2

Formation of $\Delta E/\Delta B\rho$ from Gerholm's tables [16]) to simulate energy loss at about 2.8 MeV.

$B\rho$ (gauss cm)	E_{keV}	ΔE	$\Delta E^{\dagger}/\Delta B\rho$	$f^{\dagger\dagger}$
11 000	2826.10	0.0		
10 900	2796.48	29.62	0.2962	1.0000
10 400	2648.46	177.64	0.2961	1.0001
10 000	2530.19	295.91	0.2959	1.0010
9 600	2412.04	414.06	0.2958	1.0015
9 200	2294.05	532.05	0.2956	1.0021
8 800	2176.23	649.87	0.2954	1.0027

† Applies to the interval.

†† f is $(\Delta E/\Delta B\rho)_0/\Delta E/\Delta B\rho$ or initial quotient for first interval divided by the same property for the larger intervals. ΔE is counted from 2826.10 keV which is regarded as initial energy of an imagined loss experiment.

theoretically show s to be about 2640 gauss·cm/amp.[10]). This is not inconsistent with Hall data and direct measurements of flux density before introduction of the spectrometer tube but casts doubt on the Na^{24} 2.5 MeV calibration point. (This inconsistence will be studied with other beta- and gamma emitters in this region.) On the other hand it is not settled whether the theory should include energy loss due to bremsstrahlung or not in this narrow geometry[10]).

In the case of Au^{198}, two converter foils were used each one covering half of the entrance slit. Two K-conversion lines were therefore obtained —separated by the difference in the K-electron binding energies of U and Au (example: see fig. 12). Originally it was hoped that this method could be applied for absolute energy difference calibrations in the region 2.8 MeV but the intensity did not permit this.

At lower energies, it should be quite feasible, as judged from fig. 12, since a lot of converter elements are available.

The use of the momentum as representative for the electron energy requires a close linearity to hold, unless corrections are to be made. Accordingly we have to study changes of momenta $\Delta B\rho$ versus corresponding energy changes ΔE for an interval that is equal to the range covered by the energy loss records. Thanks to Gerholms' tables[16]) it is easy to demonstrate that this relation is close to linear for simulated energy loss up to 20% even at lower energies (1 MeV). The region below 2.8 MeV is of largest interest in the present study. Already the interpolation factors of Gerholm show that $\Delta E/\Delta B\rho$ changes very little. This can be shown from the relation between these properties. Nevertheless we shall

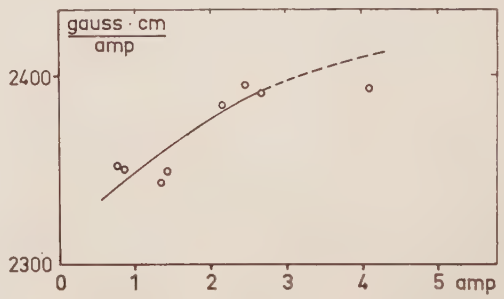

Fig. 13. Apparent spectrometer constant $S = B\rho - 200/I$ as a function of current. The upward trend is evident.

present, for entirety, in table 2 some numerical data illustrating that the deviation from linearity is less than 0.3% in the range 2.83 MeV down to 2.18 MeV. Most energy loss data to be used are lower than 300 keV and are relative measurements and so the correction might be wholly neglected.

5. Evaluation of Energy Loss Properties

5.1. PROCEDURES

The XY-record is obtained on an ordinary 21 × 26 cm paper (A 4 size) and various energy loss properties are to be evaluated from it. In order to preserve the original record, all work is made on copies. These are made with a rapid copying method ("Helioprint"). Special measurements have shown that no appreciable

distortion takes place in the copying. The absolute scale can move 0.1% but this is negligible in comparison with the reproducibility and moreover only relative data are taken.

The record of which figs. 3 and 14 are examples contains most of the information needed. A record of the primary line as well as of two or even three energy loss spectra are obtained on the same sheet of paper (cf. fig. 14). One of the latter corresponds to an aluminium or beryllium absorber serving as a standard. The mean excitation potential and other energy loss properties of these materials are well known from proton work and there is little hope that electron work can be made with better precision than this. Most of the work therefore consists of relative measurements with respect to these standards. The following properties are evaluated:

The most probable energy loss corresponds to the peak of the energy loss spectrum. It is found by taking the distance on the record from the peak of the primary line to that of the energy loss peak. The peak is found by taking mean values of successive chords of the peaked curves and joining these points to a new curve which intersects the spectrum.

The method has been used for the same purpose by MacDonell (ref. 18 of[1])) and is illustrated in fig. 14. As MacDonell points out, the whole upper part of the peak is used for the determination and not only the top points. Random variations or real intensity variations of the records are to some extent eliminated by this method. The same procedure is repeated for all runs. The half-widths of the energy loss distribution curves are directly noted and are corrected for instrumental transmission properties. The reproducibility expected for the most

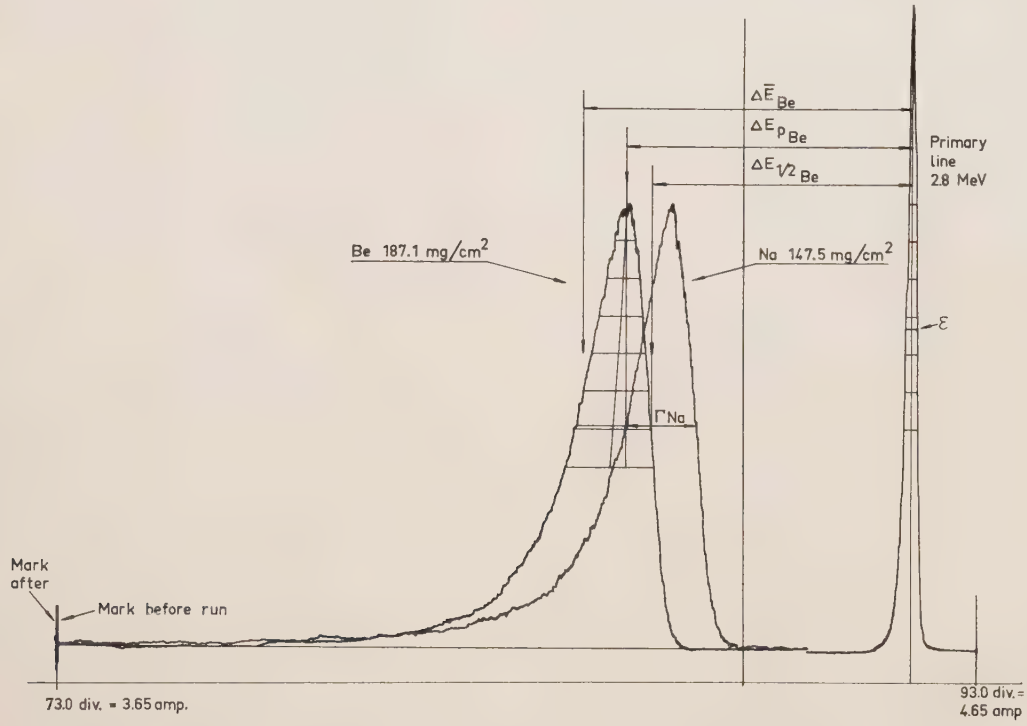

Fig. 14. Energy loss spectrum of Na and Be as well as primary line. Method of finding maximum of energy loss spectrum is shown. The arrow shows the position of the center of gravity used for evaluation of average energy loss. Record is one of the best achieved. It is seen that the part between primary peak and energy loss spectrum does not show any background. The intensity scale is different for the different curves and has been adjusted to use the chart efficiently. Without further sensitivity data, intensity conditions should not be judged from the diagram. Fig. 14 shows many improvements in relation to fig. 3.

probable energy loss measurement might be discussed in the same manner as any spectroscopic line in physics even if the Landau distribution is asymmetrical. It seems to be generally agreed that the peak position in general can be localized to better than 10% of the half-width as a conservative judgement. 1% is only claimed when very high precision is obtained and is often regarded as too exaggerated. Most beta-spectroscopists seem to agree upon 5% as a realistic figure. This figure was therefore compared with the experimental experience gained here. To this end, many copies of the same energy loss run were made and the evaluation made independently but with the same method for each copy. The relative stopping powers were then calculated as follows:

$$S_p = \left(\frac{\Delta E_p}{\Delta m_s}\right)_{subst} \Big/ \left(\frac{\Delta E_p}{\Delta m_s}\right)_{stand}. \qquad (1)$$

The standard deviation of S_p turned out to be 0.2–0.4% which is less than that from different runs. Thus neither the copying nor the personal peak evaluation work (which to some small extent includes a subjective judgement) introduces any decisive error. The half-width divided by the most probable energy loss ranges from 20 to 30% for the cases studied. The estimated reproducibility would then be 1–1.5% or, for the ratio, $\sqrt{2}$ times more, i.e. 1.4–2.1% for S_p. The results found are of the same order as the expected ones.

The half-width is obtained directly (after a small correction) and is related to the most probable energy loss or the average energy loss (see below). It can also be multiplied by the spectrometer constant to yield the half-width directly in keV.

The average energy loss is found by finding the center of gravity of the energy loss distribution. First, however, the ordinate has to be corrected for the change in the width of the momentum band. The numerical procedure thus involves the division of the energy loss distribution into 40–50 areas of constant widths and the mean ordinates found for each area. The ordinates are divided by the mean abscissa to fulfill the correction mentioned. For this purpose it seems justified to assume the calibration curve (cf. fig. 11) to be linear. The average energy loss in relative units is then found by the conventional procedure of dividing the sum of all products of ordinate times energy loss (related to the center of gravity of the primary line) by the sum of the corrected intensity ordinates. The average energy loss found without the correction is only 0.3% smaller than that found with the correction. This is certainly caused by the relatively small losses used and at the same time shows that an intensity drift of the corresponding magnitude (8% from one end of the energy loss spectrum to the other) would not introduce large errors. As for the most probable energy loss, a relative stopping power is found based on these average energy losses:

$$\bar{S} = \frac{\Delta \bar{E}_{subst}}{m_{s\,subst}} \cdot \frac{m_{s\,stand}}{\Delta \bar{E}_{stand}}. \qquad (2)$$

The evaluation of the average energy loss has the merit of using the whole energy loss curve and therefore the reproducibility might be expected to be better than for the most probable energy loss. On the other hand the large energy losses play an important part in the averaging as pointed out by Paul and Reich (ref. 13 of [1]) and others. We have been able to detect intensities as small as 0.5% (or somewhat lower) of the peak intensity but smaller intensities will escape the evaluation. It was found by treating the experimental records that the tail intensity decreases approximately exponentially on the low-energy side and thus it proved possible to perform a numerical integration to correct for tail intensities escaping detection[10]).

If absolute measurements are attempted, the data found in relative units (mms on a ruler) are transformed to current units by means of the markers for the end points of the record (illustrated in fig. 14).

Comments

Some further methodological points have to be discussed:

The response of the ionization chamber

detector is somewhat dependent on the electron energy. The specific ionization in various gases has been measured by Barber[7]) for the energy region of interest. As our chamber is filled with SF_6, we might best compare with neon. It is found from Barber's data and Nelms' tables (1, ref. [29])) that the response is 1.2% lower at 2.6 MeV as compared with 2.8 MeV. This should only affect the average energy evaluation. The effect is, however, so small (less than 0.1%), as found after numerical introduction of the correction, that it can be simply neglected. (It should be pointed out that scattering in the windows and gas and on parts of the ionization chamber, in particular the bottom plate, complicates an accurate correction procedure.) The arguments are further supported by considering the fact that relative stopping power measurements are made.

A change in the spectrometer transmission curve in the energy range should exist (cf. fig. 21 of [2])) but it should be very small and need not be considered.

The background, which is mainly due to X-rays, is very low. The trace between the high energy end of the energy loss spectrum and the primary line is wholly horizontal and corresponds to the mechanical zero point of the Y-axis. The trace rests on this level if the Y-sensitivity is increased by a factor of ten. This is a very favourable circumstance since it means that the intensity at the low energy side can be measured down to small figures compared with the peak intensity, a thing which is of fundamental importance for average energy loss measurements.

Thanks apparently to the exit aperture slit, no "ghost" lines have been detected. Such ghost lines have troubled Ziegler (ref. 15 of [1]) and Hudson (ref. 12 of [1])) and reduce the precision of the average energy loss.

Rejection of a record obtained of course takes place when failure occurs during the run. This also is done if the intensity record shows a large drift or larger intensity variations than $\pm$ 5% for the time covered by the energy loss spectrum. [This figure was also used by Goldwasser, Mills and Hansson (ref. 14 of [1])), see Warner and Rohrlich[12]).] If the XY-record itself shows signs of irregularity, even if the intensity record is good, records are of course rejected (and the instrument has to be repaired). If the marker pulses before and after the run differ by more than what corresponds to $\Delta B\rho/B\rho = 0.5‰$, some drift has occurred and causes rejection.

The number of records rejected was less than 30% after the platinizing of the inside of the doughnut (see above).

Theoretical interpretation

There is a well-developed theory for the energy loss properties and comparisons are possible. The experimental figures have to be corrected for the envelopes and cell windows, multiple scattering[1]) and radiation losses. No account of the details will be given here but the first results obtained are given elsewhere[10]).

6. Discussion

Some methodological comparisons with earlier works shall be given here.

The present method, involving the 5 MeV-betatron, double-focusing spectrometer and recording device which have all been studied in detail, provides energy loss records for elements and chemical compounds of low atomic number. The most probable energy loss is about 7% of the primary energy. The half-width of the primary line is about 0.3% or less and the half-width of the energy loss curve a factor 5–9 larger than this. No X-ray background is seen and no ghost lines.

Paul and Reich's work ([1]) ref. 13) introduced a new era of accurate electron energy loss measurements. The width of the primary line is

[6]) Brochure from the Siemens-Halske Company on Hall generators.

[7]) W. C. Barber, Phys. Rev. **97** (1955) 1071.

[8]) H. Frank, Z. f. Naturforschung **12** a (1957) 750.

[9]) T. Westermark, Arkiv f. Fysik **13** (1958) 294; *ibid.* **16** (1960) 525–26, (Short notes).

[10]) T. Westermark, Some measurements of energy loss of 2.8 MeV electrons in light elements and chemical compounds Arkiv Kemi, **17** (1960) 101.

[11]) Hütte, Des Ingenieurs Taschenbuch I (Berlin 1955) p. 942.

[12]) C. Warner and F. Rohrlich, Phys. Rev. **93** (1954) 406.

perhaps the weakest point, 1.8–3.1 %, and so corrections had to be made[13]). The reason for the large width is apparently the thick windows and energy spread of the betatron. The properties of the beam have apparently been improved later on as judged from a paper by Franck on scattering[8]).

The instrumentation of the Illinois group (ref. 14 a, b and c of [1])) seems to be very good. Our final results can be claimed to be of about comparable accuracy. Typical data are: most probable energy loss 6–7 % of primary energy, ratio of half-width of energy loss spectrum to that of primary line 6.5, intensity stability $\pm$ 5 %. A warm-up period of about one hour is needed by them to get stable energy whereas none is required in our case. The angular spread 2° is larger than our case (0.93°).

The conditions of Hudson's work are very good with regard to width of primary line (1.3‰) but are disturbed by ghost lines.

Ziegler's conditions are 2–3 % energy loss, ratio of half-width of energy loss curve to primary half-width less than two. Disturbances due to ghost lines were found.

Future improvements should be possible in our instrumentation. The intensity variations might be improved. They might perhaps be largely eliminated by mechanically moving the flux density step-wise and by plotting intensity data both for betatron output and for spectrometer output with some sacrifice in speed. The introduction of quadrupole lenses would increase the intensity and permit somewhat thicker absorbers to be used. The correction for multiple scattering would then be increased but would not affect the final precision too much. Care must however be taken so that the width of the primary line does not thereby increase.

Acknowledgements

The author is greatly indebted to Mr. B. Sjöstrand who has not only operated the accelerator and its auxiliary equipment but also introduced many technical improvements. Thanks are due to Prof. K. Siegbahn for the suggestion of the Hall generator for recording flux density and to Drs. E. Smårs and O. Wernholm for much advice on the accelerator details. The author is further indebted to Mr. P. Pedersen for his assistance with electronic maintenance and measurements.

[13]) W. Schultz, Z. f. Physik **129** (1951) 530.

[14]) A. M. Hudson, Phys. Rev. **105** (1957) 1.

[15]) B. Ziegler, Z. f. Physik **151** (1958) 556.

[16]) T. R. Gerholm, in Beta- and Gamma-Spectroscopy, Ed. K. Siegbahn, (North-Holland Publ. Company, Amsterdam, 1955) p. 926.

[17]) A. C. G. Mitchell, *ibid.* p. 224 ff.

[18]) R. D. Evans, Compton effect in Handbuch der Physik Bd. **34** (Springer-Verlag, Berlin, 1958) p. 218ff.

NUCLEAR INSTRUMENTS AND METHODS **10** (1961) 185–188; NORTH-HOLLAND PUBLISHING CO.

EINFLUSS DER QUELLENDICKE AUF DIE GEMESSENE FORM EINES BETA-SPEKTRUMS

D. FEHRENTZ und H. DANIEL

Max-Planck-Institut für Kernphysik, Heidelberg

Eingegangen am 13. Dezember 1960

The effect of the source thickness on the measured shape of the P^{32} beta spectrum has been investigated with a double-lens beta-ray spectrometer. Two methods were used: the source was covered with aluminium films of various thickness, or sources of various thickness were prepared by evaporation in vacuo. The thickness of the aluminium films was varied between 0.27 and 10 mg/cm² while the thickness of the evaporated sources was varied between 0.01 and 10 mg/cm². For the shape factor determination the maximum energy determined with the source under investigation was taken. It was found that a source thickness of 1 mg/cm² changed the shape factor by about two per cent per mc^2. The coefficient for the energy dependence of the undistorted shape factor was found to be $a = (-4.2 \pm 1.0) \times 10^{-2}/mc^2$; the quoted error is three times the standard deviation. The results are discussed.

1. Ziel der Untersuchung und Messmethode

Bei der Messung kontinuierlicher Beta-Spektren mit einem Magnetspektrometer entstehen leicht Fehler durch die Benützung zu dicker Quellen. In älteren Untersuchungen[1]) über den Einfluss der Quellendicke wurden recht dicke Quellen benutzt, oder es fanden hauptsächlich die starken Verfälschungen am energiearmen Ende des Spektrums Beachtung. Die Deutungen der beobachteten Formänderungen zogen hauptsächlich Energieverlust und Rückstreuung in Betracht. Zweck der vorliegenden Arbeit war es, den Einfluss der Quellendicke genauer zu untersuchen und dabei auch kleine Aenderungen zu erfassen.

Gemessen wurde mit einem Doppellinsen- Spektrometer[2]) an P^{32}. P^{32} hat 14.2 d Halbwertzeit. Das Beta-Spektrum besitzt eine Grenzenergie von 1705 keV und weist eine nahezu erlaubte Form auf. Zwei verschiedene Methoden fanden Verwendung: Entweder wurden auf ein- und dieselbe Quelle nacheinander Aluminiumfolien aufgelegt (Methode I), oder es wurden Quellen verschiedener Dicke durch Aufdampen von Natriumphosphat hergestellt (Methode II). Methode II ist wirklichkeitsnäher, aber die Intensitätseichung geht verloren, die bei Methode I erhalten bleibt. Außerdem besitzt Methode I messtechnische Vorteile. Die Stärke der Aluminiumauflagen bei Methode I

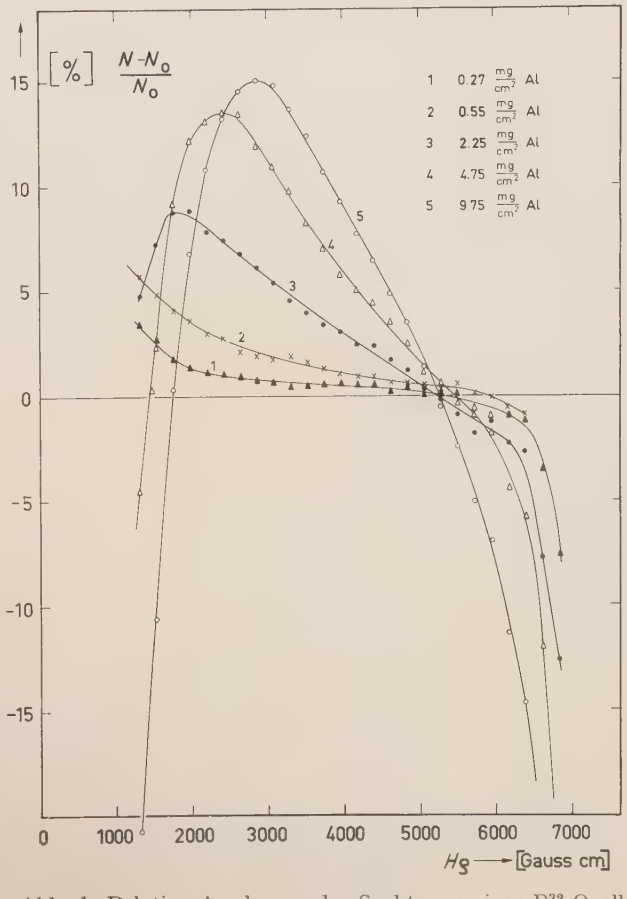

Abb. 1. Relative Aenderung des Spektrums einer P^{32}-Quelle durch Auflegen von Folien.

[1]) K. Siegbahn (Herausgeber), Beta- and Gamma-Ray Spectroscopy (North-Holland Publishing Company, Amsterdam, 1955), Kap. VIII (II) und XI, und dort zitierte Literatur.

[2]) H. Daniel und W. Bothe, Z. Naturforschg. **9a** (1954) 402; H. Daniel, Z. Naturforschg. **12a** (1957) 194.

betrug 0; 0.27; 0.55; 0.82; 1.09; 1.67; 2.25; 4.75 und 9.75 mg/cm², die Stärke der aufgedampften Quellen bei Methode II etwa 0.01; 0.6; 3 und 10 mg/cm². Die Quellenunterlage bestand aus rückseitig mit Gold bedampftem Glimmer von 0.2 mg/cm² (Methode I) oder aus Aluminiumfolie von 0.27 mg/cm² (Methode II). Die Messungen wurden wie früher beschrieben[3]) ausgeführt.

[3]) H. Daniel und U. Schmidt-Rohr, Nuclear Physics 7 (1958) 516.

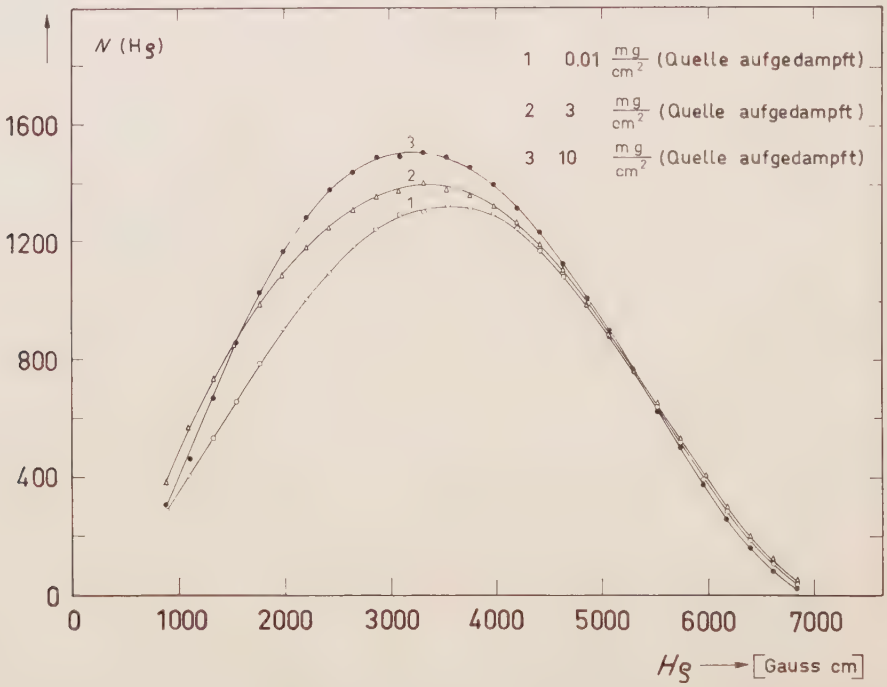

Abb. 2. Spektren von drei verschieden dicken aufgedampften P^{32}-Quellen, normiert bei 5300 Gauss-cm.

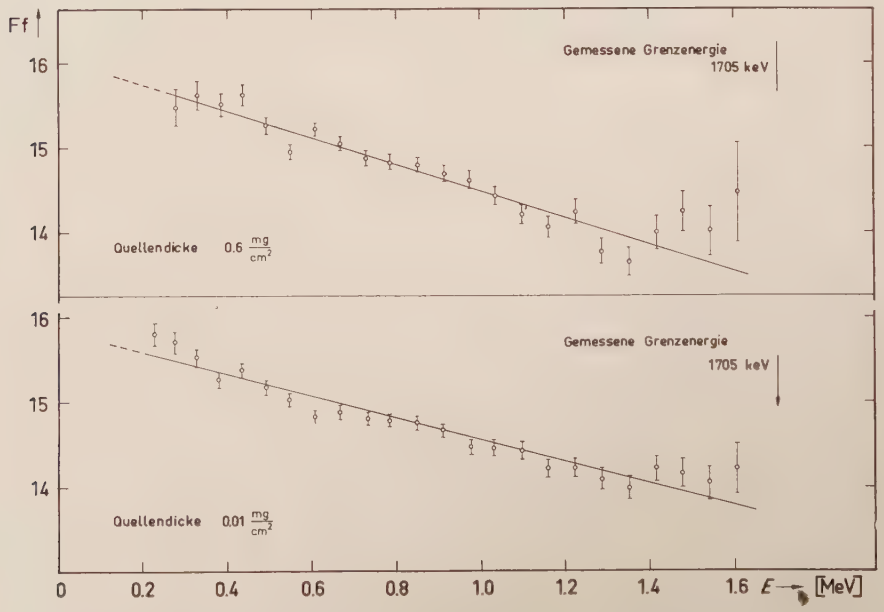

Abb. 3. Gemessener Formfaktor für aufgedampfte P^{32}-Quellen von 0.01 und 0.6 mg/cm².

2. Messergebnisse und Diskussion

Abb. 1 zeigt die relative Aenderung $(N - N_0)/N_0$ der gemessenen Intensität bei verschiedener Dicke der aufgelegten Folien (Methode I); N ist dabei die Intensität mit aufgelegter Folie, N_0 die Intensität ohne Folie. Abb. 2 zeigt die Impulsspektren von aufgedampften Quellen verschiedener Dicke (Methode II).

Abb. 3, 4 und 5 zeigen den Formfaktor[3]) für die aufgedampften Quellen. Als Grenzenergie wurde

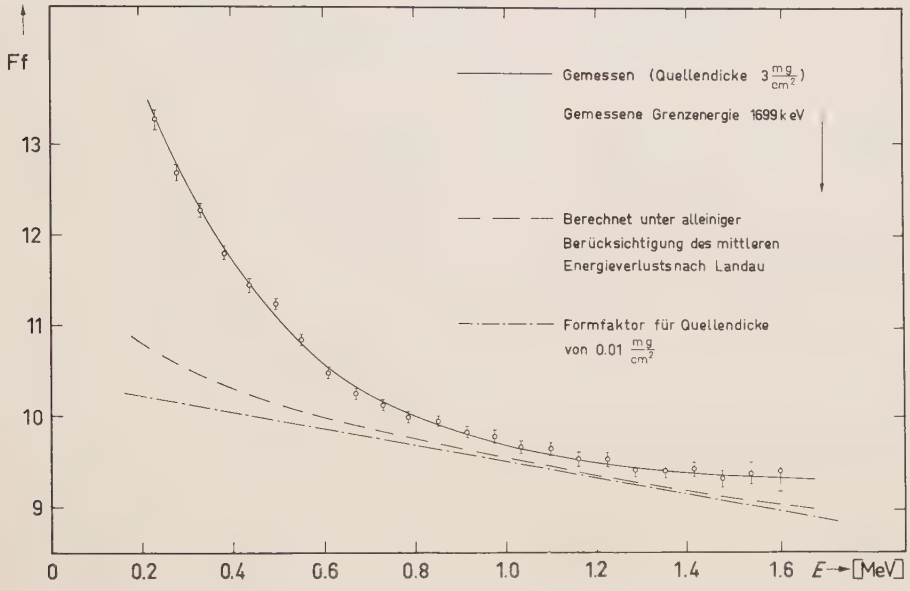

Abb. 4. Gemessener Formfaktor für die aufgedampfte P^{32}-Quelle von 3 mg/cm². Zum Vergleich sind der gemessene Formfaktor für die Quelle von 0.01 mg/cm² und der daraus unter alleiniger Berücksichtigung des mittleren Energieverlusts nach Landau konstruierte Formfaktor miteingezeichnet.

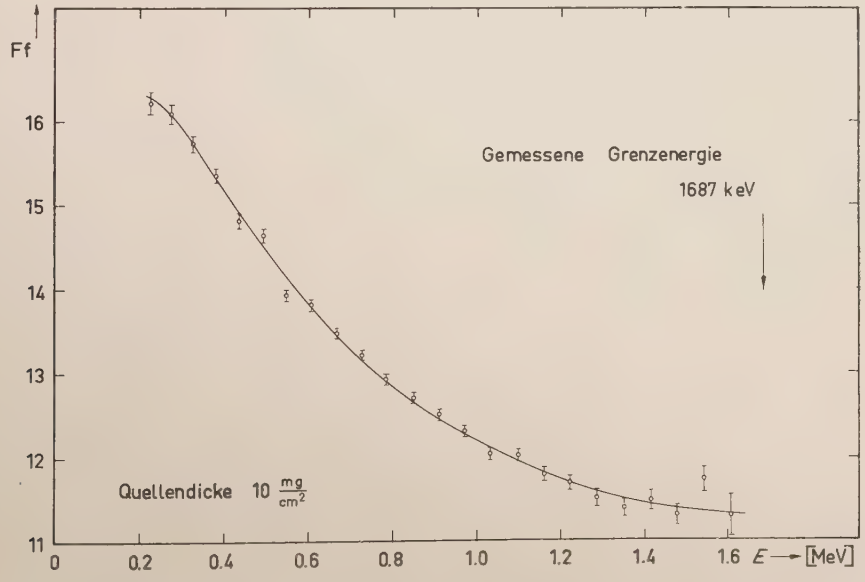

Abb. 5. Gemessener Formfaktor für die aufgedampfte P^{32}-Quelle von 10 mg/cm².

dabei stets der Wert genommen, der mit der untersuchten Quelle gemessen worden war, z.B. 1687 keV im Fall der Quelle von 10 mg/cm². Der Formfaktor ist im wesentlichen das Verhältnis von gemessener Intensität zu theoretischer für erlaubte Spektralform, ist also konstant für ein Spektrum erlaubter Form.

Die Messungen zeigten, daß die bei Quellen endlicher Dicke durch Fermi-Analyse des energiereichen Endes des Spektrums[3]) ermittelte Grenzenergie um den mittleren Energieverlust nach Landau[4]) gegenüber der wahren Grenzenergie des P^{32} verringert ist; hierbei ist berücksichtigt, daß die Elektronen die Schicht schräg durchsetzen. Des weiteren zeigte sich, daß die über das Spektrum integrierte Intensität mit wachsender Dicke der aufgelegten Folien (Methode I) zunächst zunimmt und zwischen 5 und 10 mg/cm² praktisch konstant 7% über dem Wert ohne Folie liegt. Dasselbe Verhalten erkennt man auch an den Kurven Abb. 1. Der auf den ersten Blick paradoxe Effekt lässt sich durch Richtungsstreuung erklären. Wegen der größeren effektiven Schichtdicke für Elektronen, die mit größerem Winkel gegen die Spektrometerachse in der Quelle ausgesandt werden, werden mehr Elektronen in den Oeffnungskonus des Spektrometers hineingestreut als hinaus.

Insgesamt wirkt sich der Einfluß der Quellendicke auf das Energiespektrum der austretenden Elektronen so aus: Die Verschiebung durch den Energieverlust führt zu einer Verringerung der Intensität bei größeren Energien (rechts vom Intensitätsmaximum) und zu einer Erhöhung bei kleineren. Die reine Richtungsstreuung führt bei den in Frage kommenden Oeffnungswinkeln stets zu einer Intensitätserhöhung. Dieser Effekt wächst stark mit abnehmender Energie; als wichtiger Parameter geht die Ordnungszahl des Quellenmaterials ein. Bei sehr kleinen Energien und großen Foliendicken führt die Absorption schließlich wieder zu einer Intensitätsverminderung. Wie früher[3]) gezeigt, spielt die Rückstreuung bei den verwendeten Präparat- und Unterlagendicken keine wesentliche Rolle. In Abb. 4 sind zum Vergleich der Formfaktor bei vernachlässigbarer Quellendicke und der daraus unter alleiniger Berücksichtigung des mittleren Energieverlusts konstruierte Formfaktor miteingezeichnet.

Mit der dünnsten Quelle wurden ferner die Grenzenergie zu 1705 ± 4 keV und die Konstante für die Abweichung des Formfaktors vom Formfaktor eines erlaubten Spektrums zu $a = (-4.2 \pm 1.0) \times 10^{-2}/mc^2$ gemessen (dreifacher mittlerer Fehler). Abweichungen von der erlaubten Form im gleichen Sinne, aber teilweise von etwas anderer Größe oder Energieabhängigkeit oder ohne nähere Angaben sind auch von anderen Autoren mitgeteilt worden[5]). Energieproportionale Abweichungen lassen sich quantitativ durch Interferenz zwischen erlaubten und zweifach verbotenen Termen erklären[6]).

Herrn Prof. Gentner danken wir herzlich für sein förderndes Interesse, Herrn Dr. Mayer-Kuckuk für manche Unterstützung.

[4]) K. Siegbahn (Herausgeber), Beta- and Gamma-Ray Spectroscopy (North-Holland Publishing Company, Amsterdam, 1955), Kap. I, und dort zitierte Literatur.

[5]) F. T. Porter, F. Wagner jr und M. S. Freedman, Phys. Rev. **107** (1957) 135;
H. Daniel, Nuclear Physics **8** (1958) 191;
R. L. Graham, J. S. Geiger und T. A. Eastwood, Can. J. Phys. **36** (1958) 1084;
O. E. Johnson, R. G. Johnson und L. M. Langer, Phys. Rev. **112** (1958) 2004.

[6]) G. B. Henton und B. C. Carlson, ISC-1006 (1957);
I. Iben, Phys. Rev. **109**, (1958) 2059.

NUCLEAR INSTRUMENTS AND METHODS **10** (1961) 189–192; NORTH-HOLLAND PUBLISHING CO.

A FAST SCALER FOR PULSED ACCELERATORS

F. LACOSTE and J. LEISS†

Laboratoire des Hautes Energies, Ecole Normale Supérieure, Orsay, France

Received 12 December 1960

A fast scaler using the well known principle of adding standardized pulses with a diode integrating circuit has been built and tested for experiments conducted with a pulsed linear accelerator.

With this scaler, it has been possible to count an average of one event per machine pulse of duration 10^{-6} sec, with a counting loss smaller than 1 %.

The resolution time of the scaler is approximately 10^{-8} sec.

1. Introduction

The low duty cycle of pulsed accelerators and especially of linear accelerators leads to the need of very fast electronics if one wishes to benefit from the high counting rates which are often possible.

This article describes a fast scaler which has been developed for electron scattering experiments conducted with the electron linear accelerator now in operation in this Laboratory. This accelerator gives 50 pulses per second, each pulse lasting approximately 10^{-6} sec.

The basic idea of the fast scaler is old and simple: it consists in adding the output pulses from a fast discriminator with a diode integrating circuit, using the long dead time between consecutive beam pulses to record the out-put of the integrating circuit with a slow multichannel pulse-height analyzer.

Scattered electrons, the energy of which has been selected by a magnetic spectrometer, are counted by a lucite Čerenkov counter surrounded by lead shielding 20 cm thick. At forward scattering angles, electron scattering cross-sections are often so large that it would be possible to record several hundred counts per second if the circuits could handle sufficiently large counting rates during the short operating time of the machine.

2. Description of the scaler

In fig. 1 is shown the block diagram of the scaler:

Positive pulses are taken from the last dynode of a 14 stages 56 AVP photomultiplier. With a 10 cm long lucite Čerenkov counter, we obtain, on a 110 ohms load, pulses as large as 8 volts. Their duration is less than 10^{-8} sec.

The input gate opens only during the electron pulse from the machine. This reduces the number of spurious counts due to cosmic rays. The fast discriminator separates the "real" events from the background events, which give signals at least three times smaller, for the Čerenkov counter and electron energies used here. The gating is done by the diodes D_1 and D_2 of fig. 2 and the discrimination by diode D_3 which has an adjustable bias.

The limiter standardizes the height of the pulses coming from the discriminator. This function is fulfilled here by two Hewlett Packard amplifiers (460A) in series, with their gain set near minimum. The saturated output is then approximately 3 volts. The curve giving the size of the out-put of the limiter as a function of the input before the discriminator has a transition region of about 1 volt in which the out-put rises linearly from less than 1 volt up to 3 volts. This circuit therefore can only be used if the input pulse height distribution has a small number of pulses in this transition region. This was the case in our work, but in many instances it might be more convenient to use the scaler after a fast coincidence circuit, which should have the proper pulse-height distribution.

The integrating circuit is the core of the scaler. It gives a slow output proportional to the number of standardized pulses fed into it during one machine pulse. This function is fulfilled here by the diode D_4 with its associated RC network. D_4 is a fast

† Visitor from the National Bureau of Standard, Washington, D.C.

switching silicon diode (Transitron S226G) with a forward resistance of approximately 150 ohms and a backward resistance of 6 megohms. The 470 ohms in series with D_4 and the 1 megohm resistance in the time interval between two consecutive machine pulses. The output of the integrating circuit is 0.05 volt per input pulse. Some care must therefore be taken to reduce stray pickup. For instance it was

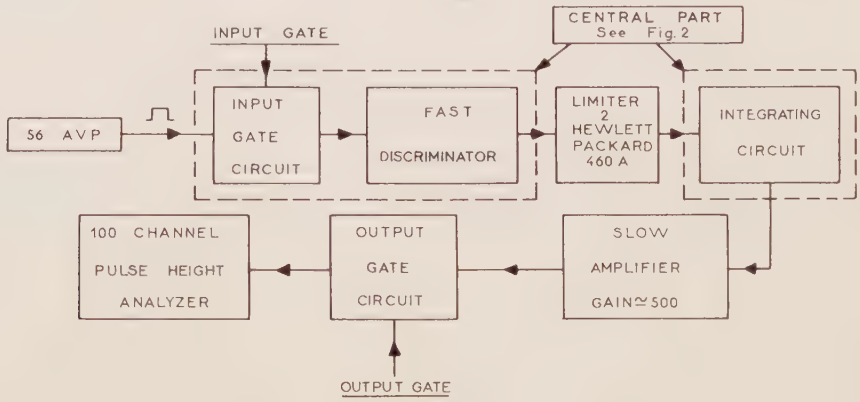

Fig. 1. Block diagram of the scaler. The circuits inside the dotted lines are given in detail in fig. 2.

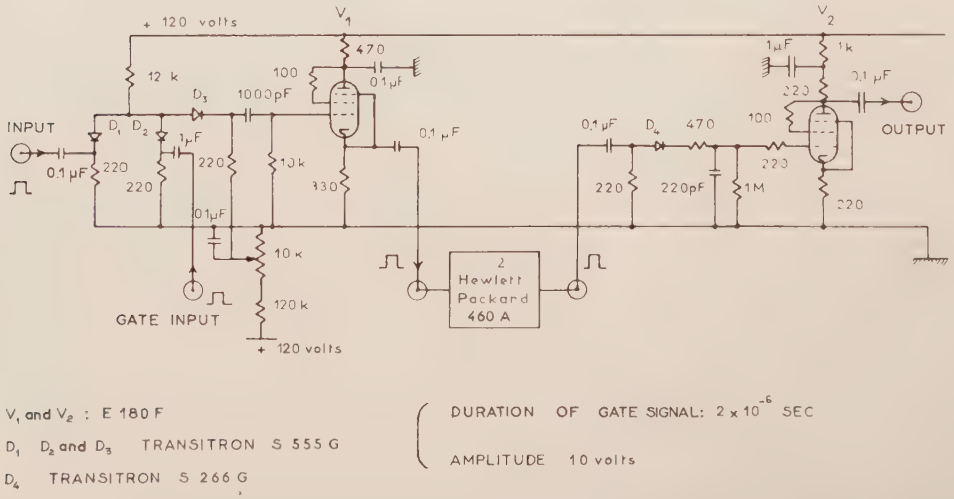

Fig. 2. Circuit diagram of the input gate, the discriminator and the integrating circuit.

parallel are used to reduce the effects of possible unstabilities in the forward or backward resistance of D_4. The charging time of the 220 pF capacitor is long compared to the duration of the standardized pulses. The decay-time-constant of the output pulses, set by the 220 pF capacitor and the 1 megohm resistor, is long compared with the duration of a machine pulse and short compared with found necessary to use a D.C. supply for the filaments of V_2.

The output gate opens only after the end of a machine pulse. This prevents the paralysis of the pulse-height analyzer before the integrating circuit has given its peak output. With some pulse-height analyzers such an output gate would probably not be necessary.

3. Performance

Fig. 3 shows a typical pulse-height spectrum obtained with a high counting rate. One can see five peaks, equally spaced, corresponding respectively

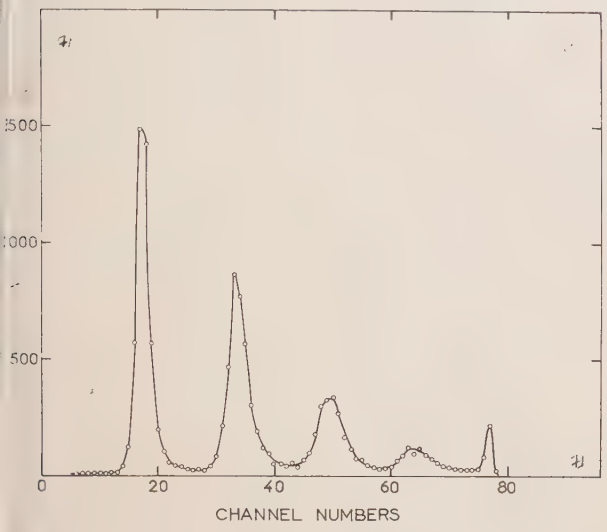

Fig. 3. Pulse-height spectrum obtained on the pulse-height analyzer with a high counting rate ($m > 4$).

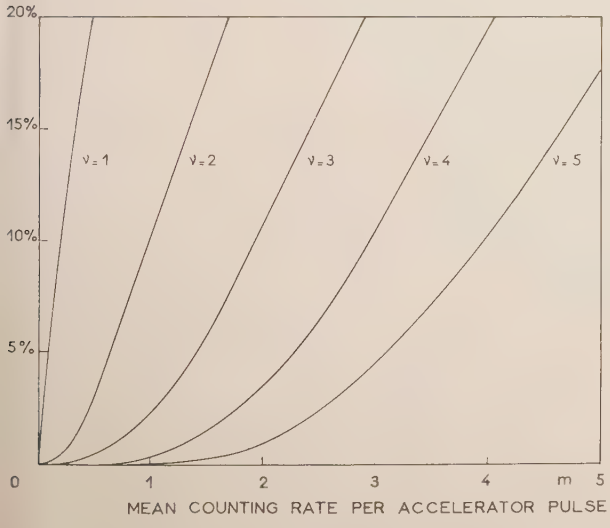

Fig. 4. Counting losses of a scaler. The number ν affixed to the curves gives the maximum number of counts which the scaler can count in one machine cycle. The curves are calculated assuming a Poisson time distribution for the events.

to 1, 2, 3, 4, and 5 Čerenkov pulses per machine pulse. Only 5 peaks are visible because of the saturation of the output gate placed before the pulse-height analyzer. Therefore, the fifth peak gives the number of machine pulses where 5 *or more* Čerenkov pulses were registered.

If we define m as the average number of events per machine pulse, it is shown in fig. 4 that, for counting rates up to $m = 2$ (i.e. 100 events per second for this accelerator), the counting losses are smaller than 1% for a scaler which can count up to 5 events per machine pulse. This is what our scaler should do, although some caution should be exercised as the curves of fig. 4 are calculated assuming a Poisson time-distribution for the events. This assumption is only true if the accelerator has the constant pulse to pulse intensity which is seldom true for many accelerators. We have therefore usually restricted the use of the scaler to counting rates smaller than $m = 0.5$.

From the spectra obtained on the pulse-height analyzer, one can deduce the five numbers $N_1, \ldots N_5$ corresponding to 1, 2 . . . , 5 or more, events per machine pulse. The "true" number of counts is then given with good accuracy by

$$N = \sum_{\alpha=1}^{5} \alpha N_\alpha .$$

Some uncertainty is introduced by the choice of the limits between each peak. The most sensible method seems to attribute the same number of channels to each peak and to place the limits in the region of low counting rate between consecutive peaks. This is the method that was used and it seems proper as it gives constant results when the counting rate is varied.

3.1. TEST WITH VARIABLE COUNTING RATES

The number N was measured for counting rates varying between $m = 0.083$ and $m = 1.5$, keeping all the other parameters in the experiment fixed. In this range, N stayed constant within the statistical accuracy of about 1%. Table 1 gives the detailed results for the eight measurements made consecutively during a period of 4 hours.

3.2. COUNTING STABILITY OBTAINED WITH THE ČERENKOV COUNTER

The sensitivity of the Čerenkov counter was measured by varying the photomultiplier voltage

TABLE 1

Experimental results of a test of the scaler with variable counting rates. N_1, N_2, ... N_5 give the number of accelerator pulses where 1, 2, ..., 5 or more, Čerenkov pulses were registered. For the mean counting rates used, the "true" number of Čerenkov pulses is given with good accuracy by $N = \sum_{\alpha=1}^{5} \alpha N_\alpha$. The mean counting rate per machine cycle is then $m = N/50t$, if t is the duration of the measurement in seconds. In the last two columns we compare the predictions based on a Poisson time distribution with the experimental ratio $N_1/50t$. The agreement is quite good because the accelerator was stable during this test.

m	N_1	N_2	N_3	N_4	N_5	$\sum_{\alpha=1}^{5} N_\alpha$	$\sum_{\alpha=1}^{5} \alpha N_\alpha$	$N_1/50t$ (%)	me^{-m} (%)
0.177	7090	814	77	8	0	7989	8981	13.9	15
0.57	4755	1443	345	66	11	6620	8995	30	32
0.188	7872	547	41	1	0	8461	9093	10.3	10.5
1.38	2109	1455	764	316	159	4724	9020	32.5	35
1.50	1917	1361	748	316	159	4501	8942	32	33.5
0.64	4479	1526	397	62	17	6481	9055	32	33
0.23	6999	940	91	5	1	8036	9177	18	18
0.083	8289	387	19	1	0	8696	9124	7.7	8

by $\pm 5\%$ and the discriminating level between 4 and 6 volts. In this range, N stayed constant within 2%. As the actual variations of the photomultiplier supply and of the discriminating level are expected to be much smaller, it is felt that the Čerenkov counter with these circuits can be used with confidence in experiments where 1% stability is required.

3.3. RESOLUTION TIME OF THE SCALER

When two events occur in close succession, the scaler will give the proper answer as long as the corresponding pulses do not overlap. The resolution time of this scaler should therefore be approximately 10^{-8} sec. This is verified experimentally as the counting losses for $m = 1$ are smaller than 1%.

4. Conclusion

The scaling circuit described in this report is somewhat inconvenient to use in its present state of development because of the need for an associated pulse-height analyzer. It does have the advantage, however, of being reliable, of being extremely easy to construct, and to possess good time resolution.

Acknowledgements

We wish to thank Professor Halban for his constant support and for accepting one of us as a visiting physicist for eight months.

The help of all the physicists in this laboratory is gratefully acknowledged. In particular, we wish to thank G. R. Bishop, D. Isabelle, D. Frèrejacque, B. Milman, J. Perez y Jorba and R. Taylor for help during the necessary tests.

NUCLEAR INSTRUMENTS AND METHODS **10** (1961) 193–201; NORTH-HOLLAND PUBLISHING CO.

DETECTION OF HIGH ENERGY γ-RAYS BY PLASTIC PHOSPHORS

L. KESZTHELYI, I. BERKES, I. DEMETER and I. FODOR

Central Research Institute of Physics, Budapest

Received 21 November 1960

Pulse height distributions of 3–20 MeV energy γ-rays in a 3 in. × 3 in. NaI(Tl) crystal and in an 8 cm diameter × 16 cm long plastic phosphor are compared with each other. It is found that for measuring high energy γ-rays in some cases plastic phosphors can be used instead of NaI(Tl) crystals.

1. Introduction

The spectrum of monochromatic γ-rays of energies above 2–3 MeV as obtained from NaI(Tl) scintillation counters usually gives a curve consisting of three peaks and an almost horizontal part[1,2,3]). The maximum energy peak corresponds to the total absorption of the γ-energy, other peaks appear if one or two annihilation γ-quanta escape from the crystal. The flat part of the spectrum is produced by Compton electrons and by such processes in which, owing partly to the escape of secondary electrons, partly to bremsstrahlung produced by the latter, the total energy of the γ-rays is not absorbed by the crystal. At higher energies (10–20 MeV) the three peaks, in general, are fused to produce a peak of 20–35% relative half-intensity width.

The triple peak and the losses due to bremsstrahlung are due to the large cross section of NaI(Tl) crystals for pair production and bremsstrahlung, which is a consequence of the high atomic number of I. These effects are small in organic scintillators (liquids, plastics) containing elements of low atomic number. In the energy range in question (3–20 MeV) chiefly the Compton effect occurs and the bremsstrahlung is negligible. Thus for organic scintillators the line shape is expected to be simpler and the rise time of pulses considerably faster, the counting efficiency, however, will be somewhat lower. In order to confirm this assumption, some experiments were carried out to compare the pulse height distributions obtained from these two types of scintillators for γ-energies in the range of 2–20 MeV.

2. Experiments

The measurements were performed with a 3 in. × 3 in. NaI(Tl) crystal mounted on a Dumont photomultiplier and with a 8 × 16 cm plastic phosphor on a Zeiss M12FS 100 photomultiplier. As γ-sources radioactive samples (Cs^{137}, Zn^{65}, ThC″) and (p, γ) nuclear reactions Li^7 (p, γ) Be^8, B^{11} (p, γ) C^{12}, F^{19} (p, $\alpha\gamma$) O^{16}, Na^{23} (p, γ) Mg^{24}, were used. The spectra were recorded by a 100 channel ferrit memory analyser. Before the counter a 12 cm long lead collimator having an aperture of 4, 2 and 1 cm in diameter, respectively could be mounted.

Some of the results of the comparative measurements are shown in figs. 1–3. Since, according to fig. 3b, collimator apertures below 4 cm do not considerably affect the amplitude distribution, all spectra from plastic phosphor were obtained with a collimator of 4 cm aperture.

As seen from the pulse height distributions of the γ-radiation in the nuclear reaction Na^{23} (p, γ) Mg^{24} shown for both counters in figs. 4a, b, respectively, the spectrum for plastic phosphor is obviously simpler.

[1]) M. I. Berger and I. Doggett, J. Res. N.B.S. **56** (1956) 355.
[2]) N. W. Koch and I. M. Wyckoff, J. Res. N.B.S. **56** (1956) 319.
[3]) I. Kockum and N. Starfelt, Nucl. Instr. **4** (1959) 171.

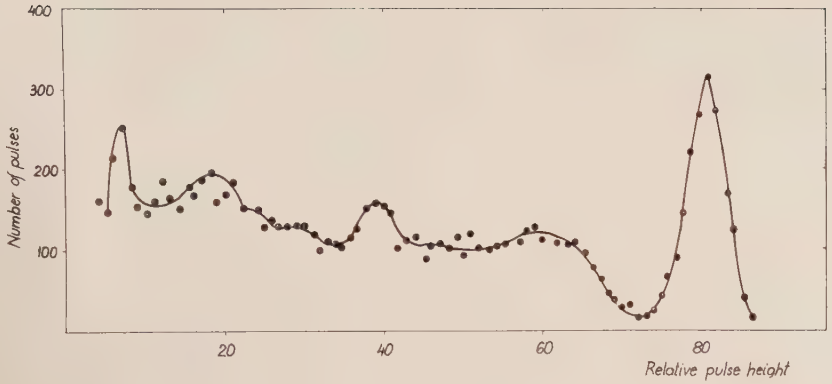

Fig. 1a.

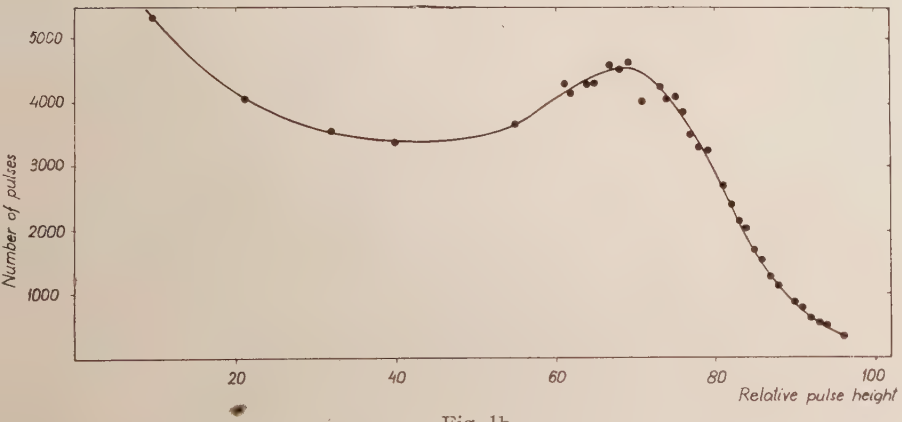

Fig. 1b.

Fig. 1. Pulse height distribution of Zn^{65} produced γ-radiation: a. in a NaI(Tl) crystal; b. in a plastic phosphor.

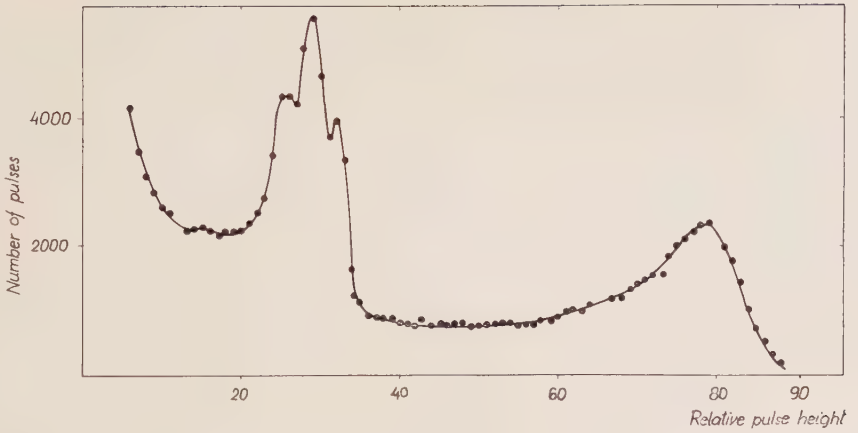

Fig. 2a.

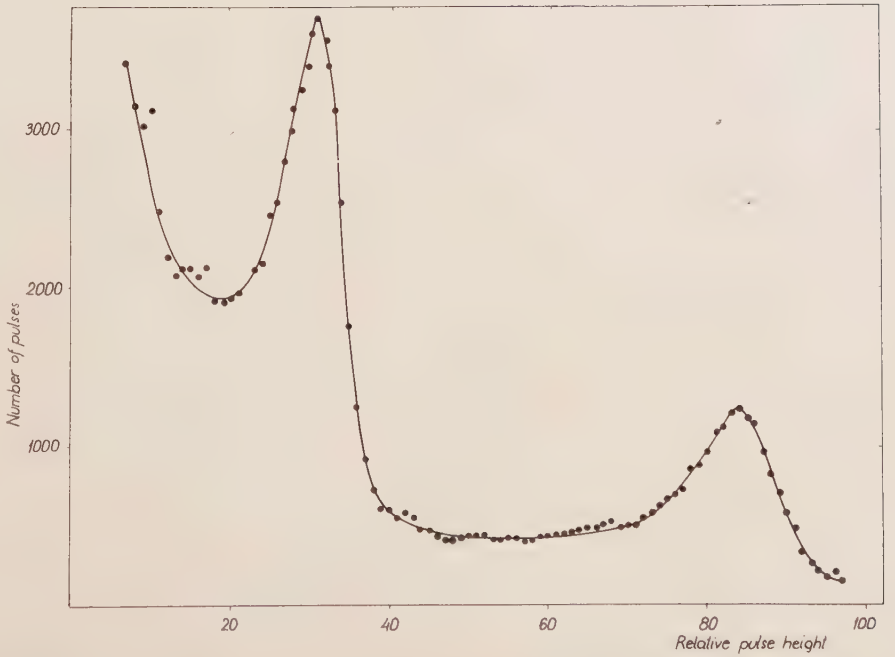

Fig. 2b.

Fig. 2. Pulse height distribution of 4.4 MeV and 11.7 MeV γ-rays produced by the $B^{11}(p,\gamma)C^{12}$ reaction: a. in a NaI(Tl) crystal; b. in a plastic phosphor.

3. Discussion

3.1. SHAPE OF THE LINE

The absorption coefficients calculated from the Compton effect and the pair production in terms of energy are shown in fig. 5. For the calculations the tabulated values in[4]) have been used. It is apparent that for plastic phosphors the absorption of γ-rays is primarily due to the Compton effect in the energy range under investigation.

[4]) K. Siegbahn, β- and γ-Ray Spectroscopy (North-Holland Publ. Comp., Amsterdam, 1955) p. 857.

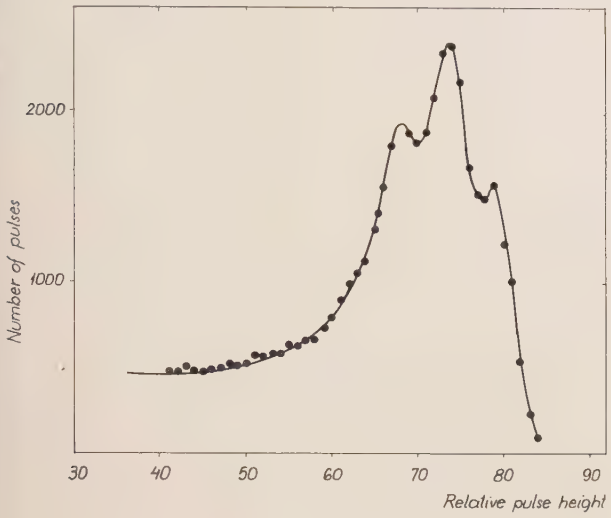

Fig. 3a.

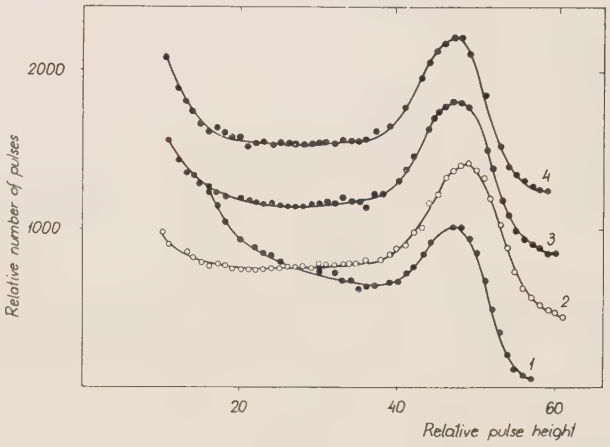

Fig. 3b.

Fig. 3. Pulse height distribution of 6.14 MeV γ-rays produced by the $F^{19}(p, \alpha, \gamma)O^{16}$ reaction:
a. in a NaI(Tl) crystal; b. in a plastic phosphor. 1. Without collimation; 2. 4 cm aperture; 3. 2 cm aperture; 4. 1 cm aperture. The distributions have been normalised at the peaks. The curves 2, 3 and 4 are shifted in the vertical direction.

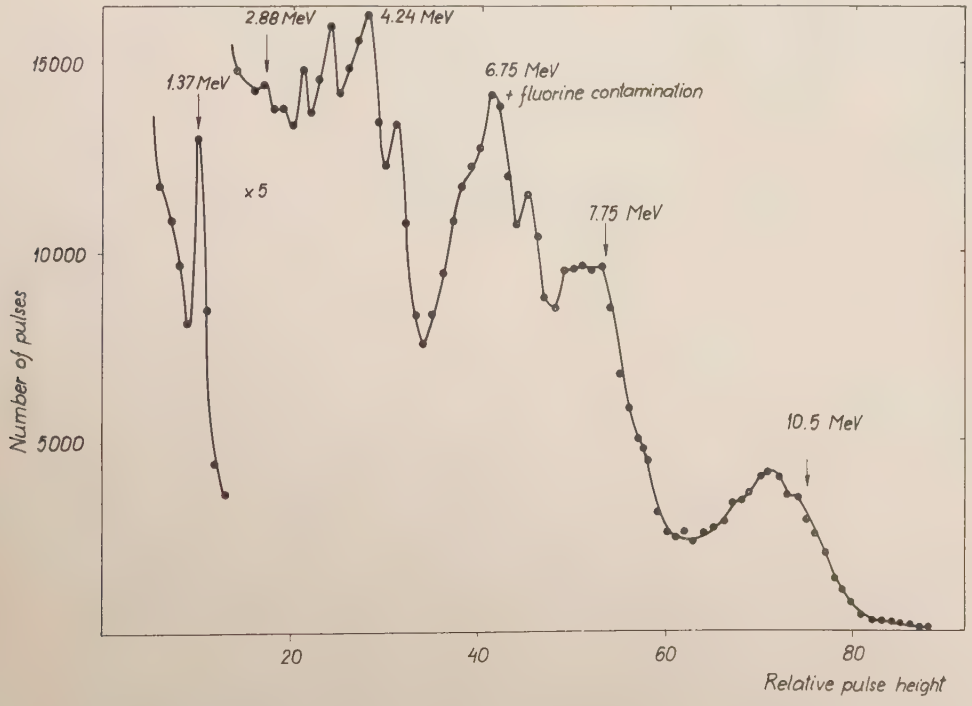

Fig. 4a. Pulse height distribution of γ-rays produced in the $Na^{23}(p,\gamma)Mg^{24}$ reaction in a NaI(Tl) crystal.

Let γ be the energy of γ-rays and E that of Compton electrons, both values given in m_0c^2 units. Then the energy distribution of Compton electrons is given by

$$\frac{\mathrm{d}\,\sigma\,(E)}{\mathrm{d}E} = \frac{2.5 \times 102^{-25}}{\gamma^2}\left[2 + E\,\frac{E\,(\gamma+1)^2 - \gamma\,(E^2+2\gamma)}{\gamma^2\,(\gamma-E)^2}\right] \tag{1}$$

where

$$0 < E < \frac{2\gamma^2}{2\gamma+1}\,.$$

The shape of the energy distributions for various γ-energies is seen in fig. 6[5]).

As known, the cross section for Compton effect increases with decreasing energy and since the energies of the scattered γ-rays are lower than their

[5]) H. W. Koch and I. M. Wyckoff, IRE Transactions NS5 (1958) 127.

[6]) D. Maeder, R. Müller and V. Wintersteiger, Helv. Phys. Acta **27** (1954) 3.

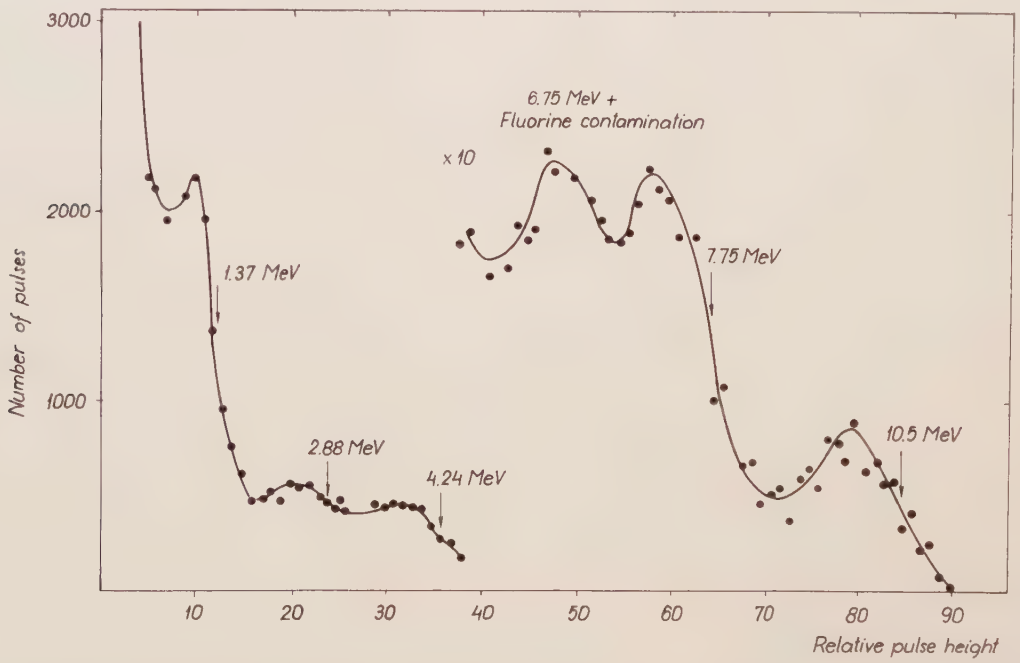

Fig. 4b. Pulse height distribution of γ-rays produced in the $Na^{23}(p,\gamma)Mg^{24}$ reaction in a plastic phosphor.

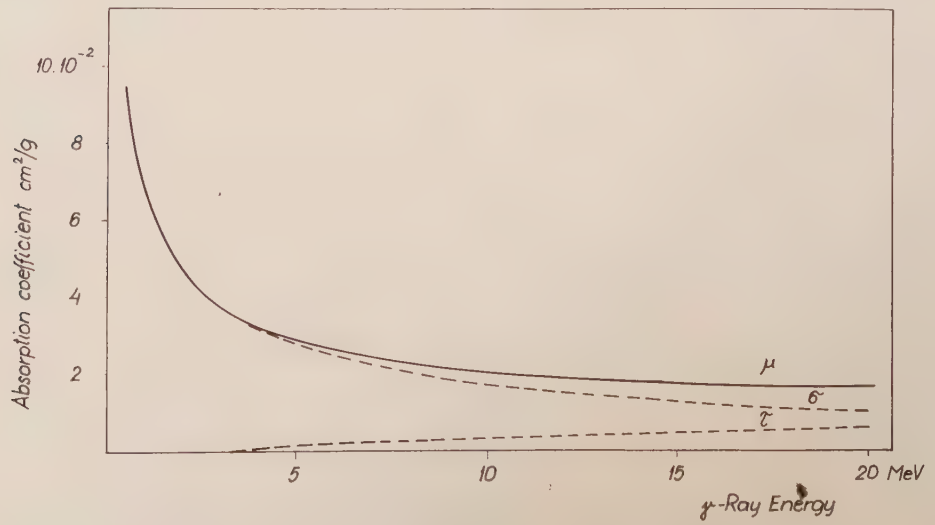

Fig. 5. Energy dependence of the absorption coefficient for a plastic phosphor.

initial energies, the probability for secondary Compton absorption also increases. By considering this effect the energy distribution – as shown by the calculations of Berger and Dogget[1]) – will be only slightly different from that given by (1) (fig. 7). The difference in spectral shapes becomes even less with increasing γ-energies. Thus the spectrum of the energies absorbed by the crystal is very similar to the Compton electron spectrum.

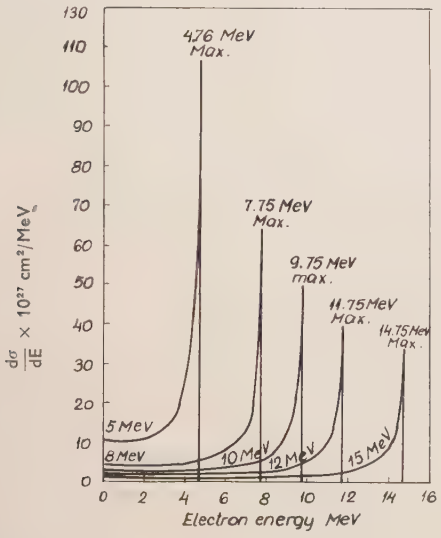

Fig. 6. Energy spectrum of Compton electrons for various γ-energies. The γ-ray energies are indicated on the curves.

This relation is well known for NaI(Tl) crystals where – at least for energies $E\gamma < 2$ MeV – the half-intensity width Γ of the photopeaks is proportional to $\sqrt{E}$ (the relative half-intensity width to $1/\sqrt{E}$). This relation, however, cannot hold at energies above 2–3 MeV, since it is based upon the assumption that the spread of pulse height occurs only in consequence of the statistical nature of pulse production in scintillation counters. At higher

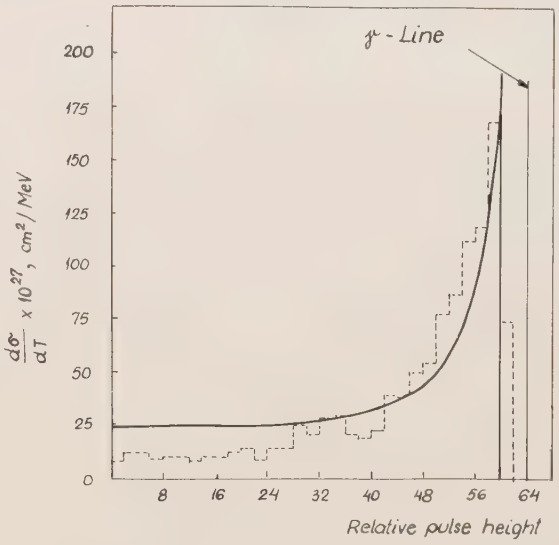

Fig. 7. Energy spectra of single Compton effect (continuous curve) and of multiple Compton effect calculated by the Monte Carlo method (histogram) for 4.5 MeV γ-energy in a 5 in. × 9 in. NaI(Tl) crystal[1]).

In the phosphor the spectrum of the electrons having energy E is given by a Gaussian distribution of the form[6])

$$\frac{\mathrm{d}n(E')}{\mathrm{d}E'} = \frac{1}{\varphi\sqrt{\pi}}\,\mathrm{e}^{-[(E-E')/\varphi(E)]^2}\,, \qquad (2)$$

where φ is the spread of the line in m_0c^2 units. The half-intensity width of the line is

$$\Gamma = 2\sqrt{\ln 2}\varphi = 1.66\,\varphi \qquad (3)$$

and therefore, instead of the Compton distribution (1) the spectrum will have the form

$$\frac{\mathrm{d}n(E')}{\mathrm{d}E'} = \frac{1}{\sqrt{\pi}}\int_{E=0}^{\frac{2\gamma^2}{2\gamma+1}} \frac{1}{\varphi(E)}\,\frac{\mathrm{d}\sigma}{\mathrm{d}E}\,\mathrm{e}^{-[(E-E')/\varphi(E)]^2}\,\mathrm{d}E\,. \qquad (4)$$

In order to determine the line shape, the value of $\varphi(E)$ and its energy dependence have to be known.

energies, however, the half-intensity width is not a useful quantity, since the peak for higher energy γ-rays is not produced by the broadening of one monoenergetic line only, but in addition by the fusion of several lines. For plastic phosphors the energy distribution of Compton electrons also contributes to the half-intensity width. Relative half-intensity widths for some γ-energies as measured both with NaI(Tl) crystals and plastic phosphors are given in table 1. The data for the two phosphors used here are seen to be approximately equal. The value of φ, however, must be different for the two phosphors in consequence of the very different light efficiency. Thus from the half-intensity width Γ the value of φ at higher energies cannot be accurately determined.

Therefore, it seems desirable to define some other

TABLE 1

γ-energy (MeV)	3 in. × 3 in. NaI(Tl) crystal			8 cm × 16 cm plastic phosphor	
	relative width (%)	relative slope (%)		relative width (%)	relative slope (%)
		with aperture 2 cm	without aperture		
0.667	9.7	3.8	3.8	—	18
1.114	8.9	3.4	3.4	—	12.8
2.62	—	2.5	2.5	—	7.6
4.46	35	2.6	3.0	31	7.5
6.14	22	2.7	3.2	25	6.7
10.5	17	—	4.6	15	5.7
11.5	17	3.75	4.7	16	5.4
17.6	—	—	5.0	—	4.9

characteristic quantity which may be measured more uniformly in the entire spectral range under investigation: We define the energy difference between the $\frac{3}{4}$ and $\frac{1}{4}$ values of the heights S on the high energy side of the peak as the reciprocal of the slope. For a monochromatic line, assuming a Gaussian distribution, we have

$$S = 0.6464\,\varphi = 0.39\,\Gamma\,. \tag{5}$$

According to the above relation S/E has to be proportional to the relative half-intensity value Γ/E, thus to $1/\sqrt{E}$. The values of $(S/E)^2$ as a function of $1/E$ are shown in fig. 8 plotted for the NaI(Tl) crystal and in fig. 9 for the plastic phosphor.

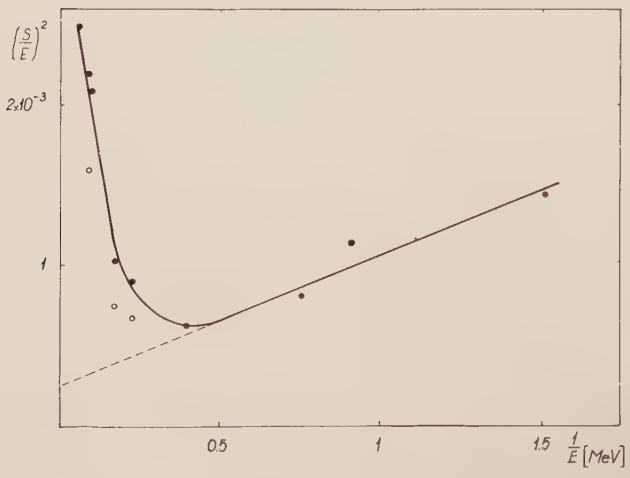

Fig. 8. Square of the relative slope as a function of the reciprocal value of energy for a NaI(Tl) crystal: ● without Pb-collimator; ○ with a 2–4 cm diameter Pb-collimator. Error in experimental points 10-15 %.

The two curves are quite different in shape. For NaI(Tl), at energies above 3 MeV, S/E rapidly increases and departs considerably from the straight line representing the law $1/\sqrt{E}$ which, as seen in fig. 8, proves to be correct for energies below 3 MeV. For plastic phosphor the relation is nearly linear and only a slight deviation can be observed at the high energy end. The rather marked deviation for NaI(Tl) may be due to several effects such as the escape of bremsstrahlung, fusion of pair peaks and escape of secondary electrons. High energy secondary electrons may produce bremsstrahlung

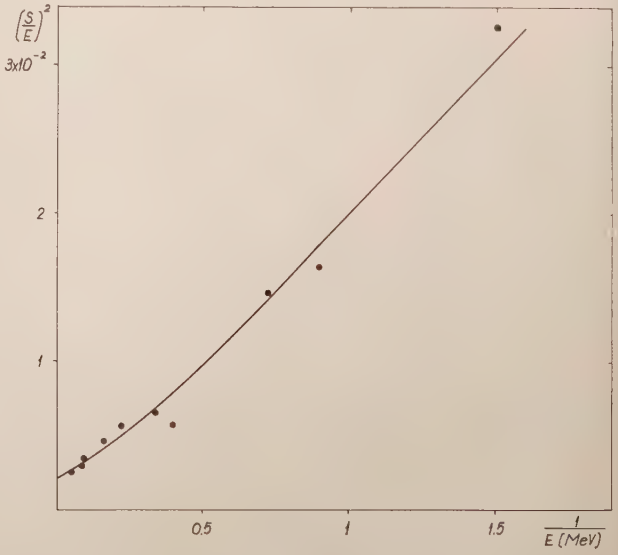

Fig. 9. Square of the relative slope as a function of the reciprocal value of energy for plastic phosphor. Error in experimental points 10–15 %.

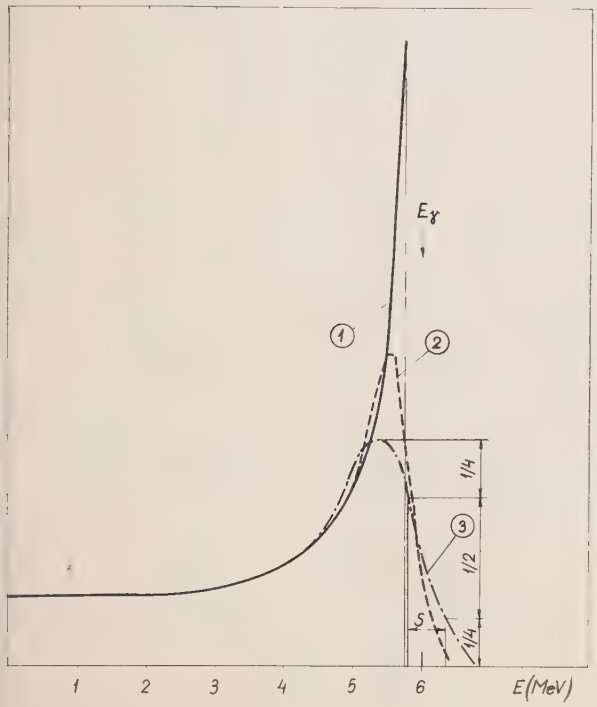

Fig. 10. Energy spectrum of single Compton scattering (curve 1) Pulse height distribution calculated from (4). with $\varphi = 0.83$ (curve 2) and with $\varphi = 1.15$ (curve 3).

quanta of various energies, a fraction of which may escape from the crystal. This assumption is supported by the fact that in case of collimated γ-beams a decrease in S/E can be observed (see fig. 8). In our case for $E_\gamma \geq 11$ MeV the pair peaks have been already fused causing an additional increase in the value of S/E. The effect of escaping electrons is probably negligible, since the effect of electron escape should be considerably more pronounced in plastic phosphors in which the electron range is appreciably higher; there, however, this high increase in the value of S/E could not be observed.

Let us return to the initial problem, the determination of the pulse height distribution as given by (4). By numerical integration we determined from equation (4) the pulse height distribution of 6.15 MeV energy γ-rays in the plastic phosphor. Since φ is a slowly varying function of the energy, it was considered as constant in the energy range 4.5–6.5 MeV. In fig. 10 we have shown also the Compton-energy distribution (curve 1) and the pulse height distribution calculated with $\varphi = 0.83$ (curve 2) and $\varphi = 1.15$ (curve 3). It is seen that for energies below 4.5 MeV, the spectra do not differ any more from the compton distribution. (The value $\varphi = 0.83$ was calculated from the spectrum of Zn^{65} with the assumption $S/\sqrt{E} =$ const.) When comparing the distribution predicted by our calculation with the experimental values (fig. 11), a good agreement was obtained for $\varphi = 1.15$ considering the measurement performed with the Pb-collimator. (The energy dependence of φ on the energy had been taken into account with the assumption $\varphi \sim \sqrt{E}$ as a correction.) From fig. 9 we obtained for 6.15 MeV $\varphi = 1.2$ making use of (5). This implies that at least for higher values of S–the slope of the pulse height distribution is not appreciably affected by the fact that it is due to the broadening of a Compton distribution and not to that of a spectral line.

Without collimation the pulse height distribution is very different from the predicted spectrum since, owing to their relatively high range, a considerable fraction of the high energy electrons does not lose its total energy in the crystal but is able to escape. The collimation on the other hand, as seen from the measurements (fig. 3), prevents radial escape even for collimators of 4 cm diameter, since the amplitude distribution does not change for collimator apertures below this value. This phenomenon is consistent with the fact that for high energy γ-radiation the Compton electrons are scattered in small angles.

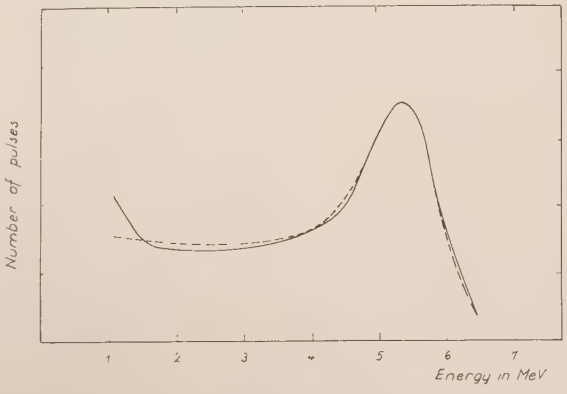

Fig. 11. Pulse height distribution as calculated/dashed curve/ and as measured/solid curve/for 6.14 MeV energy γ-radiation (measured with a Pb-collimator of 4 cm aperture).

3.2. COUNTING EFFICIENCY. ENERGY RESPONSE

In fig. 12 the variation in total efficiency with the energy is shown for the plastic phosphor used. The values of the efficiency were computed from the

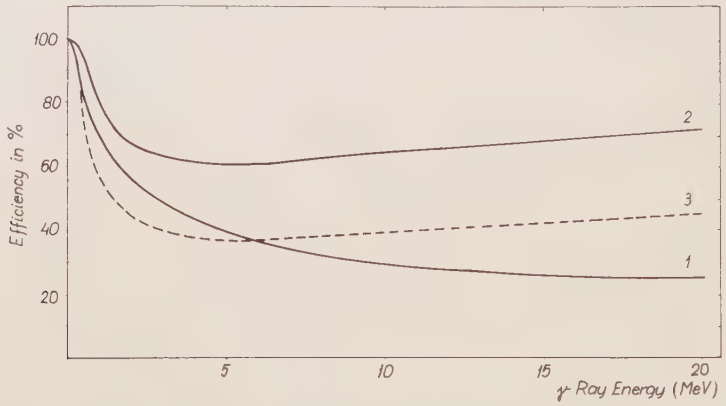

Fig. 12. Variation of efficiency with the energy for γ-source at infinite distance: 1. in the plastic phosphor used; 2. in a 3 in. × 3 in. NaI(Tl) crystal; 3. in a 1.5 in. × 1.5 in. NaI(Tl) crystal.

absorption coefficients shown in fig. 5. For comparison the efficiencies versus energy are shown also for 3 × 3 and 1.5 × 1.5 in. NaI crystals. These values are calculated by assuming the source at infinite distance.

In order to determine the response of the phosphor to the γ-energy the upper half-intensity point is assigned to the total γ-energy (fig. 10). According to the efficiency relation seen in fig. 12 the scattered γ-quanta having energies equalling the difference between the total γ-energy and the maximum energy of the Compton electrons (about 250 keV) are probably completely absorbed. The assignment of pulse height to energy value is generally not unambiguous since the former depends—as seen from fig. 10—also on the value of φ. It is of interest to note that this difficulty is even more marked in the detection of high energy γ-quanta by NaI(Tl) crystals owing to the rather complicated energy spectrum involved. The pulse

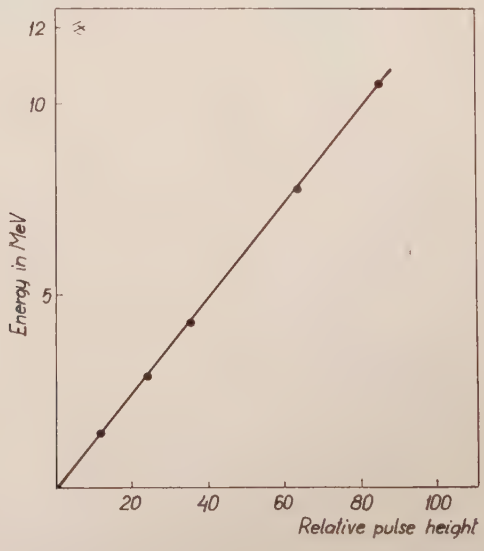

Fig. 13. Variation in pulse height with the γ-energy for γ-rays produced in the $Na^{23}(p,\gamma)Mg^{24}$ reaction as measured by plastic phosphor.

height dependence on energy thus obtained from the Na^{23} (p, γ)Mg^{24} spectrum (fig. 4) is shown in fig. 13. The dependence is seen to be linear.

4. Conclusions

As a result of our comparative experiments it can be stated that for energies above 3 MeV plastic phosphors can be used for energy measurements instead of NaI(Tl) crystals in the following cases:

1. if quick operation seems more important than counting efficiency (coincidence measurements),

2. if only NaI(Tl) crystals of small size are available.

3. if, owing to some nuclear properties of the nuclei in the NaI(Tl) crystal (e.g. to prevent the activation by neutrons) some other scintillator has to be used,

4. if, because of the complicated γ-spectrum the measurement performed with NaI(Tl) crystals has to be checked (e.g. the existence of some γ-line has to be confirmed).

Acknowledgements

Thanks are due to Prof. Dr. P. Görlich, Dr. A. Krohs and Dr. H. J. Pohl (VEB Carl Zeiss, Jena) for the M12FS100 photomultiplier put at our disposal and to Mr. Gy. Binder of our Institute for the preparation of the plastic phosphor.

NUCLEAR INSTRUMENTS AND METHODS **10** (1961) 202–204; NORTH-HOLLAND PUBLISHING CO.

DISCRIMINATEUR D'AMPLITUDE RAPIDE

A. SARAZIN, J. SAMUELI et G. BOUGNOT

Institut d'Etudes Nucléaires d'Alger

Reçu le 21 novembre 1960

A fast amplitude discriminator is described. The threshold bias is adjustable from 1 to 30 volts. The positive output pulse has a standard amplitude (1.5 volt) and length (200 ns). The difference of the lecture for pulses of 100 and 2 ns width is of the order of 1 db.

Le problème de la discrimination de l'amplitude maximum d'impulsions électriques rapides est relativement difficile car on demande aux circuits de mesure d'amplitude de donner une indication indépendante, si possible, de la durée et du temps de montée du signal étudié.

Un discriminateur d'amplitude est habituellement constitué d'un élément discriminateur suivi d'un trigger. Afin de rendre la réponse indépendante de la durée et du temps de montée du signal étudié, nous avons tenté d'améliorer la bande passante de l'élément discriminateur et d'uniformiser la sensibilité et la réponse du trigger à des signaux de largeurs différentes. Pour cela nous avons adopté une discrimination par tube bloqué permettant une contre réaction favorisant les hautes fréquences. Ce tube est suivi d'un circuit de mise en forme qui fournit au trigger de sortie un signal de largeur constante ce qui permet d'éviter une variation de la sensibilité du trigger avec la forme du signal d'entrée.

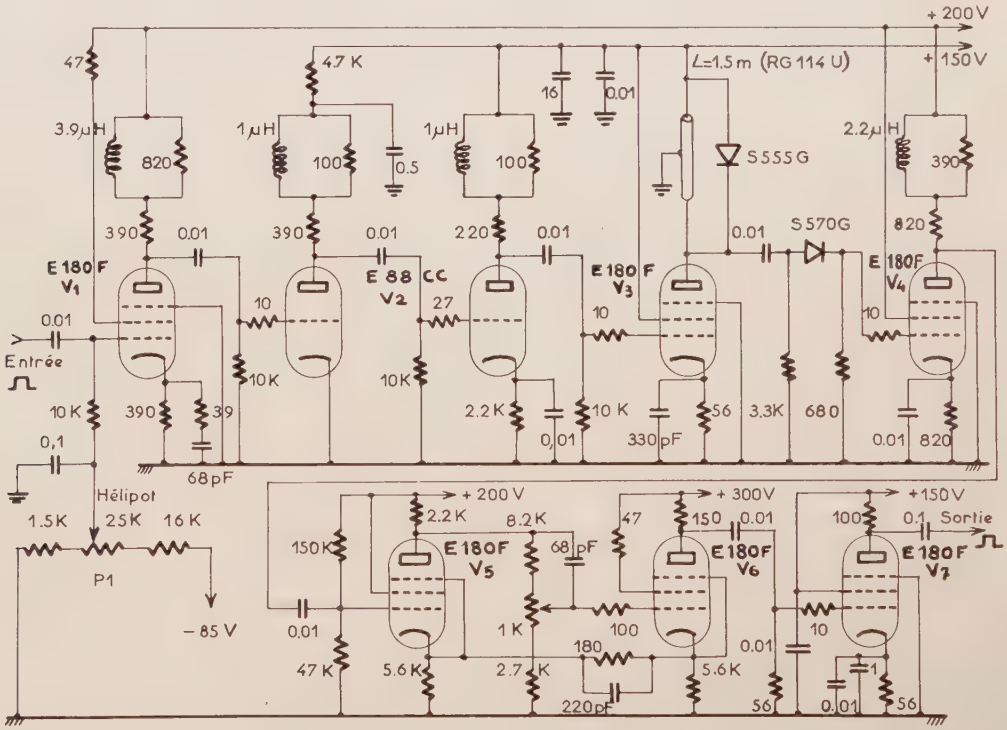

Fig. 1. Schéma général du discriminateur.

Le schéma du circuit est donné figure 1. L'élément discriminateur est le tube V_1 dont la polarisation grille définit le seuil. Ce seuil est réglable par l'hélipot P_1. La discrimination s'effectuant par tube bloqué, les signaux d'entrée doivent être de polarité positive. Dans le cas contraire, on peut utiliser un transformateur d'impulsions à ferrite ferromagnétique. La charge du tube V_1 est constituée d'une résistance de 390 ohms et d'une inductance de ligne à retard utilisée comme charge de V_3 coupe les impulsions à deux fois sa longueur électrique, soit 12 nanosecondes. Le tube V_4 sert d'amplificateur. Les tubes V_5 et V_6 constituent un trigger de Schmitt. Afin d'obtenir une impulsion de sortie à front raide. V_5 conduit en permanence, cependant que V_6 est bloqué. Cela permet d'avoir un courant important dans V_6 lors du déclenchement et d'utiliser une faible charge d'anode pour ce tube.

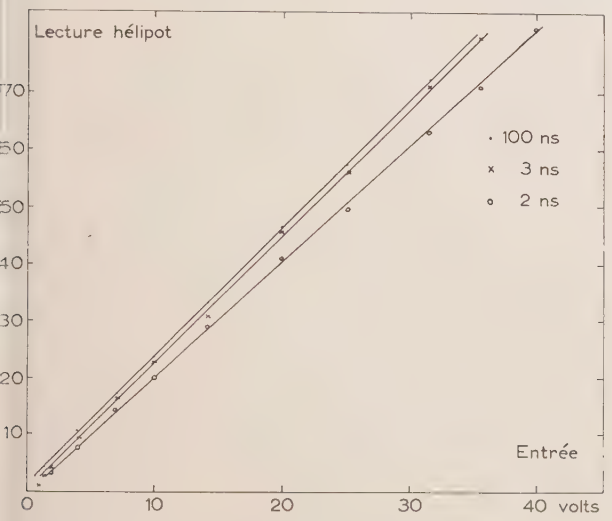

Fig. 2. Réponse du circuit.

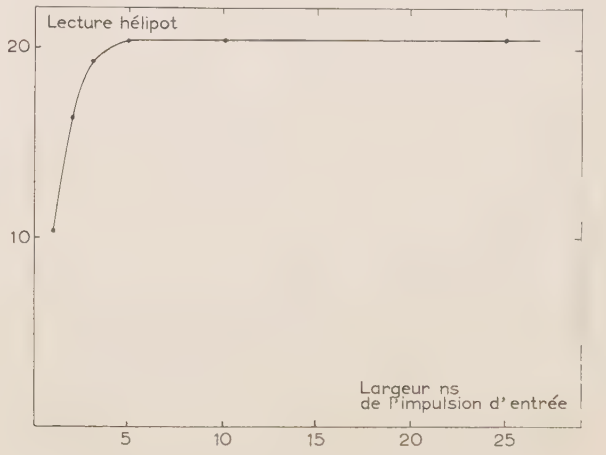

Fig. 3. Performance du discriminateur.

compensation. Pour augmenter la bande passante de l'étage, la résistance de cathode du tube est découplée par une capacité de 68 picofarads en série avec 39 ohms ce qui introduit une contre-réaction sélective favorisant les hautes fréquences. De plus, pour augmenter la pente du tube près du cut-off, les tensions d'anode et d'écran sont plus élevées qu'en utilisation normale. La réponse du tube ne respecte pas la forme des signaux d'entrée mais la réponse aux impulsions courtes est améliorée.

La largeur du signal fourni par V_1 étant celle des signaux analysés au niveau du seuil du discriminateur, nous avons fait précéder le trigger de sortie d'un circuit de mise en forme destiné à standardiser la largeur des signaux et à limiter leur amplitude. Ce circuit de mise en forme est constitué des tubes V_2 et V_3. La première triode de V_2 ainsi que V_3 sont montés en limiteurs. Les deux éléments de V_2 intègrent les signaux très courts, cependant que la

Enfin, le tube V_7 sert d'adaptateur d'impédance.

Les caractéristiques essentielles du circuit sont les suivantes:

– gamme de discrimination d'amplitude: 1 à 30 volts.

– impulsion de sortie: positive, 1.5 volt, temps de montée inférieur à 10 nanosecondes.

– durée de l'impulsion de sortie: 200 nanosecondes.

– stabilité du seuil: 0.1 volt (les tensions de chauffage étant stabilisées).

Afin d'éviter de perturber le fonctionnement du circuit par des impulsions de très grande amplitude, un blindage doit être disposé entre les connexions de grille et d'anode du tube d'entrée V_1. De même, toutes les tensions d'alimentation doivent être soigneusement découplées.

Les courbes d'étalonnage de l'amplitude de l'impulsion en fonction de la lecture sur l'hélipot ont été tracées à l'aide d'un générateur du type relai à

mercure pour des largeurs d'impulsions de 2, 3 et 100 ns. L'impédance d'entrée était ramenée à 75 ohms. Ces courbes sont données figure 2. La figure 3 indique les performances de l'appareil pour une impulsion d'entrée de niveau constant et de largeur de 1, 2, 3, 5, 10 et 25 ns.

On a également vérifié à l'aide d'impulsions de largeur 2.5 ns données par un générateur à tubes, que l'indication de l'appareil était indépendante de la fréquence de répétition du signal d'entrée. Lorsque la fréquence croît de 10 c/s à 2 Mc/s, la lecture varie de moins de 1 %.

Remerciements

Les auteurs souhaitent exprimer leurs remerciements à Monsieur le Professeur A. Blanc-Lapierre, Directeur de l'Institut d'Etudes Nucléaires d'Alger pour les conseils et l'aide qu'il leur a apportés.

NUCLEAR INSTRUMENTS AND METHODS **10** (1961) 205–211; NORTH-HOLLAND PUBLISHING CO.

SELECTION DE MESONS K^+ DANS UN FAISCEAU SECONDAIRE DE "SATURNE"

J. SEGUINOT et J. TEIGER†

Laboratoire de Physique Corpusculaire de la Faculté des Sciences de Caen

et L. VAN ROSSUM

S.P.C.H.E., Saclay

Reçu le 21 novembre 1960

The electronic device is described which permitted the determination of the number of K^+ mesons produced in a secondary beam of the "Saturne" proton synchrotron.

The selective criteria and the tests which allowed the identification of the K^+ mesons, are analysed in detail. For the ratio $\pi^+/K^+ = 400$, and with a momentum of 600 MeV/c, less than 5% of the detected particles corresponded to spurious events.

1. Introduction

Le montage électronique qui va être décrit a servi a mesurer, auprès du synchrotron à protons de Saclay, l'intensité des mésons K^+ de 600 MeV/c d'impulsion produits dans des cibles de carbone, cuivre et plomb par des chocs proton-nucléon à 35° (dans le système du Laboratoire) par rapport à la direction des protons incidents. Le but du travail était l'étude des variations des sections efficaces de production en fonction d'une part de l'énergie des protons, d'autre part de la dimension des noyaux de la cible[1]). Nous décrivons ici seulement les diverses parties du montage utilisé.

Etant donné un sélecteur de coïncidence dont le pouvoir de résolution est de l'ordre de 3 à 4 $\times 10^{-9}$ sec, une séparation par temps de vol des mésons K^+ impliquerait une base de temps de 5×10^{-9} sec au minimum. Or, pour une impulsion de 600 MeV/c à laquelle nous nous proposions de travailler, la différence entre le temps de vol des mesons légers et celui des mésons K^+ ($\beta = 0.775$), est de 8.8×10^{-10} sec/m. Il faudrait donc une base de 6 à 10 m après l'analyse magnétique, alors que le libre parcours moyen n'est que de 4.50 m dans le système du laboratoire pour cette énergie.

Il peut être ainsi remarqué, que compte tenu du taux de production attendu des mésons lourds (environ 1 méson K^+ pour 400 π), leur séparation suivant cette méthode présente des difficultés importantes d'autant plus que le résiduel des mésons π et des protons est difficile à estimer au niveau des mésons K^+ de la courbe de résolution.

Nous avons de ce fait préféré une méthode qui consiste à éliminer toutes les particules autres que les mésons K^+, en utilisant les propriétés d'émission d'un rayonnement Čérenkov, au moyen de détecteurs appropriés.

Le dispositif est constitué:

1. d'un télescope formé de compteurs à scintillation, définissant le passage d'une particule dans le faisceau;

2. d'une compteur Čérenkov sensible surtout aux mésons légers et à leurs produits de désintégration;

3. d'un compteur Čérenkov sensible surtout aux mésons lourds (compteur du type Fitch).

On verra plus loin que nous nous sommes servis aussi de l'information donnée par les scintillateurs sur la perte d'énergie par ionisation pour séparer les protons.

En fait, l'élimination des particules autres que les mésons K^+ est assurée par plusieurs méthodes indépendantes, chacune d'elles n'assurant pas un taux de réjection suffisant.

2. Dispositif Expérimental

2.1. LE FAISCEAU

La disposition des divers éléments du faisceau est donné par la fig. 1.

Les mésons K^+ sont produits par des protons du synchrotron heurtant la cible interne à énergie donnée, variable.

† Partie d'un travail présenté pour thèse de Doctorat ès-Sciences près de l'Université de CAEN (No. 40 Avril 1960).

[1]) Publication à paraître, lettres "Nuovo Cimento".

Une lentille électromagnétique est placée à 4.30 m de la cible suivant un axe faisant un angle de 35° avec la direction des protons incidents. Cette lentille est composée de trois quadrupôles.

Un aimant d'analyse, placé immédiatement après le dernier quadrupôle permet d'obtenir un

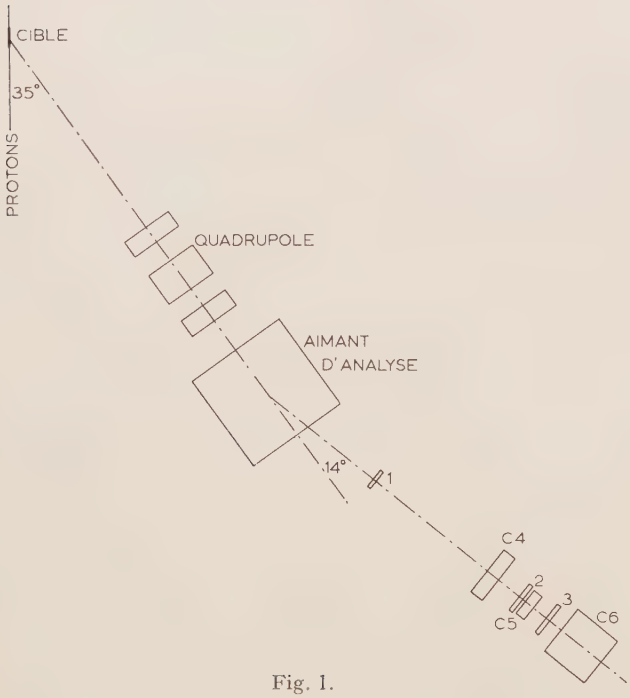

Fig. 1.

faisceau de particules d'impulsion bien définie à l'endroit de l'image de la cible.

La largeur de la bande d'impulsion était égale à $\pm$ 7% de l'impulsion moyenne correspondant aux $\frac{2}{3}$ des particules d'une distribution sensiblement gaussienne.

2.2. LE TELESCOPE DE SCINTILLATEURS

Le compteur à scintillation I a une épaisseur de 6 mm et un diamètre de 60 mm. Il est couplé optiquement à un photomultiplicateur RCA type 6810 A.

Les scintillateurs 2 et 3 ont aussi 6 mm d'épaisseur mais ils ont un diamètre de 90 mm. Chacun d'eux est monté sur un photomultiplicateur Radiotechnique Type 56 AVP.

Tous ces compteurs placés respectivement à 2.50 m, 4.50, 5.50 m du centre de l'aimant d'analyse, sont montés en coïncidence sur le sélecteur C_1 (fig. 2). Ce circuit de coïncidence, comme tous ceux que nous avons utilisés dans ce montage, est du type additif à trois voies, avec possibilité de réaliser des coincidences ou des anticoïncidences. Il a un temps de résolution de l'ordre de 3 à 4 $\times$ 10^{-9} sec.

La courbe de temps de vol de ce télescope en fonction du retard du compteur I, (2 et 3 sont trop voisins pour qu'il soit nécessaire de réajuster leur retard) est donné par la fig. 3.

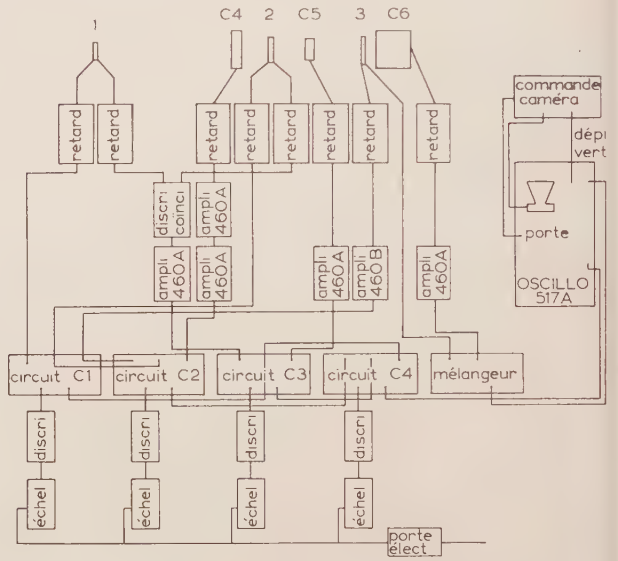

Fig. 2.

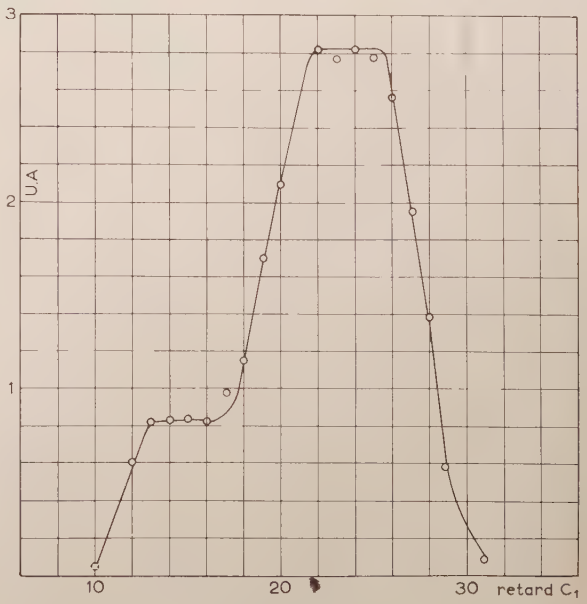

Fig. 3.

2.3. LES COMPTEURS ČERENKOV

a. Le compteur Čérenkov à seuil de vitesse de détection des mésons π

Il est constitué par une substance fluorée fabriquée sous le nom de "Fluorochemical O–75", d'indice $n = 1.276$, tel que pour une impulsion de 600 MeV/c,

$$\beta_\pi > \frac{1}{n} > \beta_K .$$

Il se présente (fig. 4), sous forme d'une cellule cylindrique de 140 mm de diamètre et de 40 mm d'épaisseur. La face d'entrée est en laiton de 0.3 mm d'épaisseur, la face de sortie, transparente, est une feuille mince de mylar afin de réduire la lumière Čérenkov produite dans cette paroi.

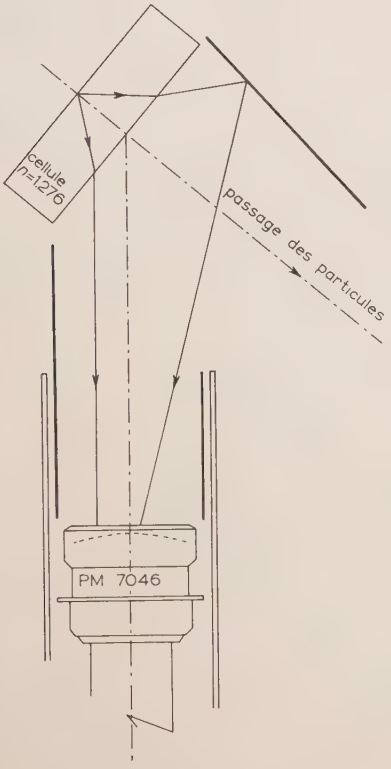

Fig. 4.

L'angle d'émergence de la lumière, soit 49°, détermine l'emplacement du photomultiplicateur RCA 7046. Un miroir plan incliné à 15° par rapport à l'axe, permet de recueillir une partie de la lumière émise dans la direction symétrique. Deux autres miroirs plans placés de chaque côté de la cellule permettent d'augmenter la collection de la lumière.

Des mesures ont permis d'évaluer à 25% l'efficacité de collection de la lumière, avec une faible dispersion.

Déterminé avec des protons le seuil effectif a été trouvé pour $\beta = 0.84$, alors qu'à 600 MeV/c, $\beta_K = 0.75$.

Nous verrons plus loin que l'efficacité de ce compteur pour les mésons légers et leurs produits de désintégration ($\beta \simeq 1$) est de l'ordre de $(1–10^{-4})$.

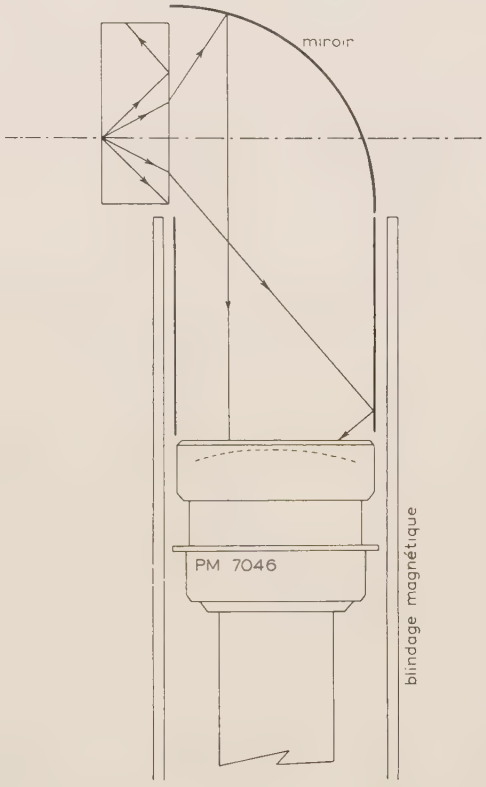

Fig. 5.

b. Le compteur Čérenkov du type Fitch de détection des mésons K^+

Le compteur (fig. 5) est constitué par un disque de plexiglass de 80 mm de diamètre et 30 mm d'épaisseur. Le pourtour et la face arrière, par laquelle pénètre le faisceau, sont dépolis et noircis. L'axe du compteur est parallèle à la direction du faisceau.

Pour atteindre la photocathode, la lumière doit sortir par la face avant qui est en contact avec l'air

et il faut donc que l'angle d'incidence sur cette face soit inférieur à l'angle de réflexion totale:

$$\theta_c = \arcsin 1/n .$$

Au-delà de cet angle, la lumière subit la réflexion totale et est ensuite absorbée par la face arrière ou la surface latérale. Ce compteur est donc sensible dans la bande de vitesse:

$$\frac{1}{n} < \beta < \frac{1}{n \cdot \cos \theta_c} = \frac{1}{\sqrt{n^2 - 1}}$$

(cette formule implique $n^2 \geqslant 2$). Pour le plexiglass $n = 1.5$ et on a

$$0.665 < \beta < 0.89 .$$

Avec ce compteur, il est possible de détecter les mésons K^+ possédant une impulsion comprise entre 0.5 et 0.8 GeV/c, sans qu'il soit sensible, en principe, aux mésons légers ou aux protons de même impulsion.

Un miroir en forme de quart de cylindre, terminé à chaque extrémité par un miroir plan, conduit la lumière sur un photomultiplicateur à grande photocathode, RCA type 7046.

Ce compteur a été essayé dans un faisceau de protons d'énergie variable; pour un β égal à 0.775 correspondant au β des mésons K^+ de 0.60 GeV/c, nous avons pu constater que l'amplitude des impulsions à l'anode du photomultiplicateur était assez élevée et uniforme pour que l'on puisse s'attendre à une bonne efficacité. Nous avons effectivement constaté que l'amplitude des impulsions diminuait lorsque la vitesse des protons approchait un β égal à 0.89.

Cependant ce compteur présente un certain nombre de défauts. Nous avons remarqué qu'une fraction des mésons π produisait des impulsions. En effet, si nous faisons l'estimation du nombre d'interactions dans le compteur Fitch, nous trouvons qu'environ 4% des mésons π interagissent en donnant un méson π à un angle supérieur à environ 10°. Ceci correspond bien à l'efficacité mesurée pour les mésons π.

De plus, nous devons tenir compte du fait que, la surface en regard du photomultiplicateur n'étant pas parfaitement polie, une certaine quantité de lumière est diffusée et réussit à sortir du disque de plexiglass.

D'autre part, des protons de 0.60 GeV/c dont la vitesse est inférieure à la vitesse de la lumière dans le plexiglass sont également comptés avec une efficacité faible, de l'ordre de 1% à 2%. Ceci pourrait être dû à une scintillation dans le plexiglass.

3. Sélections des Mésons

La figure 2 montre l'ensemble du dispositif électronique devant répondre aux conditions imposées, résumées au début de cet article.

1. Le compteur Čérenkov 4, sensible qu'aux seuls mésons légers est mis en coïncidence avec les scintillateurs 2 et 3 dans le circuit C_2.

Le compteur 1 a été volontairement écarté de facon que l'information du circuit C_2 soit indépendante du retard imposé à ce compteur quand on relève la courbe de résolution finale.

L'impulsion rapide de sortie du circuit C_2, inversée de phase et mise en forme par un amplificateur large bande Hewlett Packard 460 B, fournit le signal d'anticoïncidence pour les mésons π et les leptons chargés.

2. Le compteur Fitch mis en coïncidence dans le circuit C_3 avec l'information du circuit C_1, devrait normalement permettre de définir le passage d'un méson K^+. Mais nous avons vu qu'il comptait un résiduel de pions, qui pourra être éliminé par l'information du circuit C_2, et de protons.

Pour séparer cette dernière composante, nous nous sommes servis du fait qu'à 600 MeV/c, la perte d'énergie par ionisation des protons est sensiblement plus grande que celle des particules plus légères et qu'ils produisent, par conséquent, des impulsions plus grandes dans les scintillateurs. Afin d'augmenter la sensibilité de cette discrimination, les signaux des compteurs 1 et 2 sont envoyés dans un circuit d'addition avant d'être discriminés en amplitude. L'impulsion résultante fournit le signal d'anticoïncidence de C_3.

Le circuit C_3 donne donc en définitive une impulsion pour les mésons K^+ et un résiduel de mésons légers.

3. Finalement le circuit C_4, fait la synthèse de toutes ces informations. Il reçoit en coïncidence les sorties de C_1 et C_3 et en anticoïncidence la sortie de C_2. Le signal de sortie de C_4 est alors considéré

comme provenant du passage d'un méson K^+ dans le faisceau.

La courbe de résolution finale, fonction du retard du compteur 1, est donnée par la fig. 6 sur laquelle

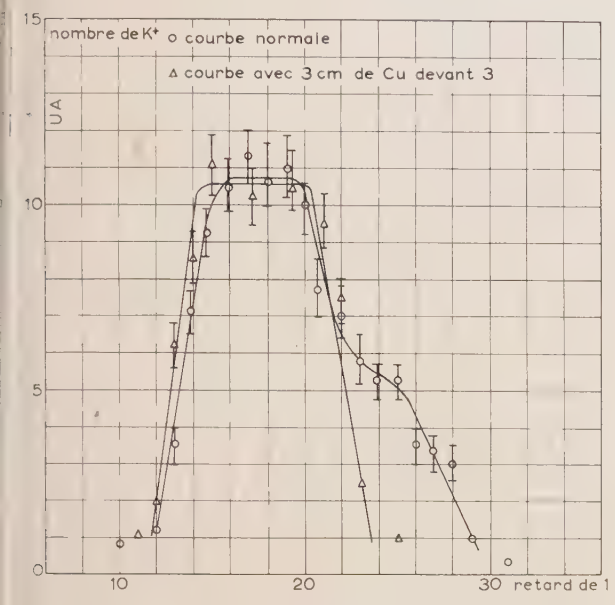

Fig. 6.

on peut voir encore une déformation dûe à des protons. Ils représentent environ 1/7000 du nombre des protons traversant les compteurs. La comparaison avec la deuxième courbe de la même figure montre que la contribution des protons a disparu par interposition de 3 cm de cuivre devant le compteur 3.

3.1. REMARQUE SUR LA SELECTION DES K+

La disposition des compteurs telle qu'elle a été décrite résulte du souci d'écarter le maximum de coïncidence fortuites.

Il doit être signalé cependant deux possibilités dangereuses de fortuites:

1. Une particule quelconque passant dans le scintillateur I, tandis qu'un proton simultané passe dans les compteurs 2, 3 et les compteurs Čérenkov 4 et 5. La seule barrière qui puisse éliminer cette coïncidence fortuite, indépendante du retard du compteur I, est le compteur Fitch.

2. Mais l'évènement le plus dangereux est un méson π interagissant, en amont ou à l'entrée du compteur 4, de façon à ne pouvoir donner le signal d'anticoïncidence. Nous obtiendrons un comptage parasite si cette interaction donne lieu à l'émission d'une particule plus lente capable d'exciter les scintillateurs 2 et 3 et le compteur Fitch.

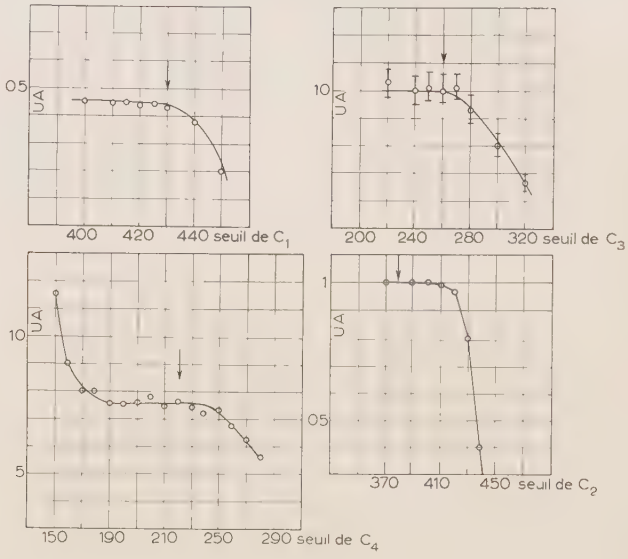

Fig. 7.

3.2. REGLAGE DES CIRCUITS DE SELECTION

Sur la fig. 7 ont été groupées les courbes de seuil de chacun des circuits de coïncidence. Ces courbes correspondent au spectre intégral de l'amplitude de l'impulsion après addition des impulsions des diverses voies, en fonction du niveau de discrimination.

Circuit C_1

La courbe de seuil a été relevée avec des mésons π négatifs afin d'avoir un faisceau pratiquement pur. On notera une plage de stabilité très satisfaisante. Elle serait d'ailleurs meilleure avec les mésons K^+ puisqu'ils sont moins rapides et que par conséquent, ils donnent une impulsion de scintillation plus grande.

Circuit C_2

Etant donné le rapport π^+/K^+ attendu, égal à 400, ce circuit doit avoir une efficacité beaucoup plus critique.

Nous avons trouvé qu'un méson π du faisceau sur 10000 échappait à la détection. Cette valeur détermine donc l'efficacité de l'anticoïncidence π.

Circuit C_3

Son réglage est déterminé sans l'anticoïncidence des protons. Il a été obtenu en utilisant des protons dont la vitesse est égale à celle des mésons K^+ de 600 MeV/c.

Reste ainsi à ajuster la valeur de la discrimination des protons qui ne peut être faite qu'au niveau du circuit C_4.

Circuit C_4

Il est réglé en faisceau positif à 600 MeV/c au retard correspondant du compteur I, des mésons K^+.

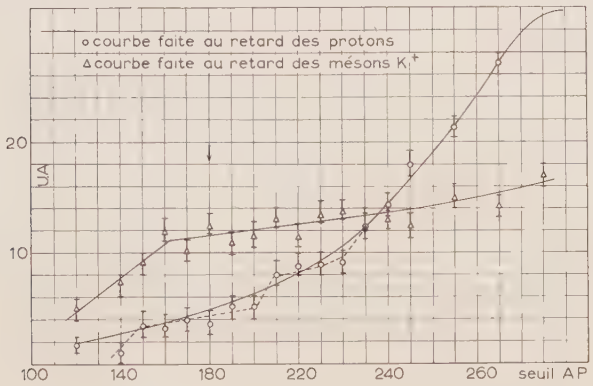

Fig. 8.

Une courbe de seuil relevée de cette facon ne permet pas d'obtenir un plateau de fonctionnement, puisqu'un certain nombre de protons sont comptés par le circuit C_3 en donnant à sa sortie, quel que soit le gain, un spectre d'amplitude.

La fig. 8 indique le taux de comptage normalisé du circuit C_4 en fonction du niveau de discrimination de l'anticoïncidence des protons, lorsque le retard du scintillateur I est ajusté soit au retard des mésons K^+ ou sur celui des protons. Pour le point de fonctionnement de l'anticoïncidence noté sur la courbe, la courbe de seuil du circuit C_4 est celle donnée par la fig. 7.

4. Efficacité de la Détection

La courbe 8 montre que pour le point de fonctionnement choisi, au retard des protons on compte à la sortie du circuit C_4 un nombre de protons égal au tiers du nombre des mésons K^+.

Il en résulte qu'au retard des K^+ il doit rester un nombre négligeable de protons qui pourraient être comptés comme des mésons K^+. C'est bien d'ailleurs ce que nous avions noté à partir de l'étude de la courbe de résolution de la fig. 5 après interposition de 3 cm de cuivre dans le faisceau. Remarquons que l'atténuation du nombre des protons au niveau du circuit C_1 a été trouvée beaucoup plus faible que l'atténuation résultante du résiduel au niveau du circuit C_4.

L'ensemble de ces tests nous a permis de déduire que le comptage du circuit C_4 inclut plus de 90% des mésons K^+ passant par les compteurs.

L'essai de l'anticoïncidence des mésons π dans le faisceau négatif et la forme de courbe de retard du circuit C_4 permettent de conclure que notre sélection inclut moins de 5% de particules autres que les mésons K^+ après soustraction des coïncidences fortuites.

5. Identification des Mésons K^+

5.1. MESURE DU PARCOURS RESIDUEL

Nous avons effectué un certain nombre de contrôles afin de prouver que la sélection électronique identifiait bien des mésons K^+:

En premier lieu, la mesure du parcours dans le cuivre des particules sélectionnées. A cet effet, nous disposons devant le scintillateur 3 des plaques de cuivre de différentes épaisseurs. Pour une épaisseur de cuivre donnée, on enregistre le nombre de particules rapporté au même nombre de protons sur la cible.

En portant le nombre de particules qui ont traversé une épaisseur de cuivre donnée, en fonction de cette épaisseur, nous obtenons la "courbe de parcours" (fig. 9).

On observe une diminution lente pour les faibles épaisseurs; le taux de cette diminution correspond à la section efficace totale pour la géometrie utilisée.

Il vient ensuite une descente rapide qui correspond à l'arrêt des particules par ionisation. Cette descente est étalée dans un intervalle Δx qui correspond essentiellement à la bande d'impulsion Δp des particules contenues dans le faisceau.

La courbe obtenue pour les particules sélectionnées est bien celle que l'on attend pour les particules de masse égale à environ 0.5 GeV, ayant une impulsion moyenne de 0.6 GeV/c et un $\Delta p/p$ de $\pm$ 7%. L'atténuation du faisceau sélectionné, produite par interaction est nettement inférieure à celle qui correspondrait à la section efficace des mésons π^+ et des protons.

Elle est compatible avec la section efficace d'absorption des mésons K+.

Sur cette courbe, on observe d'autre part une queue d'un faible pourcentage du comdtage maximum. En effet les mésons K+ s'arrêtant dans le cuivre émettent des secondaires dont certains si-

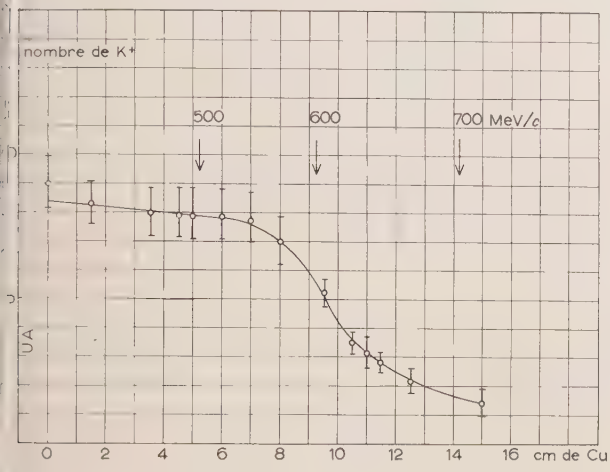

Fig. 9.

muleront un parcours plus long. Une estimation montre que ce phénomène explique bien cette déformation observée de la courbe de parcours.

Les particules sélectionnées ont donc bien une masse d'environ 0.5 GeV.

5.2. MESURE DE LA VIE MOYENNE

Une vérification supplémentaire consiste dans la mesure de la vie moyenne de désintégration de ces particules arrêtées à l'intérieur d'un compteur Čérenkov.

Nous employons pour cela une cuve de 150 × 150 × 150 mm³ en plexiglass de 5 mm d'épaisseur, remplie d'un liquide d'indice $n = 1.276$ dans lequel le méson K+ ne donne lieu à aucune lumière Čérenkov. Une certaine épaisseur de cuivre est disposée devant la cuve de façon que les mésons K+ s'y arrêtent. Parmi les produits de désintégration, (π, μ, électrons) un certain nombre produisent du rayonnement Čérenkov. Le retard de l'impulsion correspondante par rapport à l'instant d'entrée du méson K+ doit être distribué suivant une loi exponentielle correspondant à la vie moyenne.

La cuve Čérenkov est noircie sur toutes ses faces à l'exception d'une qui est en contact optique avec un photomultiplicateur Radiotechnique, type 58 A.V.P. De cette façon, nous ne conservons que des rayons lumineux qui sont approximativement isochrones. Environ 15% des K+ du faisceau se désintégrent dans la cuve d'une manière à produire une impulsion utile à la sortie du détecteur.

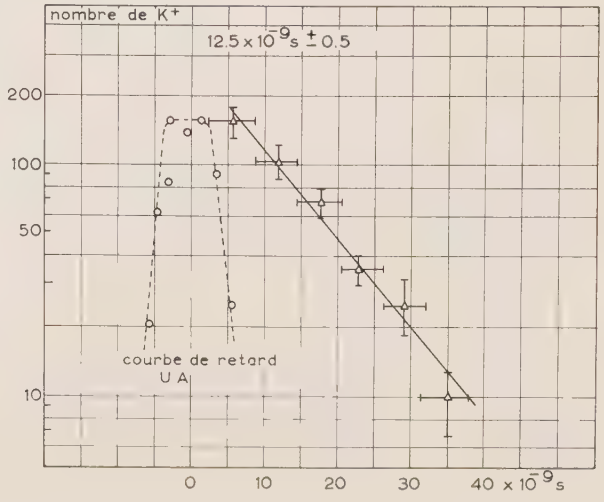

Fig. 10.

La déviation horizontale d'un Oscillographe Tektronix, type 517 A, à vitesse de balayage connue est déclenchée par la sortie rapide du circuit C_4 qui sélectionne les mésons K+ du faisceau. Dans un mélangeur d'impulsions sont envoyées les sorties du compteur 3 et de ce compteur Čérenkov. La sortie du mélangeur attaque l'amplificateur vertical de l'oscillographe. Sur la photographie de la trace on mesure la distance entre les deux impulsions. Nous avons trouvé une durée de vie de la particule comprise entre 1.18 et 1.25 × 10^{-8} s, ce qui achève l'identification d'un méson K+ (fig. 10).

Remerciements

Les auteurs remercient, Monsieur le Professeur Schérer pour son encouragement qui a rendu possible le travail, et pour l'intérêt qu'il y a apporté, Monsieur Berthelot pour l'hospitalité qu'il a accordée[1]) dans les Laboratoires de Saclay. Nous remercions Monsieur Levy-Mandel, ses ingénieurs et techniciens qui ont fait fonctionner l'accélérateur "Saturne".

[1]) à deux d'entre nous.

NUCLEAR INSTRUMENTS AND METHODS 10 (1961) 212–216; NORTH-HOLLAND PUBLISHING CO.

PHOTONS FROM POSITRON BEAMS IN THE GeV RANGE

D. M. BINNIE

Physical Laboratories, University of Manchester†

Received 7 November 1960

High energy positrons in liquid hydrogen produce, in addition to bremsstrahlung, pairs of quanta by annihilation with atomic electrons. An interesting separation of the annihilation and bremsstrahlung radiation should be obtained at a small angle to the positron beam. This appears to offer a method of producing GeV photons relatively free from bremsstrahlung. The technique could be especially applicable to bubble chamber investigations of strange particle and other photoproduction reactions.

1. Introduction

Recently, some interest has centred on the possibility of utilising annihilation radiation from high energy positrons in hydrogen as a "monochromatic" source of photons. Thus, with this possibility in mind, Gunn and Moorhouse[1]) estimated that a focused linear accelerator should be capable of accelerating positrons from a few MeV to the GeV range to give 2×10^9 positrons/pulse, 500 pulses/sec, with an overall energy spread of 3%. The annihilation photon spectrum is sharply peaked just below the positron energy and for experiments in which we might require an energy resolution of a few MeV, such as the investigation of threshold phenomena, gives a photon contribution, in photons/MeV, up to an order of magnitude greater than the bremsstrahlung background.

One of the most interesting fields of elementary particle research lies in the study of photoproduction of strange particles in which work so far has been confined to the lowest energies and "two body" reactions. At higher energies, the three or more body kinematics, the variety of possible reactions and the short mean decay distances of many of the secondary particles would appear to limit severely the possibilities of counter techniques. On the other hand, bubble chamber investigations, while aided by the short lifetimes, are very much limited by the background of electron-positron pairs in the chamber[2,3]). In both cases also, due to the form of the bremsstrahlung spectrum the only a priori photon energy information is an upper bound. The complete and unambiguous identification of the reaction and a good measure of its kinematics is therefore required before the primary photon energy is known.

The positron beam seems of little help here, for although the annihilation radiation is well peaked over a few MeV, its total intensity is relatively small. We might compare the total number of annihilation quanta N with the "number of equivalent quanta" Q of the bremsstrahlung. At 1 GeV this ratio is of the order of $\frac{1}{50}$. The great majority of interactions, either for electron pair or for strange particle production, will still arise from the bremsstrahlung spectrum.

The purpose of this paper is to point out that it appears possible to remove a large fraction of the bremsstrahlung background, still retaining adequate annihilation intensity and energy resolution, by accepting radiation at a small angle to the positron beam only (see fig. 1).

2. Theory

We have to consider the various processes that can give rise to photons at an angle θ to the in-

† Now at Physics Department, Imperial College, London.

[1]) J. Gunn and R. G. Moorhouse, National Institute Symposium at Liverpool, 1960.

[2]) J. M. Sellen, G. Cocconi, V. T. Cocconi and E. L. Hart, Phys. Rev. **110** (1958) 779.

[3]) D. C. Gates, R. W. Kenney, D. A. McPherson, W. P. Swanson, Rev. Sci. Inst. **31** (1960) 565.

cident positron beam when the latter strikes a liquid hydrogen target. Let E_0 be the positron energy, μ the electron rest mass. Relativistic approximations are used where permissable.

2.1. ANNIHILATION RADIATION

The positron annihilates in flight with an electron at rest to produce 2 photons. The photon energy and angle are related by

$$\theta = \sqrt{2\mu\ (E_0 - k)\ /E_0 k}.$$

The total cross section/electron for the production of photons from $k = E_0 - \delta$ to E_0 is

$$\phi_\delta = \pi r_0^2 \frac{\mu}{E_0}\left\{\ln\left[\frac{(\mu + 2\delta)\ E_0}{\mu k}\right] - \frac{2\delta}{E_0}\right\}$$

derived from results given by Heitler[4]). For k close to E_0 this gives the approximation

$$\mathrm{d}\,\phi_\delta \propto \frac{\mathrm{d}k}{E_0 - k} \quad \text{or} \quad \frac{\mathrm{d}\theta}{\theta}.$$

Thus the annihilation radiation at a given angle has a unique energy and the differential cross section falls relatively slowly with angle.

2.2. BREMSSTRAHLUNG

Most of the bremsstrahlung emission lies within an angle of μ/E_0 and we are interested in angles of 10 to 100 times this value. Consequently we can distinguish two main mechanisms for the production of bremsstrahlung photons which turn out to have comparable importance and which we refer to as "direct" and "indirect" emission. "Direct" emission refers to the case in which the bremsstrahlung process gives rise directly to a photon at the angle θ. "Indirect" emission requires the positron to suffer a single "large angle" scatter to the angle θ and subsequently give a normal bremsstrahlung photon in the forward direction.

For target thicknesses in the region of 1 g/cm² of hydrogen, all the processes considered have a probability $\ll 1$. Consequently we note that whereas the annihilation and direct bremsstrahlung probabilities are proportional to the target thickness "t", indirect emission is proportional to t^2. Over the range of parameters considered, direct emission is the rather more probable of the two bremsstrahlung processes.

It is possible to estimate fairly accurately the total probability for "indirect" emission. The cross section for the scattering of electrons or positrons on protons can, for our purposes, be taken as

$$\mathrm{d}\phi \quad -8\pi r_0^2 \left(\frac{\mu}{E_0}\right)^2 \frac{\mathrm{d}\theta}{\theta^3}.$$

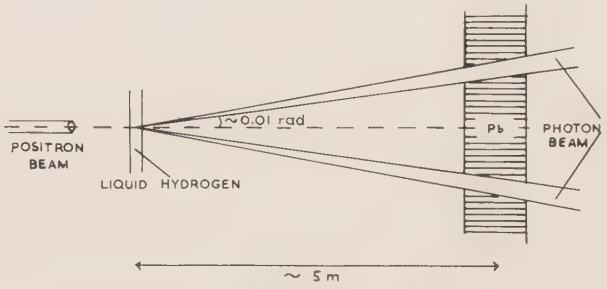

Fig. 1. Schematic geometry of photon beam.

For the positrons on the atomic electrons the calculation is given by Bhabha[5]): to the first approximation the cross section is identical with the e–P scattering cross section, but decreases somewhat more rapidly for larger angles. A reasonable approximation is therefore to double the e–P cross section. This gives a probability $\mathrm{d}P_\mathrm{s}$ for a positron to be scattered at an angle θ in t g/cm² of hydrogen of

$$\mathrm{d}P_\mathrm{s} = -2.4\left(\frac{\mu}{E_0}\right)^2 t\,\frac{\mathrm{d}\theta}{\theta^3}$$

(θ large, single scatters only). We also require the total bremsstrahlung cross section for positrons in hydrogen. This again is close to twice that of electrons on protons[6,7,8]) and hence we find, for the higher energy photons and in the region of complete screening, a probability $\mathrm{d}P_\mathrm{b}$ for bremsstrahlung giving a photon of energy k of $\mathrm{d}P_\mathrm{b} = 0.014t\ \mathrm{d}k/k$ (ref.[4]). The coefficient 0.014 increases to about 0.021 as k approaches zero.

[4]) W. Heitler, The Quantum theory of radiation, 3rd edition (Oxford, 1954).

[5]) H. J. Bhabha, Proc. Roy. Soc. A **154** (1936) 195.

[6]) D. Bernstein and W. K. Panofsky, Phys. Rev. **102** (1956) 522.

[7]) P. C. Fisher, Phys. Rev. **92** (1953) 420.

[8]) J. A. Wheeler and W. E. Lamb, Phys. Rev. **55** (1939) 858.

The probability of both processes in the same target is thus simply $\frac{1}{2}\,dP_s\,dP_b$.

The cross section for the direct emission of a bremsstrahlung photon at an angle θ when an electron or positron is incident on a nucleus is given by Schiff[9]), who integrated the Bethe-Heitler equation over the angle of the scattered electron, taking into account the effect of screening. For angles $x \gg 1$, $x = E_0\theta/\mu$ we have

$$\sigma(k, x)\,dk\,dx =$$

$$-4\overline{\phi}\frac{dk}{k}\frac{dx}{x^3}\left\{-\frac{E_0^2 + E^2}{E_0^2}\ln M(x) - \frac{(E_0 + E)^2}{E_0^2}\right\}$$

where $M(x) = (\mu k/2E_0E)^2 + (\frac{1}{137\,x^2})^2$, E is the energy of the scattered electron. We must as before consider also the effect of the atomic electrons in the target. There appears to be no detailed calculation of the angular distribution expected for this source of bremsstrahlung photons. Panofsky and Bernstein[6]) have measured the intensity of e^- bremsstrahlung from hydrogen at 500 MeV. They find good agreement with the theoretical estimates of Wheeler and Lamb[8]). In making these estimates, exchange effects and also momentum transfers to the target electron greater than μ/c were neglected. The energy of the recoil is thus normally very small and probably plays little part in the reaction; the nature of the recoil particle is also of little importance. It seems unlikely therefore that the angular distributions for $e^+ - e^-$ and $e^+ - P$ will be much different. This conclusion can perhaps be supported in a rather different manner if we note that the elastic scattering of e^+ on e^- and P are very similar at small angles. We therefore expect that the radiative processes arising due to the scattering of the positrons should also be similar. Of course, for very large angles, the recoil electron energy must become large and the kinematics become very different. However this region is outside that of interest to us. We assume that it is again adequate to double the Schiff cross section to find the photon angular distribution for positrons on hydrogen.

We note that while both the "direct" and the "indirect" bremsstrahlung contain an angular dependence factor $d\theta/\theta^3$ or dx/x^3, $(x = E_0\theta/\mu)$, the angular distribution of annihilation photons resembles a dx/x distribution only. The ratio of annihilation to bremsstrahlung radiation increases with x as x^2. At 1 GeV, a value of x of 50 corresponds to an angle of about $1\frac{1}{2}°$.

3. Beams

3.1. INTENSITY

Examples of the type of results to be expected are given in figs. 2 and 3. As is customary in bremsstrahlung curves we plot the intensities, namely photon flux times energy, per MeV. Fig. 2 shows the spectrum of photons from

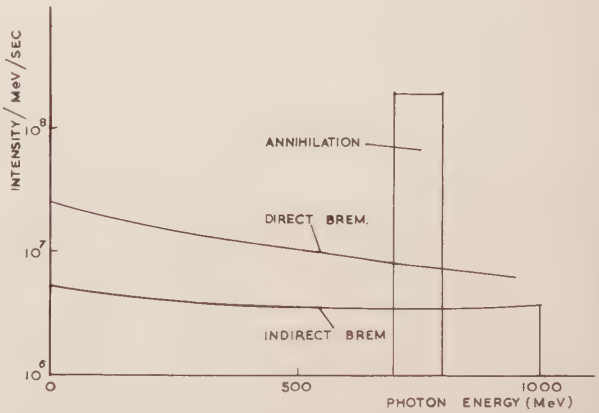

Fig. 2. The three components of the photon beam between angles of 0.0158 and 0.0207 rad for 10^{12} positrons/sec at 1 GeV incident on 1 g/sq.cm of hydrogen.

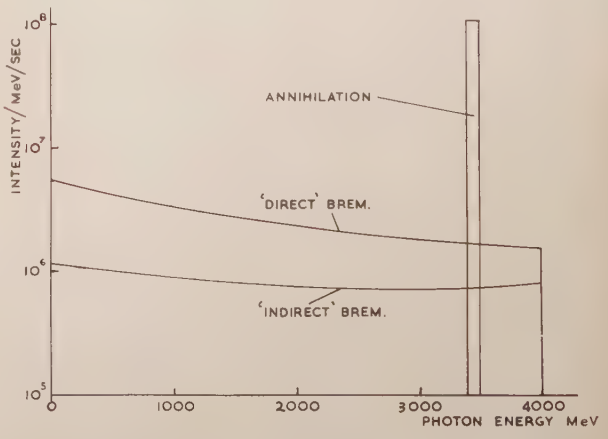

Fig. 3. The three components of the photon beam between angles of 0.00598 and 0.00664 rad. for 10^{12} positrons/sec. at 4 GeV incident on 1 g/sq.cm of hydrogen.

[9]) L. Schiff, Phys. Rev. **83** (1951) 252.

1 GeV positrons on 1 g/sq cm of hydrogen in which the angle of acceptance of the radiation, 0.0158 to 0.0207 rad, is set to correspond to a photon band of 700 to 800 MeV. Fig. 3 shows 4 GeV positrons, again on 1 g/sq cm hydrogen, producing annihilation photons of 3.4 to 3.5 GeV, corresponding angles being 0.00598, 0.00664 rad. These graphs, plotted ignoring those effects which smear out the annihilation radiation spectrum, serve to show the relative intensities of photons from annihilation and bremsstrahlung. "Direct" and "indirect" bremsstrahlung are shown separately. It will be recalled that the relative proportions of these two backgrounds depend on the target thickness. The direct bremsstrahlung curve is more peaked at the lower energies as we are mainly in the "unscreened" region. N/Q is in the region of unity or greater. Therefore a good fraction of any interactions produced by the photon beam will arise from the narrow band of annihilation photons. The beam at 4 GeV is somewhat lower in photons/second, but otherwise very similar to the 1 GeV beam.

3.2. ENERGY RESOLUTION

The annihilation photon energy is unique for a given angle θ and given positron energy E_0. In practice the positron energy resolution is mainly limited by the primary beam, as, for the targets of interest, ionisation loss is small. A variety of effects lead to a spread in the angle θ. They comprise the area and angular spread of the positron beam; the scattering of the positrons in the hydrogen and the range of angles in the photon beam (fig. 1). The relative importance of these effects depends very much on the use for which the beam is designed. This is illustrated in the next section in which we consider such a beam specifically in conjunction with a hydrogen bubble chamber.

4. The Use with Bubble Chambers

To be able to examine individual interactions in a bubble chamber, it is necessary to restrict the number of electron pairs produced[3]). Even for pure photon beams of unique energy, pair production, with a cross section of 20 mb/atom at 1 GeV, must greatly predominate over all other processes, and therefore set the limit to the flux of photons tolerable in the chamber. This level, for a 50 cm hydrogen chamber and allowing 10 pairs per picture on average, would be about 250 photons/picture. With the 1 GeV annihilation beam suggested, for the same conditions we need 100 annihilation photons/picture. These photons are therefore responsible for 4 of the 10 pairs. Most of the remaining pairs will come from photons of much lower energy.

The flux of photons required is much less than that available; this being 5×10^4/pulse at 700 to 800 MeV and 6×10^3/pulse at 3.4 to 3.5 GeV for 2×10^9 positrons/pulse. Thus something could certainly be made with a tenth or even a hundreth of the postulated positron beam. We must however allow a factor of 2 or 3 for the attenuation in a beam hardener designed to remove photons of energies less than a few MeV[3]).

For bubble chamber work the position of the interaction—and hence the final angle of the photon—will normally be very well known. This feature eliminates one of the main uncertainties in the energy of the annihilation photon. Consider the 1 GeV positron beam. This has an overall energy spread of $\pm$ 15 MeV. In a 1 g/cm^2 hydrogen converter, the r.m.s. small angle scatter is $\pm$ 0.0012 rad. Assuming an angular divergence corresponding to a transverse momentum of 2 MeV/c, an angle of $\pm$ 0.002; and a beam area of 1 sq cm, $\pm$ 0.001 at 5 m; and noting that the photon energy change from 700 to 800 MeV corresponds to an angular change of 0.005 rad we would have a final energy resolution of $\pm$ 40 MeV. Using the postulated positron beam, we could reduce the thickness of the hydrogen target—thus at the same time reducing the relative contribution of "indirect" bremsstrahlung and improving the energy resolution—and also improve the positron beam geometry. In this case, we could reasonably expect a photon energy resolution for photons in the annihilation beam of $\pm$ 20 MeV in the 700 to 800 MeV band and $\pm$ 50 MeV in the 3.4 to

3.5 GeV band. As most of the high energy events would be produced by annihilation rather than bremsstrahlung photons, the spectrum of photons/MeV being at least 25 times that of the surrounding bremsstrahlung, this information should be very valuable. We also see the possibility of choosing the energy range over which to work rather than having to measure everything and attempting to sort out a complete picture.

Measurement of some of the electron pairs should give a good calibration of the energy and flux of the photons.

As a guide to the rate of events to be expected, 100 photons/picture in 50 cm of hydrogen would produce 1 event/5000 pictures for a 1 μb/nucleon cross section, and of course double this rate in deuterium. While these rates are admittedly low, there seems little possibility at present of stydying many of the "strange particle" photoproduction reactions in any other way.

Acknowledgements

I would like to acknowledge my debt to Professor S. Devons for putting me on the track of ideas connected with accelerators; also to Professor J. Gunn of Glasgow University and Dr. M. Umezawa of Manchester University for their interest and discussions.

NUCLEAR INSTRUMENTS AND METHODS 10 (1961) 217–223; NORTH-HOLLAND PUBLISHING CO.

MONOCHROMATEUR DE POSITRONS EN SECTEUR D'ORANGE

C. SCHUHL et C. TZARA

C.E.N. Saclay, Gif-sur-Yvette (S & O)

Reçu le 21 octobre 1960

An orange-sector monochromator of positrons is described. The paths of the electrons and the shape of the magnets are calculated. This monochromator is calculated to obtain monochromatic photons by annihilation in flight of the positrons. The experimental results are in good agreement with the calculus.

1. Motif du Choix d'un Aimant en Secteur d'Orange

Des photons monochromatiques d'énergie continûment variable peuvent être obtenus par annihilation en vol de positons monoénergétiques[1,2]). Ces positons sont produits par cascade à partir d'un faisceau d'électrons d'environ 30 MeV qui heurte une cible de platine d'une épaisseur de l'ordre d'une longueur de radiation. A la sortie de la cible de platine, en plus des photons et des électrons, nous obtenons un spectre continu de positons très divergents. Il importe donc que le monochromateur magnétique possède une transmission élevée tout en conservant une grande simplicité. C'est la raison pour laquelle nous avons choisi le type en "secteur d'orange"[3]) défini par deux pièces polaires planes non parallèles et telles que leur intersection contienne les points objet et image. Enfin certaines des données ont été imposées pour permettre l'utilisation d'un circuit magnétique déjà existant.

La première fonction du monochromateur est d'isoler un faisceau monoénergétique de positons. Ce rôle est rempli par un premier secteur magnétique suivi d'une fente réglable. Pour que le faisceau de photons finalement obtenu ne soit pas noyé dans le rayonnement de freinage produit jusqu'au niveau de la fente, un deuxième secteur magnétique, dont la pièce polaire a la même forme à l'entrée que le premier, reprend le faisceau de positons et le dévie.

Le système des deux aimants a dû être choisi symétrique par rapport à la fente pour des raisons d'encombrement du local où ils sont installés alors que la symétrie par rapport à un plan eût été préférable pour l'optique du système. La cible de lithium où a lieu l'annihilation est située au sein du champ magnétique et sa forme est telle que les tangentes aux trajectoires convergent en un point. Ces tangentes sont les axes des faisceaux de photons issus des divers points de la cible. De cette manière, on obtient l'intensité maximum de photons dans une certaine surface autour du point de convergence. Le calcul de forme de la cible n'a pas à être corrigé d'effet de champ de fuite. Le seul changement de la forme de la cible de lithium permet de modifier à volonté le point de convergence du faisceau. Le champ du deuxième secteur se prolonge au-delà de cette cible et les positons qui la traversent sans subir d'interaction radiative sont refocalisés aussi loin que possible du faisceau de photons pour que le rayonnement qu'ils émettent ne puisse atteindre la zone utile.

2. Optique d'un Champ en Secteur d'Orange

2.1. EQUATION DU MOUVEMENT

Le champ magnétique ne dépend que de la distance r à l'axe Oz (fig. 1). Le travail du champ magnétique H est une constante entre les deux pôles P et P′:

$$\int_{P}^{P'} \boldsymbol{H}\cdot \mathrm{d}\boldsymbol{l} = \theta r H = \text{constante}\,. \qquad (1)$$

[1]) C. Tzara, Rapport C.E.A. no. 814; C.R. **245** (1957) 56.

[2]) J. Miller, C. Schuhl, G. Tamas et C. Tzara, C.R. **249** 2543 (1959).

[3]) O. Kofoed-Hansen, J. Lindhard et O. B. Nielsen, Kgl. Danske Vidensk. Selsk. Mat. Fys. Med. **25** no. 16 (1950).

La variation de l'induction en fonction du rayon s'écrit:

$$B = \alpha/r \,. \tag{2}$$

Le rayon de courbure de la trajectoire d'un

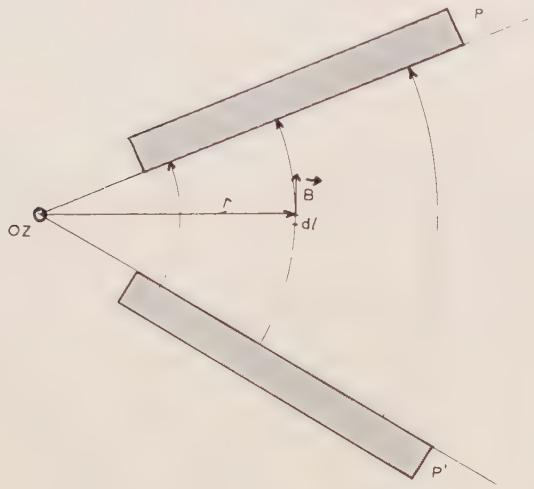

Fig. 1. Aimant en secteur d'orange.

électron d'impulsion p est, à la distance r de l'axe Oz:

$$\rho = \frac{cp}{eB} = br \,. \tag{3}$$

Si l'on pose

$$b = \frac{cp}{e\alpha} \,. \tag{4}$$

l'équation de la trajectoire dans un plan passant, par l'arête du dièdre des deux faces polaires s'écrit

$$\rho \frac{\mathrm{d}^2 r}{\mathrm{d}z^2} = \left[1 + \left(\frac{\mathrm{d}r}{\mathrm{d}z}\right)^2\right]^{\frac{3}{2}} = -br \frac{\mathrm{d}^2 r}{\mathrm{d}z^2} \,. \tag{5}$$

La solution de l'équation (5) peut se mettre sous la forme

$$z = z_0 + \int_{r_0}^{r} \frac{\log \dot{r}/a}{\sqrt{b^2 - (\log r/a)^2}} \,\mathrm{d}r \tag{6}$$

où a est une constante qui correspond à la valeur de r pour laquelle $\mathrm{d}r/\mathrm{d}z = \infty$ et b est défini par la relation (4). Remarquons que lorsque a et b sont déterminés, r varie entre $r_{\max} = a\mathrm{e}^{b}$ et $r_{\min} = a\mathrm{e}^{-b}$.

Si nous choisissons un système de coordonnées tel que $r = r_{\max}$ pour $z = 0$, en ne nous intéressant qu'à l'arc ABC, la solution (6) devient:

$$u = \int_{\mathrm{e}^{b}}^{t} \frac{\log t}{\sqrt{b^2 - (\log t)^2}} \,\mathrm{d}t \tag{7}$$

où $u = z/a$ et $t = r/a$.

Cette dernière expression montre que toutes les trajectoires qui correspondent à une certaine valeur de b, c'est-à-dire à une impulsion de particule et à un courant magnétisant donnés et qui ont leurs tangentes parallèles à l'axe des z pour $z = 0$ sont homothétiques par rapport à O. Il suffit donc de calculer la trajectoire pour la valeur $a = 1$ que nous appellerons *"trajectoire réduite"*.

2.2. PRINCIPE DU CALCUL DES TRAJECTOIRES

Posons

$$F(t) = \frac{\log t}{\sqrt{b^2 - (\log t)^2}} \,. \tag{8}$$

Nous pouvons calculer $F(t)$ et intégrer $F(t)\,\mathrm{d}t$ graphiquement. Nous nous limiterons

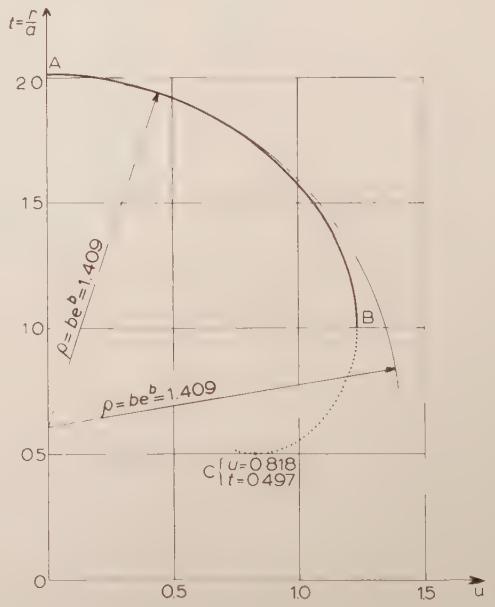

Fig. 2. Trajectoire réduite $u = f(t)$ pour $b = 0.7$.

au calcul de l'arc AB (fig. 2) c'est-à-dire t variant de e^{b} à 1. Pour t voisin de e^{b} l'intégration est difficile car $F(t)$ tend vers l'infini.

Au voisinage de $t = e^b$ nous pouvons calculer l'intégrale. Posons

$$t = e^{(1-\varepsilon)b} \quad \text{où} \quad \varepsilon \ll 1 , \tag{9}$$

Dans ces conditions

$$u = \int_{\varepsilon=0}^{\varepsilon_1 = 1 - \frac{1}{b}\log\tau} - \frac{b\,(1-\varepsilon)}{\sqrt{1-(1-\varepsilon)^2}}\, e^{(1-\varepsilon)b}\, d\varepsilon \tag{10}$$

ou, en tenant compte du fait que $\varepsilon \ll 1$,

$$u \simeq \tilde{u} = b\, e^b \sqrt{2\left(1 - \frac{\log\tau}{b}\right)} = b\, e^b \sqrt{2\varepsilon_1} . \tag{11}$$

Il suffit ensuite de calculer

$$u = \tilde{u} + \int_\tau^t F(t)\, dt . \tag{12}$$

Nota: Quelle erreur fait-on sur u en calculant l'intégrale de cette manière? Nous pouvons évaluer l'erreur sur $F(\varepsilon)$. En effet:

$$F(\varepsilon) = \frac{1-\varepsilon}{\sqrt{1-(1-\varepsilon)^2}} \tag{13}$$

alors que pour le calcul nous posons

$$\tilde{F}(\varepsilon) = \frac{1}{\sqrt{2\varepsilon}} . \tag{14}$$

L'erreur relative faite sur la valuer de $F(\varepsilon_1)$ est, dans ces conditions, égale à

$$\frac{\tilde{F}(\varepsilon_1) - F(\varepsilon_1)}{F(\varepsilon_1)} \simeq \tfrac{3}{4}\varepsilon = \tfrac{3}{4}\left(1 - \frac{\log\tau}{b}\right). \tag{15}$$

La valeur de $\tilde{F}(\tau)$ calculée par l'approximation est donc majorante.

2.3. CONDITIONS INITIALES

a. Nous admettons un arrangement des orbites symétrique, c'est-à-dire que toutes les trajectoires auront leurs tangentes parallèles à Oz dans le plan $z = 0$.

b. Nous imposons comme conditions:

$r = 50$ cm pour la trajectoire moyenne pour $z = 0$;

la source de positons à 75 cm de l'axe Or; l'image de la source dans le premier aimant à 75 cm de Or également. Le second aimant dont l'entrée est identique à celle du premier est dissymétrique comme nous le verrons par la suite.

c. Nous avons choisi pour b la valeur 0.7.

2.4. CALCUL DES TRAJECTOIRES DES POSITONS

a. *Trajectoire réduite*: toutes les trajectoires peuvent être calculées à partir de la donnée $b = 0.7$ qui fournit

$$\begin{aligned} b &= 0.7 \\ e^b &= 2.013753 \\ e^{-b} &= 0.496585 \\ \rho &= bt \\ \rho_{max} &= b\, e^b = 1.409527 . \end{aligned}$$

$F(t)$ est représenté sur la figure 3 jusqu'à la valeur $t = \tau = 1.9$ qui correspond à une valeur de $\tilde{u}$ égale à

$$\tilde{u} = b\, e^b \sqrt{2\varepsilon_1} = 0.5748 . \tag{16}$$

Nous avons montré que la valeur de

$$\tilde{u} = \int_0^{\varepsilon_{lim}} F(\varepsilon)\, d\varepsilon$$

était approchée par excès. Au premier ordre,

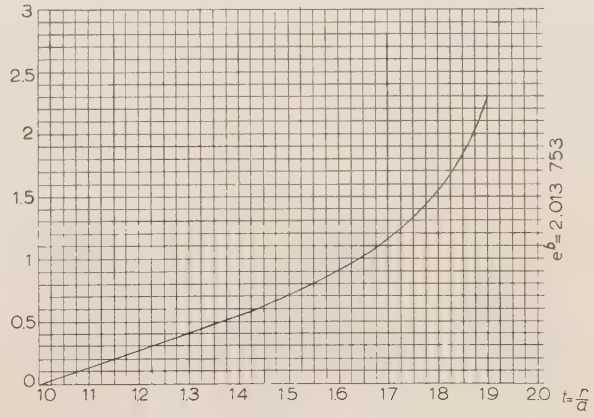

Fig. 3. $F(t)$ avec $b = 0.7$.

l'erreur sur $\tilde{u}$ est la moitié de l'erreur correspondant à ε_{lim} soit, d'après (15)

$$\tfrac{3}{8}\,\varepsilon_{lim} = 0.031 \tag{17}$$

d'où

$$\tilde{u}_{corr} = 0.5748\,(1 - 0.031) = 0.5571 . \tag{18}$$

Nous en déduisons la courbe $u = f(t)$ en intégrant graphiquement $F(t)$. Les résultats sont représentés sur le tableau 1 et la figure 2.

TABLEAU 1
Calcul de la trajectoire réduite

t	$F(t)$	u
2.013 75		0
1.9	2.299	0.5571
1.8	1.547	0.7432
1.6	0.9064	0.9794
1.4	0.5480	1.1226
1.2	0.2698	1.2046
1.0	0	1.2321

b. Réseau de trajectoires: A partir de la trajectoire réduite nous obtenons aisément toutes les autres trajectoires à partir des définitions de $u = r/a$ et $t = z/a$. Pour la trajectoire moyenne par exemple comme r_0 $(z = 0) = 50$ cm, nous calculons pour a la valeur

$$a = r_0 \, e^{-b} = 24.829 \text{ cm.} \qquad (19)$$

L'ensemble du réseau des trajectoires pour r_0 variant entre les valeurs 30 cm ($a = 14.298$ cm) et 65 cm ($a = 32.278$ cm) est représenté sur les figures 4 et 5.

3. Forme des Pièces Polaires des Aimants

3.1. FORME THEORIQUE

La forme des pièces polaires est définie par le lieu des points de contact des réseaux des tangentes issues des points objet et image désirés au réseau de trajectoires des positons correspondant à diverses valeurs de a (voir fig. 4 et 5). Rappelons que, pour le premier aimant, les points image et objet correspondent aux valeurs de $z_1 = \pm 75$ cm et pour le second aimant, si la position de l'objet est également à $z_2 = -75$ cm, l'image se situe à $z'_2 = 50$ cm.

3.2. EFFET DU CHAMP DE FUITE

Il est très difficile de calculer exactement l'influence du champ de fuite. Comme l'angle d'ouverture du secteur d'orange est relativement faible (demi angle égal à 6×10^{-2} radian) nous avons admis que l'effet du champ de fuite était équivalent à $0.8e$ le long de chaque trajectoire, e étant la valeur de l'entrefer au point considéré. D'où les formes choisies représentées sur les figures 4 et 5.

TABLEAU 2
Réseau des trajectoires

$r = 30$ cm; $a = 14.898$		$r = 35$ cm; $a = 17.380$		$r = 40$ cm; $a = 19.864$		$r = 45$ cm; $a = 22.346$	
$r = at$	$z = au$	$r = at$	$z = au$	$r = at$	$z = au$	$r = at$	$z = au$
30.00	0	35.00	0	40.00	0	45.00	0
28.306	8.300	33.022	9.682	37.742	11.066	42.457	12.449
26.816	11.072	31.284	12.917	35.755	14.763	40.223	16.608
23.837	14.591	27.808	17.022	31.782	19.455	35.754	21.886
20.857	16.724	24.332	19.511	27.810	22.300	31.284	25.086
17.878	17.946	20.856	20.936	23.837	23.928	26.815	26.918
14.898	22.195	17.380	21.414	19.864	24.474	22.346	27.533

$r = 50$ cm; $a = 24.829$		$r = 55$ cm; $a = 27.312$		$r = 60$ cm; $a = 29.795$		$r = 65$ cm; $a = 32.278$	
$r = at$	$z = au$	$r = at$	$z = au$	$r = at$	$z = au$	$r = at$	$z = au$
50.00	0	55.0	0	60.00	0	65.00	0
47.175	13.832	51.893	15.216	56.610	16.599	61.328	17.982
44.692	18.453	49.162	20.298	53.631	22.144	58.100	23.989
39.726	24.318	46.699	26.749	47.672	29.181	51.645	31.613
34.761	27.873	38.237	30.660	41.713	33.448	45.189	36.235
29.794	29.909	32.774	32.900	35.754	35.891	38.734	38.882
24.829	30.592	27.312	33.651	29.795	36.710	32.278	39.770

Remarquons que, dans le cas des aimants à faces parallèles, l'effet du champ de fuite est évalué $0.7e$ et $0.8e$ suivant les auteurs. Nous avons choisi la valeur la plus grande afin de surestimer les fuites pour les corriger par addition de fer aux pièces polaires, technique plus aisée que de meuler des pièces polaires trop grandes.

3.3. RESOLUTION THEORIQUE

Par la même méthode graphique la résolution du premier aimant est trouvée égale à

$$R = 83/\delta \qquad (20)$$

où δ est l'ouverture de la fente en centimètre.

3.4. FORME DE LA CIBLE DE LITHIUM

La forme de la cible de lithium est la forme théorique qu'aurait la face de sortie du second aimant pour focaliser les positons à 1.50 m, 2 m ou 2.50 m. Pratiquement les trajectoires des positons entre l'axe $z = 0$ et la cible de lithium se confondent avec des cercles, ce qui facilite le calcul de la forme de la feuille de lithium.

Nous savons que $\rho = br$, d'où

$$s = \rho \sin\theta = br \sin\theta\,, \qquad (21)$$

$$\sin\theta = \frac{r/L}{(1-b)^2\,(r/L)^2 + 1} \cdot \left\{ b + (1-b)\ \sqrt{1 - (2b-1)\ (r/L)^2} \right\} \qquad (22)$$

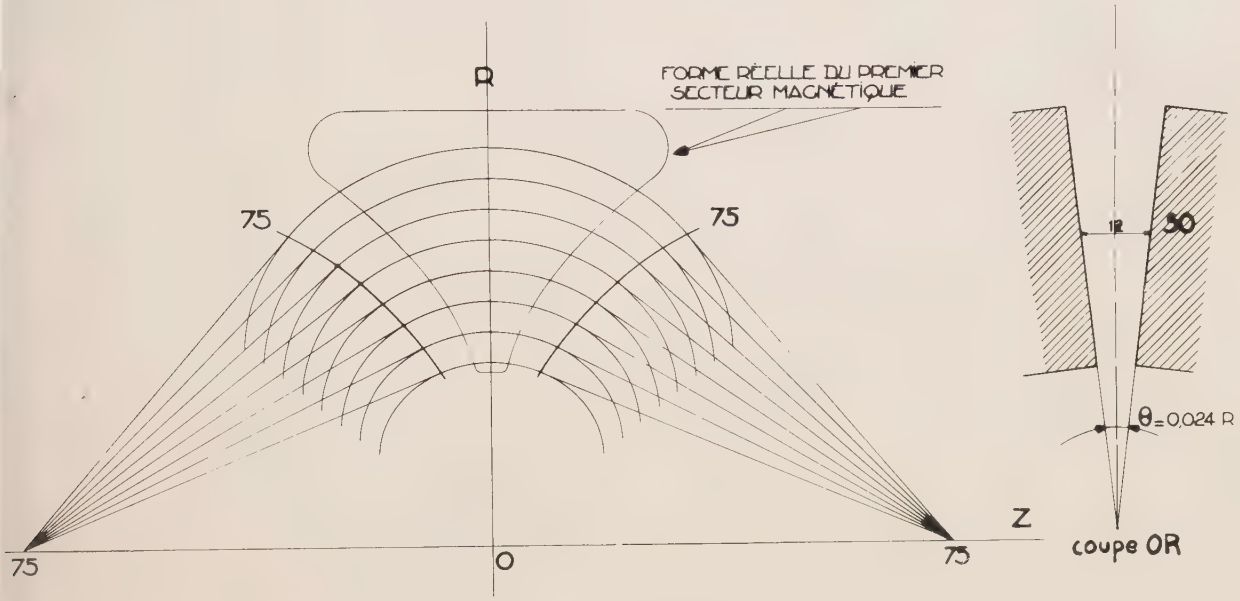

Fig. 4. Trajectoires dans le premier secteur magnétique.

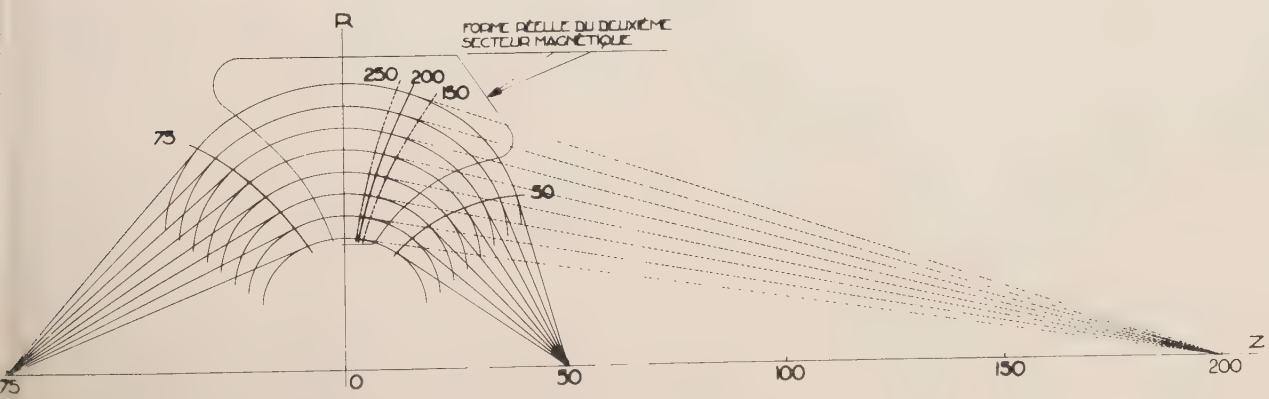

Fig. 5. Trajectoires dans le second secteur magnétique.

et par suite

$$s = \frac{b r\, r/L}{(1-b)^2 (r/L)^2 + 1} \cdot \left\{ b + (1-b)\sqrt{1-(2b-1)(r/L)^2} \right\} \quad (23)$$

et dans notre cas où $b = 0.7$

$$s = \frac{0.7\, r\, r/L}{0.09 (r/L)^2 + 1} \left\{ 0.7 + 0.3\sqrt{1-0.4\,(r/L)^2} \right\} \quad (24)$$

qui s'écrit en fait

$$s \simeq 0.7\, r\, r/L - 0.10\, r\, (r/)L^3 .$$

TABLEAU 3
Forme de la cible de lithium

	Distance de focalisation désirée		
	$L = 150$	$L = 200$	$L = 250$
r	s	s	s
30	4.20	3.15	2.52
35	5.70	4.29	3.43
40	7.46	5.59	4.48
45	9.42	7.08	5.66
50	11.61	8.73	6.99
55	14.08	10.57	8.46
60	16.74	12.57	10.07
65	19.62	14.76	11.81

L, r et s sont exprimés en cm.

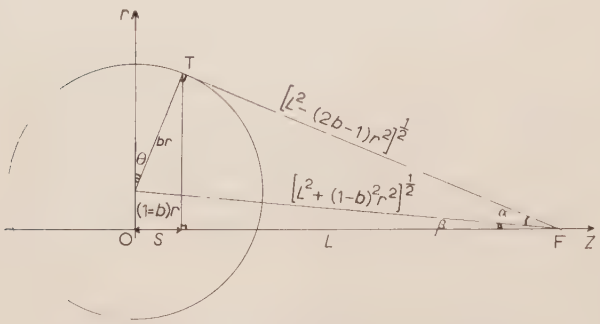

Fig. 6. Calcul de la forme de la cible de lithium.

4. Réalisation du Monochromateur

4.1. DESCRIPTION

Le monochromateur de positons (fig. 7) comprend, en plus des pièces polaires dont nous venons de calculer les formes:

a. une cible de platine qui reçoit le faisceau d'électrons primaire de l'accélérateur linéaire. Cette cible doit être escamotable afin de pouvoir utiliser directement le faisceau d'électrons.

b. un système de lèvres mobiles qui doit être l'image de la cible de platine à travers le premier aimant et l'objet du second aimant.

c. un ensemble de boîtes à vide, non magnétiques et terminées à l'entrée comme à la sortie du faisceau par des fenêtres minces f_1 et f_2 pour que la diffusion multiple des électrons soit la plus faible possible

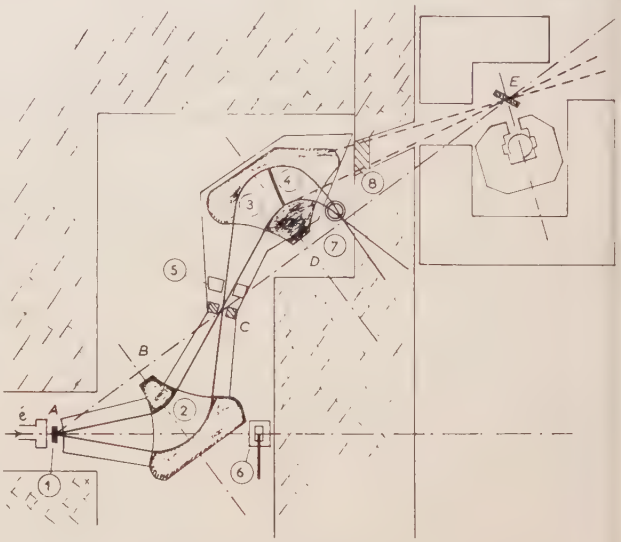

Fig. 7. Monochromateur de positons: 1. Cible de platine; 2. Premier secteur; 3. Second secteur; 4. Cible de lithium; 5. Collimateur de plexiglass; 6. et 7. Chambres d'ionisation; 8. Filtre d'aluminium; c. Fente réglable; E. Lieu de convergence des photons.

4.2. DETAILS DE FABRICATION

a. La cible de platine est soutenue par un bras de levier fixé sur la première boîte à vide ce qui permet de l'escamoter facilement.

b. La feuille d'entrée f_1 est en aluminium de $\frac{2}{10}$ mm d'épaisseur et la feuille de sortie f_2 est en mylar de $\frac{5}{10}$ mm d'épaisseur.

c. Les boîtes à vide sont en acier inox.

d. La fente est un rodage conique bronze-acier doux percé d'un trou rectangulaire et sert également de vanne. La largeur de la fente équivalente est réglée par l'angle de rotation du rodage suivant la formule

$$\delta = 6.75 \sin (36° - \theta) \text{ cm.} \quad (25)$$

e. Après la fente se trouve un collimateur de plexiglass réduisant la section du faisceau de positons entrant dans le deuxième aimant, de sorte que les positons marginaux, générateurs de rayonnement de freinage ne puissent atteindre la paroi de la deuxième boîte à vide.

g. Les bobinages des aimants sont alimentés par un groupe de 10 kW régulé en tension à mieux de 0.2%.

5. Caractéristiques Expérimentales du Monochromateur

5.1. VERIFICATION DE LA LOI DU CHAMP EN α/r ET COMPARAISON DES DEUX AIMANTS

Nous avons mesuré le champ magnétique en fonction de la distance radiale dans le plan $z = 0$, pour deux valeurs de l'intensité dans les bobines soit 30 A et 60 A; la mesure était effectuée avec une sonde à effet Hall.

Les deux aimants sont donc identiques à mieux que 1% sans qu'aucune correction n'ait été effectuée et les quantités $H_1 r$ et $H_2 r$ sont pratiquement constantes.

Tableau 4
Vérification de la loi en $1/r$ pour le champ magnétique des aimants

I_{aimant} (ampère)	r (mm)	H_1 (gauss)	$H_1 r$ (gauss·cm)	H_2 (gauss)	$H_2 r$ (gauss·cm)
30	370	1435	53100	1434	53050
	470	1135	53300	1122	52700
	570	935	53300	932	53100
60	370	2860	105800	2836	104900
	470	2270	106700	2240	105300
	570	1886	107500	1880	107200

5.2. POSITION DES IMAGES DE LA CIBLE DE PLATINE

Le faisceau primaire d'électrons est relativement large. La tache obtenue sur la cible de platine est de l'ordre de 10 mm de diamètre. Nous avons mesuré la dimension du faisceau de positons à la sortie de la seconde boîte à vide. Nous obtenons 95 mm pour 100 mm calculés.

Nous avons de même recherché la direction des tangentes aux trajectoires d'électrons issus directement de l'accélérateur linéaire au niveau de la cible de lithium en irradiant des émulsions radiographiques placées à des distances différentes avec le spectre de freinage des électrons dans l'aluminium. La mesure de la densitométrie des émulsions permet de déterminer l'axe moyen du faisceau de gamma de freinage qui est le même que celui du faisceau d'annihilation. L'intersection de cet axe et de la droite passant par le platine et la fente détermine le point de convergence des photons.

6. Conclusion

L'ensemble de l'appareillage s'est avéré répondre au but que nous lui avions fixé, c'est-à-dire nous permettre d'obtenir un faisceau de photons monochromatiques d'énergie variable et d'intensité suffisante pour les utiliser dans l'étude de leur interaction avec les noyaux[4]).

[4]) J. Miller, C. Schuhl, G. Tamas et C. Tzara, Karlsruhe Photonucl. Conf. 1960; J. Phys. Radium (lettre) **21** (1960) 755.

NUCLEAR INSTRUMENTS AND METHODS **10** (1961) 224–228; NORTH-HOLLAND PUBLISHING CO.

A HIGH GAIN IMAGE INTENSIFIER SYSTEM WITH FAST SHUTTER ACTION FOR APPLICATION IN HIGH ENERGY PHYSICS

G. GOETZE and H. KANTER

Westinghouse Research Laboratories Pittsburgh 35, Pennsylvania

Received 24 October 1960

A high speed camera system employing two Transmission Secondary Electron Intensifiers in tandem is described. This camera is capable of recording the light emission of single photoelectrons on photographic film. Possible applications of this instrument in high energy physics are discussed.

1. Introduction

The development of direct viewing high gain image amplifiers has reached a point where their use for certain applications in high energy physics has become attractive. Thus, it has recently become possible to obtain photographs of nuclear particle tracks in solid scintillators with the aid of multistage image intensifiers[1–4]). Solid scintillators are particularly desirable for high energy physics because of their fast response and extremely short recovery time. Image intensifiers which permit photographic recording of nuclear tracks in such "luminescent chambers" also appear to be useful in determining the velocity of high energy particles from their Čerenkov radiation pattern and in monitoring the profile of low intensity particle beams. The essential problem in all these applications is the registration of very low light intensities, corresponding to only a few photons per unit area of the photo-sensitive surface. For image intensifiers the theoretical performance limit is the registration of single photoelectrons. The purpose of this paper is to describe a fast acting camera system capable of single photoelectron registration, employing a new type of image amplifier that utilizes transmission secondary electron emission from thin insulating films recently developed in our laboratories[5]). The theoretical performance of the system was checked by obtaining photographs of minimum ionization cosmic ray tracks in NaI(Tl)-crystals.

2. Principle of Track Camera System

The camera system described in the present paper involves the use of two direct-viewing image intensifiers of the transmission secondary electron emission type operating in cascade, followed by an ordinary 35 mm camera. The first tube serves primarily to store the image of the desired event and the second tube acts both as amplifier and high-speed electronic shutter.

The amplifying action in the tubes employed in the camera system is based on the fact that electrons of a few kilo-volts can eject a relatively large number of slow secondary electrons from the exit side of a thin insulating foil[6]). Each tube employs 4 thin film dynodes covered with aluminum on the entrance side and a layer of high secondary electron yield on the exit side. An electron emitted from the photocathode is accelerated towards the first dynode, impinging with sufficient energy to release several secondaries at the exit side of the film while being stopped in the insulator. The slow secondaries

[1]) E. K. Zaviosky, M. M. Butslov, A. G. Plakhov and G. E. Smolkin, J. Nuclear Energy **4** (1957) 340.

[2]) L. W. Jones, K. Lai, R. Newsome and M. L. Perl, IRE Transactions on Nuclear Science **7** (1960) 145.

[3]) G. T. Reynolds, IRE Transactions on Nuclear Science **7** (1960) 115.

[4]) K. Lande, A. K. Mann, K. Reibel and D. H. White, IRE Transactions on Nuclear Science **7** (1960) 121.

[5]) Westinghouse "ASTRACON" WX 4342; M. M. Wachtel, D. D. Doughty, G. Goetze, A. E. Anderson, E. J. Sternglass, Rev. Sci. Instr. **31** (1960) 576.

[6]) E. J. Sternglass, Rev. Sci. Instr. **26** (1955) 1202.

are again accelerated to the next dynode, where this process is repeated. The electrons emitted from the last dynode are accelerated by a high potential to strike a phosphor, so that image intensification is achieved both by electron multiplication and final acceleration. Focusing is accomplished by an axial magnetic field of about 500 gauss. The operating voltage is 4 kV per stage, with 15 kV between the last stage and the phosphor. Under these conditions, the photon gain for the tubes used was measured to be 10^4. Gating of the second intensifier can be accomplished by applying the full operating voltage to the photocathode to first dynode stage. In order to achieve the lowest possible dark current, it is desirable to hold the photo cathode at ground potential since this minimizes the possibility of corona discharges in the neighborhood of the cathode which can give rise to additional dark current. The resolving power of the particular tubes used was 12 line pairs/mm across an image diameter of 25 mm. The combined resolution of the whole camera system was 7 line pairs/mm or 175 resolvable picture elements over the useful image diameter.

3. Details of Intensifying System

Referring to fig. 1, the light produced along the path of a particle traversing a scintillation crystal is imaged by a mirror system onto the photocathode of the first intensifier. The output of the first intensifier is optically coupled to the second intensifier by a standard lens pair in a front-to-front arrangement. (Two Zeiss Biotar lenses, $f1.5/75$ mm.) This second intensifier is operated only for a short time interval whenever a desired event occurs in the crystal. In the particular experiment described a photomultiplier in optical contact with the crystal triggers a pulse generator which then delivers a gate pulse to the second intensifier†. During the gate time, the track image that appears on the output of the first tube is further intensified by the second tube in order to record it on photographic film.

† In an actual experimental situation, the monitoring photomultiplier would be replaced by a suitable coincidence-counter arrangement.

The phosphor of the first tube must be designed to store the information long enough to permit operation of the gate circuit. To utilize the full light emission of this phosphor, the gate-time is

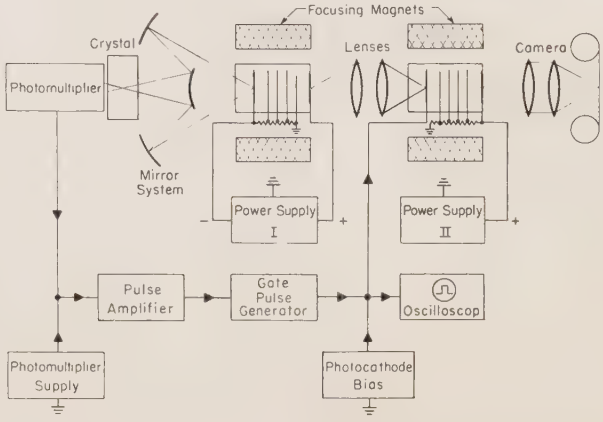

Fig. 1. Block diagram of image intensifier system.

made somewhat longer than the decay time of the phosphor. Since tubes with a P-11-type (ZnS:Cd) phosphor were used, the gate-time was chosen to be 1 msec. Shorter gate times, down to several μsec, are feasible with other phosphors. The output of the second intensifier is photographed on Ansco Super Hypan film, using an Exacta Camera with a similar lens pair as for the interstage coupling.

Light flashes due to single electrons released at the first photocathode were readily recorded as bright spots on the film. The fact that these flashes actually represent single photoelectrons was verified as follows. The output dark current of the first tube was measured and divided by the known electron gain. The resulting calculated number of electrons leaving the photocathode per second was compared with the observed flash population per second on the output screen and was found to agree within a factor of 1.5.

The number of recorded light dots per cm of track image can be estimated from the number of photons emitted per cm of track in the scintillation crystal, the light collection of the input optics, and the photocathode efficiency of the first tube. The geometric light collection of the front optics can be calculated using the approximate relation

$$L \approx [16\, Q^2\, n^2\, (1 + M)^2]^{-1}$$

where Q is the f-number of the front optics (focal length/lens diameter), n is the index of refraction of the scintillator, and M is the minification ratio. An $f/1.2$ mirror was used instead of a lens to avoid the light losses due to absorption. The minification used was 2, and the index of refraction of the sodium iodide crystal is 1.78. Therefore, the light collection of the input optics was calculated to be 1.5×10^{-3}. With an emission of 10^5 photons per cm of track for a minimum ionizing particle in a NaI (Tl)-crystal, it follows that only 300 photons per cm of track arrive at the photocathode of the first tube. The quantum efficiency of the photocathode for the blue light emitted by the crystal could not be determined accurately, but was estimated to be about 5%. One should therefore expect of the order of 15 photoelectrons per cm of track to be released at the photocathode. Actual track pictures of cosmic-ray particles obtained with this system as shown in figs. 2 and 3, show about 7 dots per cm, in reasonable agreement with the calculated value.

Fig. 2. Photograph of particle track.

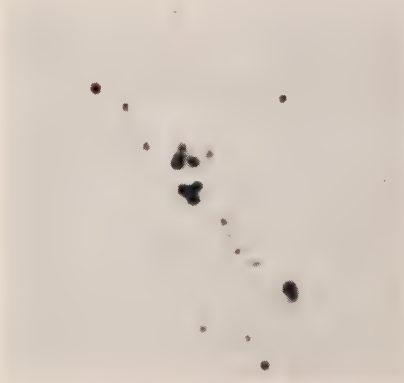

Fig. 3. Photograph of particle track.

Well-focused track pictures appearing as a straight line of dots such as reproduced in fig. 2 can only be expected if the particle track stays within the focal plane of the front optics. Whenever the track lies outside the focal plane, a "blurred" image appears, consisting of dots distributed over a certain band rather than along a straight line (fig. 3). The useful volume for a well-focused image depends on the acceptance angle of the input optics. A larger depth of focus is only feasible with a sacrifice in light collection. The limited depth of focus represents a certain serious disadvantage in most applications. The limitation may be overcome by the use of scintillators consisting of plastic fibers[7]). In such crystals, the light produced anywhere along the length of the fiber is piped to the end face so that a lens with shallow depth of focus can be used. When the area of the crystal end face is not too large, and greater light collection is desired, the fibers may be brought into direct contact with the photocathode of the image intensifier by the use of a vacuum-tight fiberglass input window†.

An over-all view of the whole camera system is shown in fig. 4. The length of the system is about 1 m, the width 25 cm, and the height 30 cm. Once the magnetic field and the individual dynode voltages have been adjusted to achieve optimum focusing, readjustments are made by controlling the operating voltage. The system has been operated successfully over periods of many hours without noticeable change of focus or overall gain. The relative insensitivity to stray magnetic fields of this type of tube was found to be a distinct advantage. Even the presence of

† At present, image tubes with fiberglass input windows 10 cm in diam are commercially available. (Westinghouse FLUOREX WX 4481.)

[7]) G. E. Reynolds, Nucleonics **16** (June 1958) 60.

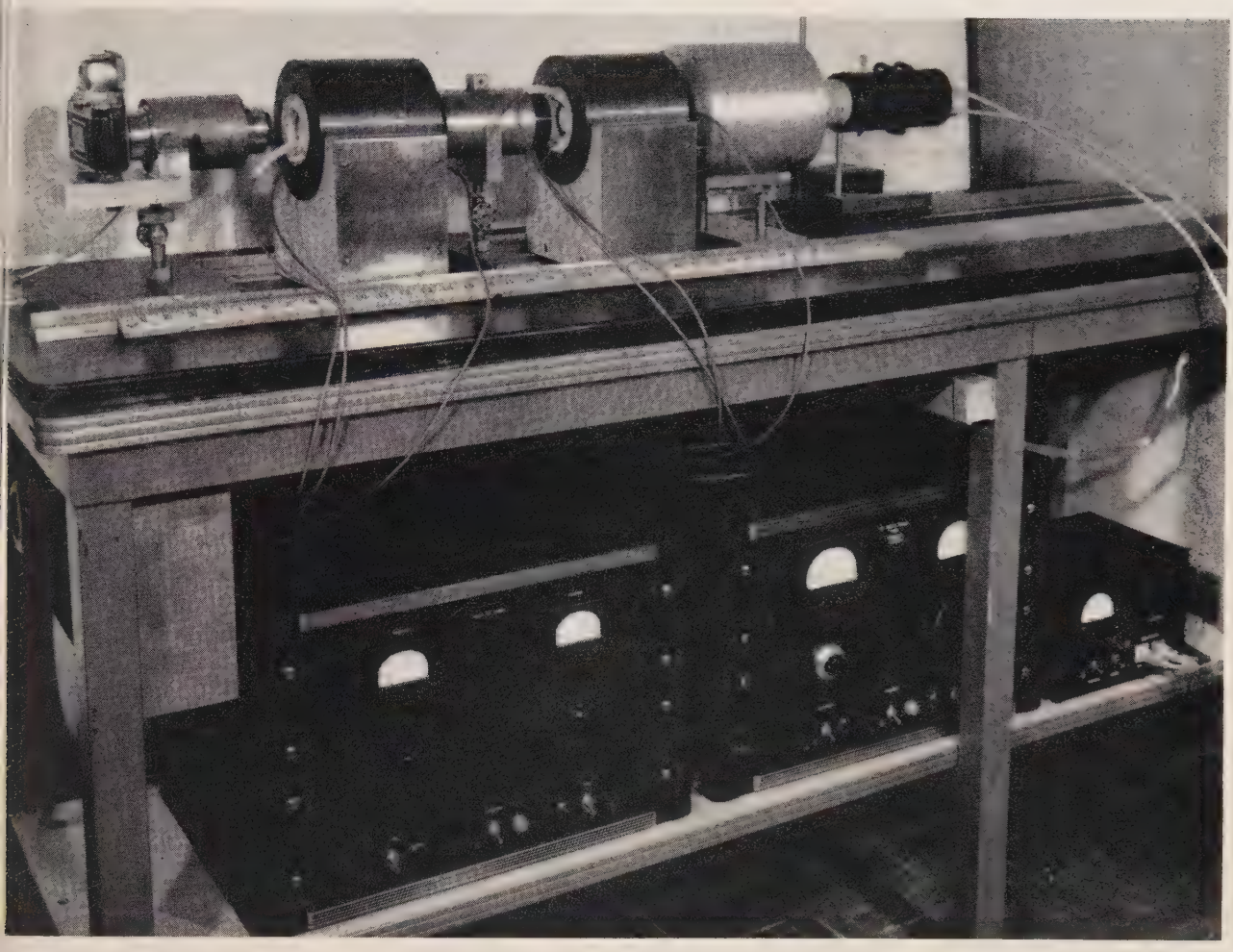

Fig. 4. Over-all view of image intensifier system.

rather strong stray magnetic fields can be compensated for by aligning the tube axis with the field lines and adjusting of the magnets until the focus is restored.

4. Discussion

The performance of the experimental system may be considerably enhanced by improved light coupling techniques at the input. This might be achieved by the use of larger scintillators coupled to an ordinary image-intensifier of large cathode diameter and small output phosphor as a first stage††. Even in its present form, the system might be very helpful for certain special applications. For example, monitoring of the low intensity secondary beams produced by high energy accelerators is feasible, thus greatly facilitating the adjustment of beam focusing magnets. The possibility of operating such systems for very short time intervals can be utilized to reduce the background illumination in viewing pulsed beams, which otherwise might be swamped out by the background illumination. Another possible application is the photography of Čerenkov radiation emitted by high-speed particles, which can be focused as a ring shaped image onto the photocathode of the intensifier[8]). The resolution of the system is good enough to permit a determination of the particle velocity and direction from the diameter and the position of the photographed image.

[8]) A. Roberts, Nucl. Instr. and Meth. **9** (1960) 55.

5. Conclusion

The characteristics which make transmission secondary emission image intensifiers particularly useful in high energy physics may be summarized as follows:

1. Sufficient gain to record each photoelectron released at the input photocathode.
2. Low dark current level.
3. High speed of response.
4. Small image distortion even in the presence of stray magnetic fields.
5. Relatively small size and weight.
6. Ease of operation.

Acknowledgement

The authors are indebted to Mr. A. E. Anderson and Drs. R. Siegel and E. J. Sternglass for their continuous interest and support.

NUCLEAR INSTRUMENTS AND METHODS **10** (1961) 229–230; NORTH-HOLLAND PUBLISHING CO.

CIRCUIT A PLUSIEURS ETATS STABLES UTILISANT DES DIODES TUNNEL

Y. HAZONI

S.M.N.F., C.E.N., Saclay, Gif-sur-Yvette (S & O)

Reçu le 6 septembre 1960

A four stable states circuit had been realized utilizing tunnel diodes.

The time needed for a change of state is of the order of 10^{-8} s. Thus, the circuit could serve as a fast prememory for a classical multichannel analyzer; being able to count recurrent pulses having repetition rate up to 40 MHz, it could serve also as the basic unit for the address scaler associated with such analyzers.

Nous avons réalisé un circuit à 4 états stables utilisant des diodes tunnel. Le temps nécessaire pour passer d'un état stable au suivant est de l'ordre de 10^{-8} seconde.

PRINCIPES DE FONCTIONNEMENT

La courbe caractéristique courant-tension d'une diode-tunnel est représentée sur la figure 1.

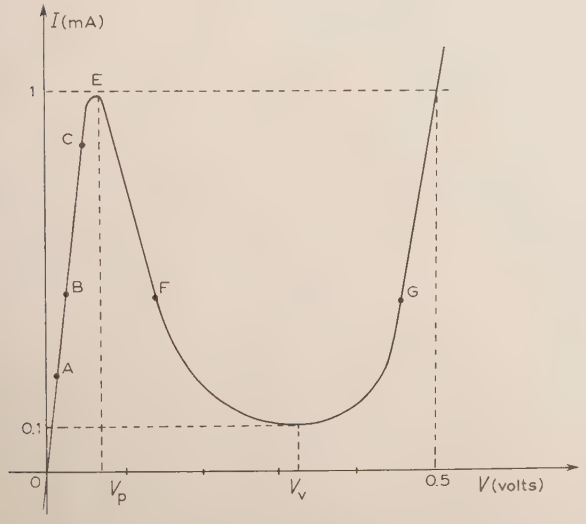

Fig. 1. La courbe caractéristique $I-V$ d'une diode tunnel G.E. 1 N 2939.

Si la diode est alimentée par un courant constant, il y a trois points de fonctionnement possible B, F et G. Si la résistance interne de la source de courant est plus élevée que la résistance négative $-R$ de la diode, seuls les points B et G correspondent à des points de fonctionnement stables. Les points de fonctionnement B et G peuvent être interchangés en appliquant à la diode une impulsion de courant de polarité convenable et d'amplitude suffisante pour charger ou décharger la capacité de la diode, avec la différence de potentiel existant entre les points de fonctionnement B et G.

Un système à quatre états stables, utilisant les propriétés ci-dessus, a été réalisé. Il consiste en un réseau (fig. 2) constitué par 3 diodes-tunnel et des résistances. Chaque diode D_i ($i = 1, 2, 3$) est alimentée par une source de courant à haute

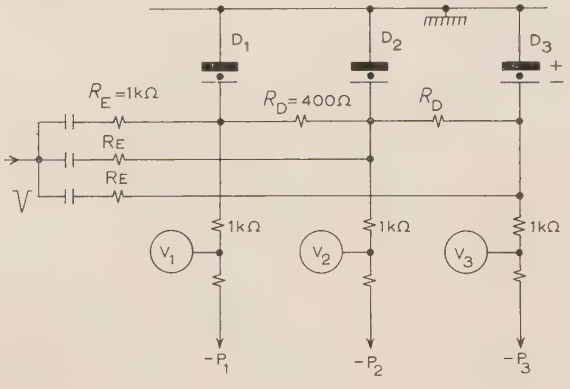

Fig. 2.

impédance, débitant un courant P_i. Pour des valeurs bien choisies des courants P_i le système possède les quatre états stables suivants:

état zéro: Les points de fonctionnement de toutes les diodes sont dans la région OE; celui de D_1 en C, celui de D_2 en A et celui de D_3 entre O et A.

état un: Le point de fonctionnement de D_1 est dans la région FG les points de fonctionnement des diodes D_2 et D_3 s'étant déplacés respectivement en C et en A.

état deux: D_1 et D_2 ont leur point de fonctionnement dans la région FG et c'est le point de fonctionnement de D_3 qui est en C.

état trois: Les 3 points de fonctionnement des diodes D_1 D_2 et D_3 sont dans la région FG.

COMPTAGE

Le circuit précédent peut être utilisé comme circuit de comptage en provoquant les changements d'état dans l'ordre 0, 1, 2, 3 par les impulsions à compter. Celles-ci sont appliquées, comme impulsions négatives de courant, aux trois diodes en parallèle, à travers les résistances R_E. L'amplitude est telle que seule la diode D_i, dont le point de fonctionnement est en C, bascule dans la région FG de la caractéristique où elle atteint un nouveau point de fonctionnement stable. Une nouvelle répartition des courants de polarisation s'établit par l'intermédiaire des résistances R_D, amenant le système à l'état stable suivant et la diode D_{i+1} dans l'état défini par le point de fonctionnement C.

Le temps minimum qui doit séparer deux impulsions est celui de l'établissement de la répartition des courants de polarisation après un changement d'état, il est déterminé par la constante de temps $R_D C_D$, ou C_D est la capacité parasite des diodes soit environ 10 pF.

Le temps minimum entre deux impulsions à compter est ainsi de l'ordre de 10^{-8} s.

REMISE A ZERO

La remise à zéro est effectuée en appliquant à l'entrée du circuit une impulsion de courant positive suffisante pour décharger la capacité des trois diodes et amener leur point de fonctionnement dans la région OE de la caractéristique.

LECTURE.

La lecture consiste à vérifier dans quel état 0, 1–, 2– ou 3 le système a été laissé. Au cours des essais cette opération a été effectuée en mesurant avec trois voltmètres la tension entre les points V_i et la terre.

PERFORMANCES

Le système a été essayé avec des impulsions négatives de courant, de durée 10 mμs. La mémoire des informations emmagasinées est, à priori, conservée aussi longtemps que les courants de polarisation P_i sont fournis.

Expérimentalement la plus longue période d'essais a été de 2 heures environ.

APPLICATIONS

Un tel système à n états stables (n pouvant aller jusqu'à 10), comportant $(n-1)$ diodes tunnel peut être utilisé pour constituer l'élément de base d'une mémoire tampon rapide destinée à diminuer le temps mort d'un sélecteur multicanaux (sélecteur à enregistrement sur bande magnétique par exemple).

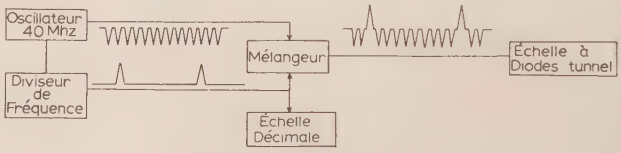

Fig. 3.

Associé à un oscillateur 40 MHz et combiné à un diviseur de fréquence, ce circuit peut aussi servir pour réaliser l' "Echelle d'adresse" d'un Sélecteur multicanaux: la figure 3 montre le principe d'une telle utilisation.

NUCLEAR INSTRUMENTS AND METHODS **10** (1961) 231–233; NORTH-HOLLAND PUBLISHING CO.

A TUNNEL DIODE UNIVIBRATOR AND PULSE HEIGHT DISCRIMINATOR

Y. HAZONI†

S.M.N.F., C.E.N., Saclay, Gif-sur-Yvette (S & O)

Received 6 September 1960

A univibrator and a pulse height discriminator using tunnel diodes and backward diodes, are described, as well as their application in pulse shaping and fast coincidence technique.

The main advantages achieved are simplicity of design and fastness.

The characteristics of the two diodes are shown in figs. 1 and 6.

The T.D. univibrator consists of a high current tunnel diode (R.C.A. G 189 or H 242 – fig. 1) which is put in the emitter circuit of a transistor 0C 170 (fig. 3). The transistor serves as a low impedance supply for the tunnel diode. The voltage applied across the T.D. is determined by the bias chosen for the base of the transistor. In the same time, the transistor serves as a collector follower, thus isolating the emitter circuit from the load. The characteristics of this circuit are shown in fig. 2; a marked "negative resistance" region can be seen.

The circuit has two modes of operation, depending on the value of the bias chosen: it can work either as an oscillator or as a univibrator.

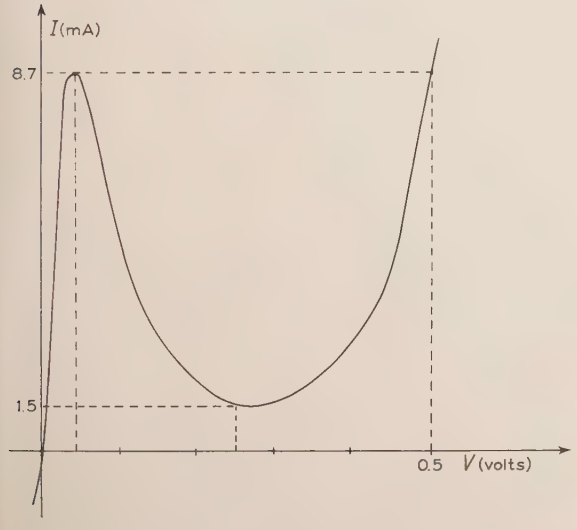

Fig. 1. $I-V$ characteristic curve of the T.D. R.C.A. G 189 and H 242.

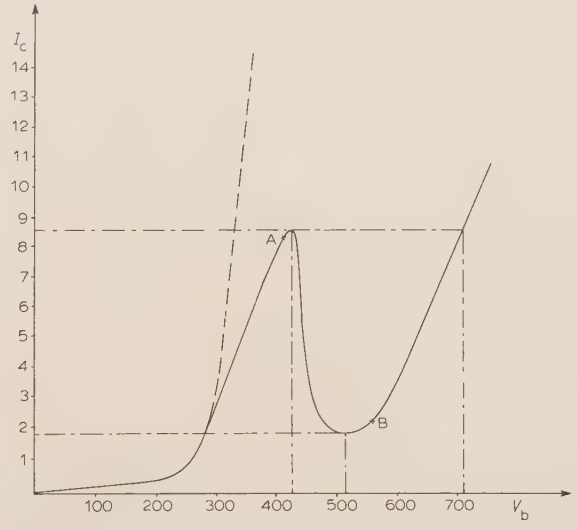

Fig. 2. I_c-V_b characteristic curve of the T.D. univibrator. – – – T.D. short circuited. ____ T.D. univibrator.

To function as an oscillator, the transistor is biased so that the T.D. operates in the negative resistance region. A detailed description of the oscillator, and its application as a high frequency analog to digital converter, has already been published††.

To function as a univibrator, the circuit is biased very near to the negative resistance

† On leave from the A.E.C. of ISRAEL.

†† Convertisseur analogique numérique rapide Y. Hazoni-C.R. Acad. de Sc., Tome 251 No. 3 (18 Juillet 1960) pp. 343.

region, either at point A or B (fig. 2) thus, a small pulse will be sufficient to trigger the oscillator for the duration of one period; in other words, it will function as a univibrator. In the circuits described later on, the univibrator is

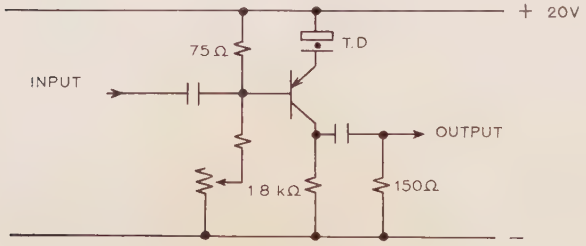

Fig. 3.

biased at point A and triggered by negative pulses. The triggering pulse should be shorter than one period of the circuit operating in the oscillator mode, otherwise it will act as a pulsed oscillator and will deliver a train of pulses for the duration of the input pulse. The output of the univibrator is a pulse of constant shape; in the particular circuit used it had an amplitude of about 7 mA (fig. 4).

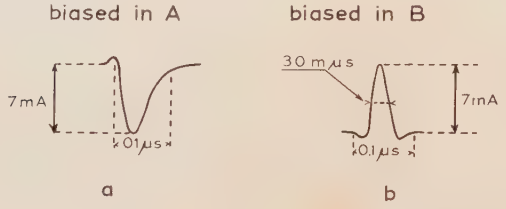

Fig. 4.

Applications

1. PULSE SHAPING

The shape of the output pulse of the T.D. univibrator is not sensitive to the shape of the triggering pulse (provided it is short enough), or to its height. The circuit was triggered with pulses of 1 mμs to 50 mμs duration. The ratio between the highest and lowest pulses capable of triggering the circuit was found to be about 20. Thus, the circuit could serve as a pulse shaper.

2. PULSE HEIGHT DISCRIMINATION

Fig. 5 represents a proposed combined circuit of the T.D. univibrator and a biased B.D. (backward diode – fig. 6), capable of discriminating mμs pulses with an accurate variable discrimination level.

The B.D. can be biased either lower than point A or higher than point B on its characteristic I–V curve (fig. 6). In fig. 5 it is biased

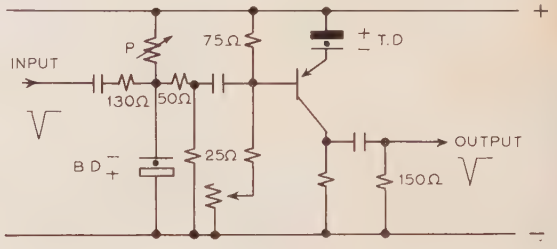

Fig. 5. T.D. Pulse height discriminator.

lower than point A because of dissipation considerations.

The bias is a current bias and the pulses to be analyzed should be negative current pulses.

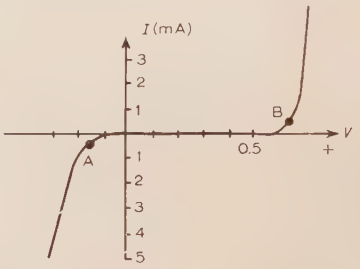

Fig. 6. $I-V$ Characteristic curve of a B.D. (taken from "Germanium and Silicon T.D.-Design, operation and Application") I.A. Lesk *et al.*, 1959 IRE, Wescon Convention Record, Part 3, ECG 441.)

Once the input current pulse is higher than the bias current, the B.D. will flip over from an operation point below A to a point higher than B. This flipping will be seen as a standard 0.2 volt negative pulse in the input of the T.D. univibrator, high enough to trigger it.

The speed of the discriminator is determined by the input time constant. This time constant is different for pulses lower or higher than the discrimination level. For pulses lower than the discrimination level, the time constant is given by the resistance of the B.D. ($< 20\Omega$) and the input capacity of the T.D. univibrator (< 100 pF); thus giving a time constant smaller than 2×10^{-9}s. For pulses higher than the discrimination level,

the time constant is governed by the dead time of the T.D. univibrator, being about 0.1 μs. This property is mainly important in experiments where the pile up problem exists.

The discrimination level is changed by changing the bias current, which is controlled by the potentiometer P (fig. 5). This bias control could be replaced by another system giving a linear readout of the discrimination level.

The discrimination range depends on the B.D. chosen and could cover the range between 0.1 to 10 mA.

The accuracy of the proposed circuit depends only on the accuracy of the bias current, and thus, on the stability of the power supply and resistances used. An analog circuit, using a conventional fast diode 1 N 914 in place of the B.D., has been tried. This experiment gives an idea about the rapidity of the proposed circuit. It was tried with pulses of 10, 25, 50 and 100 mμs duration. No change of discrimination level was found, for pulses having the same amplitude, as a function of the pulse duration down to 25 mμs. A considerable change of discrimination level was found when the pulse width was reduced to 10 mμs. Thus, pulses longer than 25 mμs are not integrated in the input of this circuit. The application of the B.D. in place of the 1 N 914 diode should increase the rapidity of the circuit up to $\approx 2 \times 10^{-9}$ s. The analogy of this experiment to the proposed circuit, is restricted to the fastness of the circuit. The diode used could not compete with a B.D. because of the marked difference between the I–V characteristic curves for the two diodes. The low current part of the characteristic curve of a conventional diode is not as sharp as that of a B.D. Moreover, this part of the characteristic curve, in the case of an ordinary diode, is very sensitive to temperature variations, which is not the case for the B.D. Thus, the circuit, operating with an ordinary diode could not have stability and accuracy comparable with the proposed B.D. circuit.

10^{-8} s coincidence circuit

A 10^{-8} s coincidence circuit was constructed by mixing two preshaped pulses in the input of the T.D. univibrator, as shown in fig. 7a. A resolution time of 10^{-8} s was achieved with two rectangular pulses, 5 mμs long, given by a pulse generator.

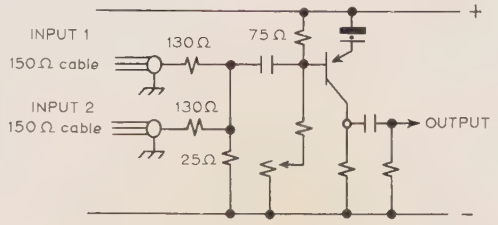

Fig. 7a.

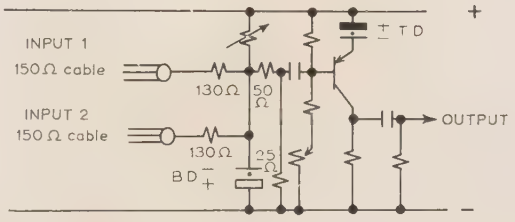

Fig. 7b.

A proposition for a 10^{-9} s coincidence circuit

A resolution time of $\approx 10^{-9}$ s could be attained by mixing two standard 10^{-9} s pulses in the input of the pulse height discriminator described above.

It is the view of the author, that this circuit will be able to discriminate the pulse height of the superposition of the two 10^{-9} s pulses, and thus, to measure their overlapping in time. The mixing could be done as proposed in fig. 7b.

Acknowledgement

The support of the "Centre d'Etudes Nucléaires de Saclay" (Département de Recherche Physique) for this work is gratefully acknowledged. The author would like to thank also M. A. M. Goodman from R.C.A. Laboratories, and the Case Institute of Technology, Cleveland, for providing the tunnel diodes needed for this work.

NUCLEAR INSTRUMENTS AND METHODS 10 (1961) 234–236; NORTH-HOLLAND PUBLISHING CO.

DIRECT CURRENT STABILIZATION OF SCINTILLATION COUNTERS USED WITH PULSED ACCELERATORS

F. P. G. VALCKX

Fysisch Laboratorium der Rijksuniversiteit, Utrecht

Received 20 October 1960

A simple system is described for the gain stabilization of the photomultiplier of a scintillation counter. Use is made of a constant light source. The stabilization factor of the system amounts to $S = 200$.

1. Introduction

Gain stabilization of photomultipliers may be necessary in high resolution scintillation spectroscopy. If the pulse spectrum contains a high intensity narrow line the circuit developed by de Waard[1]) may be used. The difference in counting rates of two channels, set on the two halves of the line, is fed back to regulate the voltage on the multiplier. In the more sophisticated circuit of de Waard one channel is modulated across the line. In many scintillation counter experiments, however, the pulse spectrum does not contain a high intensity narrow line, and it may be difficult or impossible to introduce such a line artificially. In the present paper a simple circuit is described which operates on a different principle and which can be used for the gain stabilization of scintillation counters detecting radiation or particles produced by pulsed accelerators.

The new system uses a constant light source illuminating the multiplier photo-cathode. The deviation of the d.c. anode current from a preset value is amplified and fed back to regulate the multiplier voltage. The multiplier anode current is diverted during the burst of the machine to prevent the d.c. component of the scintillation pulses from influencing the stabilization. The system has proved very reliable during experiments on the elastic and inelastic scattering of 90 MeV positive pions produced with the CERN synchro-cyclotron in Geneva. Scattered pions were completely stopped in large plastic scintillation counters. The height of the resulting pulse was used to distinguish elastic from inelastic scattering.

[1]) H. de Waard, Nucleonics **13**, no. 7 (1955) 36.

2. Stabilizer Design

Sufficiently constant illumination of the photocathode was obtained from a commercial 10 W, 230 V incandescent lamp. This lamp was mounted inside the multiplier shielding near the base of the multiplier. The light arrived from below, through the glass envelope of the multiplier, at the photo-cathode. The lamp was fed from a 300 V stabilized power supply through a variable resistor, reducing the voltage to about 40 V. The variation in light output was below 1% for changes in the ambient temperature up to 50°C. After several days of burning in at 230 V the light output has not changed measurably over a period of one month. To prevent fatigue of the photomultiplier the anode current must be kept low. With RCA 7046 multipliers the decrease in gain caused by fatigue was less than 5% for constant anode currents up to 1 μA.

The electronic circuit consists of two separate units (fig. 1). The first unit is placed near the scintillation counter in the cyclotron experimental hall. It contains the circuit to suppress the multiplier current during the machine burst, and a cathode follower, feeding the signal through a 150 m screened cable to the counting room. The second unit, placed in the counting room

together with the power supply of the multipliers consists of a d.c. differential amplifier with a cathode-follower output. Neither side of the

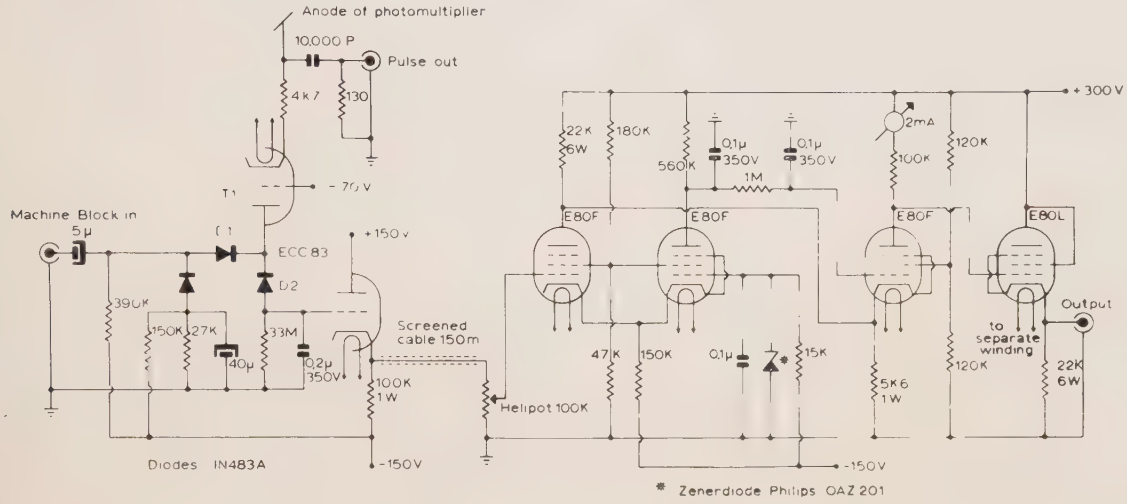

Fig. 1. Stabilization circuit. The error signal, produced in the left hand part of the circuit (placed in the cyclotron experimental hall) is fed through 150 m screened cable to the difference amplifier in the right hand part of the circuit (placed in the cyclotron counting room). The amplifier output regulates the multiplier power supply.

photomultiplier high voltage power supply is grounded, but the positive bus is connected with the amplifier output and the negativebus with the multiplier photo-cathode, via the high-voltage cable to the experimental hall. A change in input of the amplifier varies the output voltage and consequently the voltage on the multiplier, correcting the variations of the anode current of the multiplier.

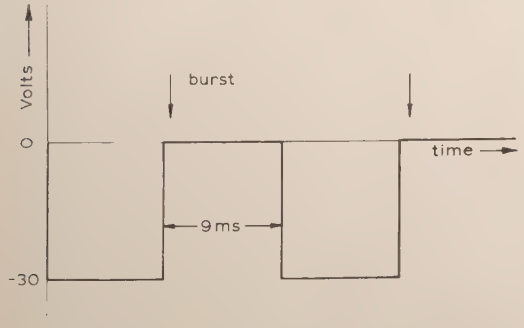

Fig. 2. Voltage at the anode of D1. The machine burst started about 0.5 ms after the fast rise of the block.

The suppression of the anode current during the burst of the machine is performed by the diode circuit in the first unit. A symmetrical block with an amplitude of 30 V is derived from the high-frequency system of the synchro-cyclotron. The repetition frequency of the machine is 54 Hz. The timing of this block with respect to the machine burst, and also the d.c. level at the anode of the diode D1 is shown in fig. 2. This block causes the diodes D1 and D2 (both IN483A) to conduct alternatingly. When the machine block is in its negative half-period, D1 is switched off and the anode current has to go through the resistor of 33 MΩ. The voltage built up over this resistor is then about — 15 V for an anode current of 1μA. The diodes have a very high back resistance. For — 50 V the inverse current is less than 10^{-8} A. But at 1μA the forward resistance also is rather high. Therefore it was necessary to install T1, as otherwise the *RC*-time of the multiplier anode would be too long. A number of different tubes were measured to select the type with the highest mutual conductance. The best proved to be the type ECC83, which has a mutual conductance of 6μA/V at $i_a = 1\mu$A. With an effective capacity of the multiplier anode of 10^4 pF this gives a *RC*-time of 1.6 ms, which is sufficiently short compared to 9 ms (see fig. 2).

The current going through the resistor of 33 MΩ is not exactly half the multiplier anode

current, but about 10% less. The reason is that when D2 is switched into conduction, the voltage at the anode of T1 is reduced from 0 V to — 15 V. Therefore, at that moment the cathode of T1, together with the condenser at the anode of the multiplier, also has to drop about 0.2 V in voltage. Consequently, during the first milliseconds of that half period a part of the multiplier anode current is used for charging the condenser.

In the amplifier the signal voltage is compared with the voltage on the Zener diode, which was — 8.3 V. The gain of the amplifier is 4000. Its output can vary from 120 V to 280 V.

The desired gain of the photomultiplier is set roughly with the light intensity of the lamp. Fine regulation is done with the helipot at the input of the amplifier. The meter in the amplifier serves to indicate if the circuit is working in its stabilizing region.

3. Fluctuations

The noise of the anode current of the photomultiplier gives an increase in the statistical fluctuations of the pulse height measured. This effect can be calculated from the fluctuations in the number of photoelectrons due to the d.c. current, in a time interval equal, roughly speaking, to the pulse length. In first approximation the relative increase of the peak width amounts to $(\tau i \sigma^2)/(2eg)$, where τ is the pulse length, i the anode current, σ the pulse height relative standard deviation, e the electron charge and g the current amplification of the multiplier. In our experiment the pulse length was 20 ns. For e.g. $\sigma = 0.1$, $g = 10^5$ the increase is completely negligible.

4. Stabilization Factor

For the stabilization factor of the system one finds $S = \alpha\, VG/E$, where V is the voltage of the Zener-diode, G the gain of the amplifier, E the voltage over the photomultiplier, and α the relative variation of the gain of the multiplier with the voltage, $\alpha = (\mathrm{d}g/g)/(\mathrm{d}E/E)$. In the present case the stabilization factor amounted to $S \sim 200$.

Acknowledgements

This work is part of the research programme of the "Stichting voor Fundamenteel Onderzoek der Materie" and was made possible by financial support from the "Nederlandse Organisatie voor Zuiver Wetenschappelijk Onderzoek" and from the "Ministerie van Onderwijs, Kunsten en Wetenschappen". The author wishes to thank E. S. Gelsema, M. Kruiskamp and B. A. Strasters for their assistance.

NUCLEAR INSTRUMENTS AND METHODS **10** (1961) 237–239; NORTH-HOLLAND PUBLISHING CO.

LETTERS TO THE EDITOR

ON THE ENERGY EXPENDED PER ELECTRON-HOLE-PAIR PRODUCED IN p–n-JUNCTION-DETECTORS

E. BALDINGER and W. CZAJA

Institute for Applied Physics, University of Basel, Switzerland

Received 1 December 1960

Recently we have shown in a short communication[1]) that it is possible to determine the true average energy expenditure per electron-hole-pair in p–n-junction-detectors.

As is well known from gas-ionization-chambers, the amount of energy ε expended in the gas per electron–ion–pair produced is determined from the saturation charge by extrapolation to infinite field strength. Theory predicts a linear relationship between the reciprocal charge collected $1/Q$ and the reciprocal electric field strength $1/F$ applied to the plates. Extrapolation to $F \to \infty$ can easily by performed[2]). In general $1/Q$ is a function of $1/v$, where v is the drift-velocity of the charge carriers. In most cases for gases as well as in semiconductors $v = \mu F$ (μ = const.), and $1/Q$ depends on $1/F$ [3]). The same ideas apply to p–n-junctions, which are in a certain sense the solid state analogs to gas-ionization-chambers, leading to the same functional dependence between $1/Q$ and $1/F$, which has been shown to hold for different types of devices[1]). The main difference between gas-chambers and p–n-junctions is the bias dependent depth of the space charge region ("active chamber volume") in solide state detectors, leading to a $V^{\frac{1}{2}}$ law for F in the space charge region of an abrupt junction and to a corresponding change in depletion layer capacity. V is the applied bias.

[1]) E. Baldinger, W. Czaja and A. Z. Farooqi, Helv. Phys. Acta **33** (1960) 551.

[2]) W. Haeberli, P. Huber and E. Baldinger, Helv. Phys. Acta **26** (1953) 145;
E. Baldinger and W. Haeberli, Ergeb. d. exakt. Naturwissensch. **27** (1953) 248.

[3]) F. Widder and P. Huber, Helv. Phys. Acta **31** (1958) 601, where the influence of pressure in the case of a F/p dependence of μ had been considered.

We measured the energy loss ε_{Si} per electron-hole-pair in silicon at room temperature[1]). Because of the limited accuracy of our equipment two

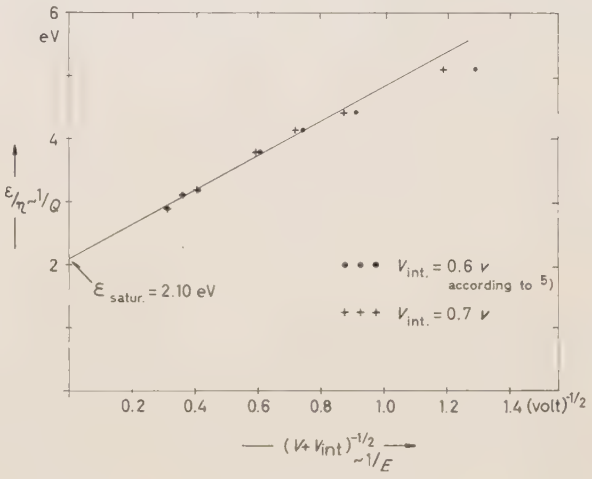

Fig. 1.
Saturation curve in Ge after Walter, Dabbs and Roberts[5]).

possible ways of extrapolation yielded the preliminary values.

$$\varepsilon_{Si} = \left\{ \begin{matrix} 3.30 \text{ eV} \\ 3.16 \text{ eV} \end{matrix} \right\} \pm 0.15 \text{ eV}$$

where both are smaller than known values in the literature[4]). This is to be expected.

In a recent paper, Walter, Dabbs and Roberts[5]) published comparable results on Ge-surface-barrier-detectors (compare fig. 8 of ref.[5])). Using

[4]) K. G. MacKay and K. B. MacAfee, Phys. Rev. **91** (1953) 1079;
W. D. Davis, J. Appl. Phys. **29** (1958) 231.

[5]) F. J. Walter, J. W. T. Dabbs and L. D. Roberts, Rev. Sci. Instr. **31** (1960) 756.

their experimental points of $(\varepsilon/\eta)_{Ge}$, where η are the charge collection losses, and

$$\frac{1}{Q} \cdot \frac{\varepsilon}{qE\eta}. \tag{2}$$

ε/η is plotted against $(V + V_{int})^{-\frac{1}{2}}$ in fig. 1. q is the electron charge, E the energy of the incident particle and V_{int} the built in or diffusion potential of the diode. In fig. 1 the value of 0.6 V for V_{int} is used according to[5]), which seems to be a little bit too small (compare their fig. 7). However it should be mentioned that the value of V_{int} is only of minor importance for the four points in the high field strength part of fig. 1, which determine the intersection with the ordinate.

Obviously ε_{Ge} determined from the saturation charge is smaller than the value of 2.94 eV given by the authors. From fig. 1 we conclude

$$\varepsilon_{Ge} = 2.10 \text{ eV}. \tag{3}$$

Now one may compare (1) and (3) with the finding that

$$\frac{\varepsilon_{Si}}{\varepsilon_{Ge}} \approx 1.5 \rightarrow \frac{\Delta E_{Si}}{\Delta E_{Ge}} = 1.46 \approx \frac{\varepsilon_{Si}}{\varepsilon_{Ge}}, \tag{4}$$

where the energy gap ΔE_{Si} is taken to be equal to 1.09 eV [6]) at 300° K and $\Delta E_{Ge} = 0.746$ eV [6]) at 77° K in accordance with the temperature used in[5]).

Taking the greater of the two values (1) the difference in the two fractions (4) is smaller than 6%. Aside from a possible accidental coincidence, the relationship (4) seems to be remarkable.

It must be mentioned that a relation

$$\varepsilon \approx x \, \Delta E \tag{4a}$$

for semiconductors is to be expected from the following reasons: The work of Fano and Erskine[7]) indicates that for gases

$$\varepsilon = k_1 + k_2 I \tag{5}$$

holds al least approximately, where k_1 and k_2 are constants and I is the ionization energy of the gas. Values of ε for a great number of gases taken from Fulbright and Valentine and Curran[8]) are plotted against the ionization potential of the atoms and molecules repsectively in fig. 2. Besides certain existing exceptions. (The surprisingly small ε for Cl_2 may be correlated to the small dissociation-energy for the Cl_2-molecule compared with H_2, N_2 and O_2 [9]).) the values for comparable gases lie on nearly straight lines. k_2 is roughly equal for all gases, while k_1 shows certain differences but seems to be approximatively equal for comparable gases. As expected, monoatomic gases show the lowest ε for comparable I (i.e. smallest k_1).

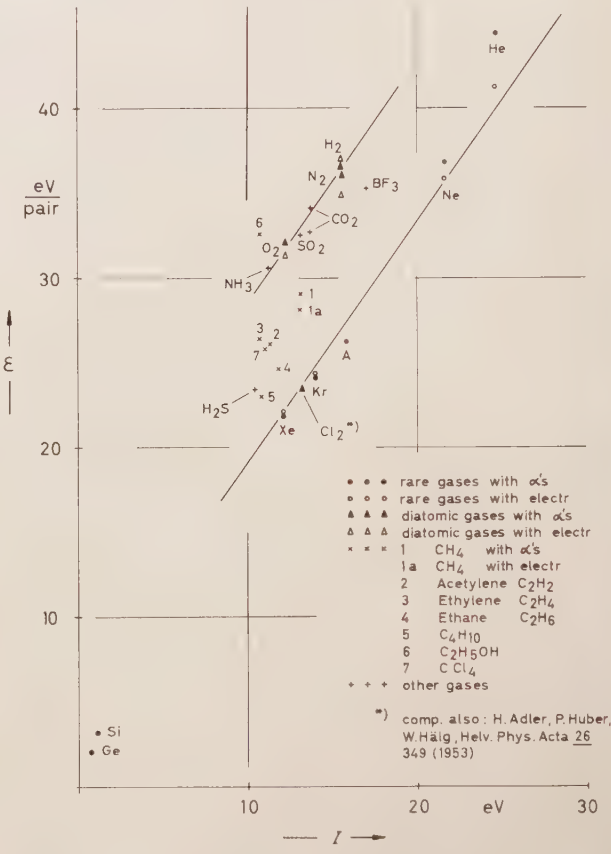

Fig. 2. Amount of energy expended per electron-ion-pair produced in gases as function of the ionization energy. Values for Si and Ge are for semiconductors with $I = \Delta E$.

[6]) Semiconductors, Ed. N.B. Hannay (Reinhold N.Y., 1959) p. 332.

[7]) V. Fano, Phys. Rev. **70** (1946) 44;
G. A. Erskine, Proc. Roy. Soc. A**224** (1954) 326.

[8]) H. W. Fulbright, Encycl. Phys., Vol. **45** (Springer-Verlag Berlin, 1958);
J. M. Valentine and S. C. Curran, Rep. Progr. Phys. **21** (1958) 1.

[9]) G. Herzberg, Molecular Spectra and Molecular Structure, Vol. **1** (D. van Nostrand N.Y. 1950) Values are Cl_2: 2.47 eV; O_2: 5.08 eV; N_2: 9.75 eV; H_2: 4.47 eV.

This correlation between ε and I found in gases suggests that (4a) holds for semiconductors, where one should use ΔE rather than I because of the different meaning of "ionization" in the two cases.

In conclusion we hope that further measurements will clarify the statements and ideas outlined here. In connection with semiconductors determinations of ε in other materials than Si and Ge are of special interest and might throw new light on the possible mechanisms of electron-hole-pair creation by energetic particles in solids. Experiments with Ga As-diodes are proposed.

Note added in proof: Recently we heard about different measurements of ε in PbO with γ's ($\Delta E = 3.0$ eV, $\varepsilon = 8.0$ eV) and CdS with α's ($\Delta E = 2.5$ eV, $\varepsilon = 7.3$ eV)[10]. The recombination effect had been taken into account[10]) and the values are in excellent agreement with our findings in Ge and Si. With electrons in CdS ($\varepsilon = 9.3$ eV) the agreement is poor, while in GaAs ($\Delta E = 1.35$ eV, $\varepsilon = 6.3$ eV) experimental difficulties may be responsible for the disagreement.

A stimulating discussion with Dr. F. Lappe, RCA-Laboratories, Zürich Switzerland, is gratefully acknowledged.

[10]) F. Lappe, Zschr. f. Physik **154** (1959) 267; J. Appl. Phys. to be published.

NUCLEAR INSTRUMENTS AND METHODS **10** (1961) 240–242; NORTH-HOLLAND PUBLISHING CO.

AN IMPROVED CIRCUIT FOR PULSE SHAPE DISCRIMINATION BETWEEN NEUTRONS AND GAMMA RAYS

J. RETHMEIER, H. J. BOERSMA and C. C. JONKER

Natuurkundig Laboratorium der Vrije Universiteit, Amsterdam

Received 29 December 1960

Recently two circuits to perform pulse shape discrimination between neutrons and gamma's have been published, by Owen[1]) and by Brooks[2]). However in some experiments a difficulty in the application of these methods arises because the anode pulse has to be used to drive other circuits (e.g. fast coincidence units).

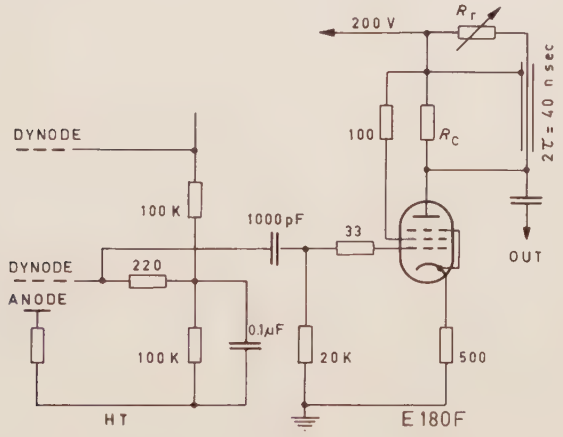

Fig. 1a.

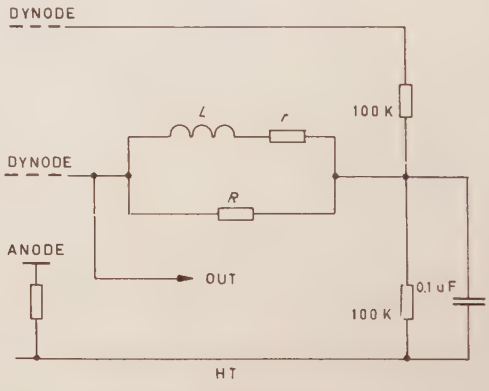

Fig. 1b.

Fig. 1. Gamma-neutron discrimination circuits.

In the method proposed by Owen, the photomultiplier is driven into saturation, and so the anode pulse can not be used for other purposes. In Brooks method the time constant of the anode pulse is already determined by the requirements of the pulse shape discrimination circuit and so it may be impossible to meet other requirements. In the following we give two circuits to accomplish the γ – n discrimination, using the pulse from only one dynode. They are able to separate the pulses from 0.8 – 14 MeV recoil protons in a stilbene crystal from those of electrons with energies in excess of 200 keV.

The first of these circuits is shown in fig. 1a. After an excitation of the crystal by a charged particle, the pulse form at the anode of the E 180 F is given in fig. 2a, if the clipping cable has been terminated with its characteristic impedance, $R_r = R_c$. The delay of the reflected signal is about 40 nsec. If R_r is somewhat smaller than R_c, a small portion of the signal will be negatively reflected. R_r can be chosen so that in the case of an α or proton scintillation, the reflected signal equals the slow component on the time of its return. For a γ-pulse the ratio between the slow and the fast component is twice as small; so there will be a positive swing now, for the same value of R_r as above (fig. 2b).

After some amplification and limiting of the fast

[1]) R. B. Owen, AERE (Harwell Report El/R 2712.
[2]) F. D. Brooks, Nucl. Instr. and Meth. **4** (1959) 151.

component (to prevent undershoot and overloading), this swing may be taken as an indication of a γ-pulse, to drive a coincidence or anticoincidence gate. The resistance R_r is easy to adjust.

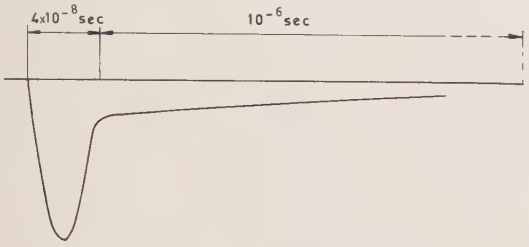

Fig. 2a. Pulse form at the anode of the E 180 F, when $R_r = R_c$.

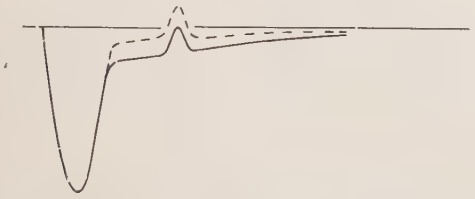

Fig. 2b. Pulse form at the anode of the E 180 F, when R_r has been adjusted. Solid curve is α particle or proton Dashed curve is electron.

The other circuit is given in fig. 1b.

The inductance L forms with the stray capacity C of the dynode a LC circuit, which is critically damped by the resistance R. After the fast component of a positive pulse, the circuit gives a small negative swing. As the load impedance for the slow component is negligible the resistance r is added to have the circuit responding to the slow component. This resistance has little influence on the LC circuit if $r < 4R$. By choosing r suitably it is possible to compensate the slow component of the proton recoil pulse, while an electron pulse gives a negative swing.

As above we have after amplification an indication of a γ-pulse. Typical values of both circuits are:

$$R_c = 135\,\Omega, \quad 2\tau_{delay} = 40\ \text{n sec}, \quad R_r \approx 100\,\Omega\ .$$

$$L = 2 \text{ or } 3\mu H, \quad R = 250\,\Omega, \quad r \approx R\ .$$

In fig. 3 and 4 some experimental results obtained with circuit no. 1a are shown. The stilbene scintillator was irradiated by 5.3 MeV α particles from a Po source, and by 1.2 MeV gamma's from Co^{60}. The spectrum was recorded by a 256 channel pulse height analyser (fig. 3, curve a). Then the analyser was gated by the output pulse of the γ – n discriminator, so that only gamma's were recorded (fig. 3, curve b).

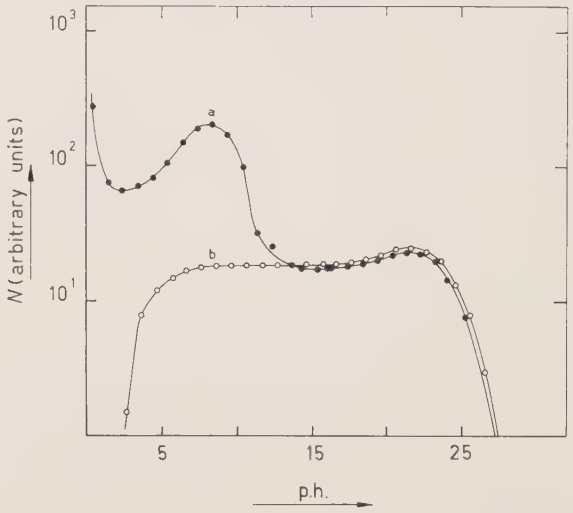

Fig. 3. a. The pulse height spectrum of Co^{60} γ-rays plus Po α-particles; b. The same spectrum gated by the pulse from the n–γ discriminator.

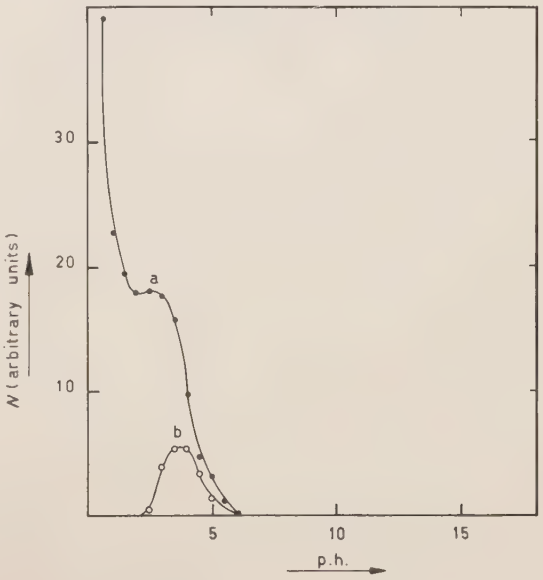

Fig. 4. a. The pulse height spectrum of Hg^{203} γ-rays; b. The same spectrum gated by the pulse from the n–γ discriminator.

Very small pulses are not able to operate the coincidence gate, and so there is a cut-off at the lower end of the spectrum. This cut-off depends on

the bias of a trigger in the gate unit, and this bias was just above the noise level.

In fig. 4a the spectrum of gamma rays from Hg^{203} (no α source present) and in fig. 4b the effect of the $\gamma - n$ discrimination gate is shown. From these results it is clear that the $\gamma - n$ discriminator is triggered by γ-pulses as low as 200 keV, but not by α-pulses.

The energy resolution, measured with the pulse height of the slow component of the scintillation is far inferior to the resolution, obtained with the fast component, because in the latter case the statistics of the photoelectrons from the cathode of the photomultiplier are much better. This is the reason, that the cut-off in fig. 3b and fig. 4b is not sharp.

We tested the performance of the circuit also with 14 MeV neutrons. In fig. 5a the proton recoil spectrum of these neutrons in a stilbene crystal and the room-background is shown. Fig. 5b gives the same spectrum, but in anticoincidence with the output pulse of the $n - \gamma$ discriminator.

The circuit is now used in a time of flight experiment with 14 MeV neutrons.

Finally we should like to remark that the $\gamma - n$ discrimination is achieved by these methods without loss of neutron pulses, and that the stability in time is ensured, because the circuits contain only passive elements.

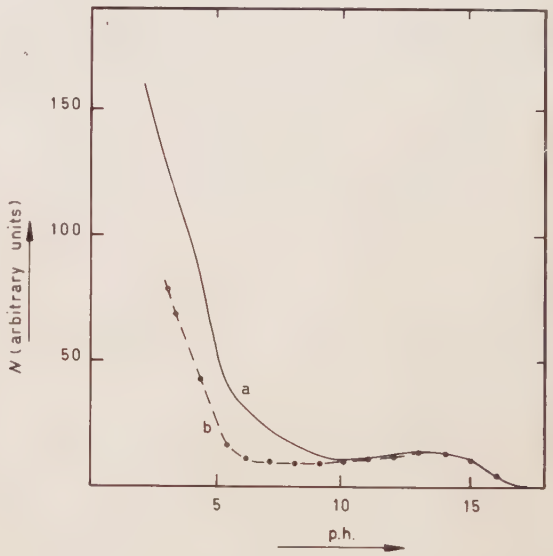

Fig. 5. a. The spectrum of 14 MeV neutrons plus background; b. The same spectrum, but in anticoincidence with the pulse from the n -γ discriminator.

This investigation was part of the joint program of the "Stichting Fundamenteel Onderzoek der Materie" and was partly made possible by financial support of the "Nederlandse Organisatie voor Zuiver Wetenschappelijk Onderzoek".

NUCLEAR INSTRUMENTS AND METHODS 10 (1961) 243–244; NORTH-HOLLAND PUBLISHING CO.

TIME-TO-PULSE-HEIGHT CONVERTER AS COINCIDENCE AND ANTI-COINCIDENCE INDICATOR†

L. CRANBERG

Los Alamos Scientific Laboratory, Los Alamos, New Mexico

Received 2 December 1960

The time-to-pulse-height converter[1]) is now in common use as a flexible tool for measuring time spectra over a wide range of conditions. It is the purpose of this note to call attention to the usefulness of the converter as a routine coincidence and anti-coincidence indicator.

In normal use of the converter a pulse from one detector is fed to the "start" input of the converter, which in effect initiates the discharge of a capacitance at constant current. A pulse from a fiducial timer or another detector fed into the "stop" input determines the time at which the discharge process is terminated, so that the charge transferred in the interval between "start" and "stop" pulses is a measure of elapsed time. This charge, in the form of an appropriately shaped pulse, may then be measured by means of a pulse-height analyser. It is clear that the converter and analyzer function essentially as a multi-channel delayed-coincidence time analyzer, but there are a number of important differences between it and the conventional coincidence circuit[2]) (e.g. of the Rossi type or its derivatives), aside from the multi-channel feature, which are sometimes overlooked.

The conventional coincidence circuit measures essentially the overlap between two pulses each of duration τ, and gives an indication which is symmetric about time zero and extends for a time $\pm\tau$. The optimum time τ and the relative phasing of the two legs of the coincidence circuit must usually be explored by careful preliminary experiments. On the other hand the converter can record the coincidence events as long as they occur anywhere within the duration of the "start" gate, and in practice the resolution observed with the converter is usually dominated by statistical considerations rather than by the characteristics of the converter itself. To achieve a comparable result with a coincidence circuit requires, in fact, a time-delay analysis.

A further advantage of the converter-analyzer combination over the conventional coincidence circuit is that it provides a more reliable basis than the latter for determination of accidental coincidences[3]). Underlying the usual method of accidental coincidence correction with simple coincidence circuits is the assumption that the accidental coincidences are random in time and may be ascertained by inserting delay in one leg of the coincidence circuit. This assumption is not a reliable one in many instances, particularly where an accelerator beam is the primary source of the events being observed. Even nominally d.c. accelerators exhibit a complex pattern of beam current fluctuations which may be erratic in time. Use of the converter-analyzer combination enables one to obtain concurrently with the bona-fide coincidences the time spectrum of accidentals. By judicious extrapolation under the peak corresponding to bona-fide events one may extract a correction to the observed coincidence rate which compensates more accurately for the accidentals. In

†) Work performed under the auspices of the U.S. Atomic Energy Commission.

[1]) J. H. Neiler and W. M. Good, "Time-of-Flight Techniques", Section IVA in "Fast Neutron Physics, Part I" ed. by J. B. Marion and J. L. Fowler, Interscience Publishers, New York, 1960.

[2]) S. DeBenedetti and R. W. Findley, "The Coincidence Method" in "Nuclear Instrumentation II", Handbuch der Physik, Vol. 45, Springer, Berlin, 1958.

[3]) J. B. Garg and N. H. Gale, Nuovo Cimento **16**, (1960) 1014.

the event that accidentals have a strongly periodic character with a maximum which coincides with the bona-fide events, as is the case in accelerator experiments with highly modulated accelerator beams, a detailed time spectrum taken over several modulation periods should facilitate extraction of an appropriate correction for accidentals.

A final point to be noted is the potential usefulness of the converter as an anti-coincidence indicator. Thus, if "start" pulses alone are present the converter delivers an output pulse of fixed height corresponding to the maximum duration, τ, of the "start" gate pulse. If "stop" pulses are occasionally present at a definite time after the start pulse and within the interval τ, then they will produce converter output pulses of uniform height less than the maximum value. If a second family of stop pulses is present which is synchronous with the start pulses and occur within the time τ but later than the first family of stop pulses, then the converter output will deliver pulses of an intermediate height when pulses of the first family are absent. Thus, in general the converter would deliver a pulse-height spectrum containing three peaks. If one designates the "start" pulses as A, the prompt "stop" pulses as B, and the delayed "stop" pulses as C, the three peaks correspond, in order of diminishing height, to events of the character A, no B, no C; A no B, C; and A, B. It is usually a trivial matter to couple together the two sources of stop pulses in proper relative phase to obtain the desired anti-coincidence action.

NUCLEAR INSTRUMENTS AND METHODS **10** (1961) 245–246; NORTH-HOLLAND PUBLISHING CO.

DOPPELSTREUEXPERIMENTE MIT AZIMUTWINKELINTEGRATION

JOACHIM KESSLER

Physikalisches Institut der Technischen Hochschule Karlsruhe

Eingegangen am 14. Oktober 1960

In order to count more particles in double scattering experiments one may integrate over the azimuthal angle. By this procedure, however, the left-right asymmetry is often greatly diminished. An arrangement is proposed, which makes it possible to integrate over the full range $0 \ldots 2\pi$ of the azimuthal angle without losing asymmetry.

Alle Doppelstreuexperimente zur Bestimmung der Polarisation und Asymmetrie von Teilchenstrahlen höherer Energie haben eines gemeinsam: Die Intensität des zweifach gestreuten Strahls ist sehr gering. so daß große statistische Fehler die Genauigkeit der Messungen begrenzen. In zwei kürzlich erschienenen Mitteilungen untersuchte Burge[1]), wie sich der relative statistische Fehler verringert, wenn der zweifach gestreute Strahl nicht, wie üblich, bei festen Streuwinkeln θ und ϕ beobachtet wird, sondern wenn die Zählanordnung bei festem θ über den Azimutwinkel ϕ integriert, so daß mehr gestreute Teilchen erfaßt werden. Fig. 1 stellt eine Anordnung dar, wie sie den Rechnungen Burges zugrunde liegt.

Deren Ergebnis läßt sich wie folgt zusammenfassen: Wird nur über einen kleinen Winkelbereich $-\phi \ldots . \phi$ integriert, so nimmt der relative mittlere statistische Fehler f annähernd mit $1/\sqrt{\phi}$ ab. Je größer jedoch der erfaßte Winkelbereich wird, umso mehr verlangsamt sich die Abnahme von f, bis schließlich der Fehler mit wachsendem ϕ sogar wieder ansteigt. Die Größe des Winkelbereichs $-\phi \ldots . \phi$, dem der kleinste Wert von f entspricht, hängt von dem bei dem Experiment auftretenden Polarisationsgrad ab und ist der von Burge berechneten Tabelle zu entnehmen.

Dieser komplizierte Verlauf des statistischen Fehlers f erklärt sich durch zwei Einflüsse, die in entgegengesetzter Richtung auf den Fehler einwirken: Einerseits ist bei fester Streuintensität die erfaßte Teilchenzahl proportional der Größe des Azimutwinkelbereichs $-\phi \ldots . \phi$, so daß der Fehler mit $1/\sqrt{\phi}$ absinken sollte. Andererseits wird jedoch die beobachtete Asymmetrie umso kleiner, je größer der Azimutwinkelbereich gewählt wird. Der Grund dafür ist, daß zur Asymmetrie nur die Komponente des Polarisa-

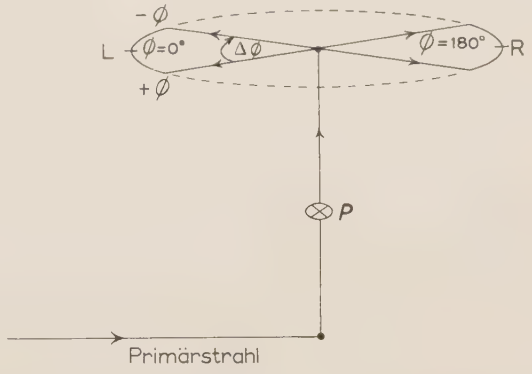

Fig. 1. Doppelstreuexperiment mit Integration über den Azimutwinkelbereich $\Delta\phi$. Der Polarisationsvektor **P** steht senkrecht zur ersten Streuebene (= Ebene, die aus einfallendem und gestreutem Strahl aufgespannt wird). Zur Asymmetrie trägt nur die Komponente von **P** bei, die senkrecht zur zweiten Streuebene steht. Deshalb erhält man bei Streuung um $\phi = 0°$ bzw. 180° maximale Asymmetrie, während bei Streuung um $\phi = 90°$ bzw. $-90°$ überhaupt keine Asymmetrie auftritt. Je grösser der Winkelbereich $-\phi \ldots . \phi$, desto mehr kommen die Richtungen mit ins Spiel, die nur einen geringen Beitrag zur Asymmetrie liefern, so dass die gemessene Asymmetrie $(L-R)/(L+R)$ umso kleiner wird, je grösser der erfasste Winkelbereich ist (L bzw. R bedeutet die Anzahl der nach links bzw. rechts in den erfassten Winkelbereich getreuten Teilchen).

[1]) E. J. Burge, Nucl. Instr. and Meth. **6** (1960) 101; **7** (1960) 221.

tionsvektors beiträgt, die senkrecht zur Streuebene steht (vgl. Unterschrift zu Fig. 1). Je kleiner aber die Asymmetrie, umso größer der bei ihrer Messung auftretende relative Fehler. Diese zwei gegenläufigen Einflüsse bewirken den von Burge errechneten Fehlerverlauf.

In der Anordnung der Fig. 1 wird also der Gewinn, den die größere erfaßte Teilchenzahl darstellt, erkauft durch einen Verlust an Asymmetrie. Die Frage ist, wie man solche Asymmetrieverluste vermeiden und dadurch den Vorteil, den die Azimutwinkelintegration mit sich bringt, voll ausschöpfen kann. Im folgenden wird eine Anordnung vorgeschlagen, die es gestattet, den gesamten Azimutwinkelbereich ohne jede Einbuße an Asymmetrie zu erfassen.

In Fig. 2 ist das Prinzip am Beispiel der 90°–90°-Doppelstreuung erläutert. Der Primärstrahl

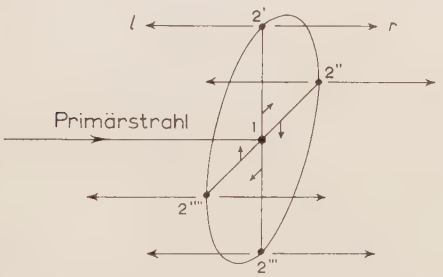

Fig. 2. Doppelstreuexperiment mit Integration über den vollen Azimutwinkelbereich ohne Asymmetrieverlust.

erfährt bei 1 die erste Streuung. Wir betrachten zunächst den gestreuten Teilstrahl, der bei 2′ zum zweitenmal gestreut wird. Erfolgt die Beobachtung in den Richtungen l und r, so mißt man maximale Asymmetrie, da der Polarisationsvektor senkrecht zur Streuebene steht. Das ist genau die Anordnung, wie sie bei den üblichen Experimenten ohne Azimutwinkelintegration gewählt wird. Entsprechendes gilt für die Teilstrahlen, die nach 2″ bis 2‴″ gestreut werden, und für jeden dazwischenliegenden Teilstrahl, dessen erste Streuung unter beliebigem Azimutwinkel erfolgte. In allen diesen Fällen steht der Polarisationsvektor, der stets senkrecht zur ersten Streuebene gerichtet ist, auch senkrecht auf der zweiten Streuebene, wenn man die Beobachtungsrichtungen so wählt, wie in Fig. 2 dargestellt. Wenn daher alle in der angegebenen Weise nach links bzw. rechts doppelgestreuten Teilchen nachgewiesen werden, so hat man über den Azimutwinkel integriert, ohne dabei Asymmetrie zu verlieren.— Selbstverständlich ist die Methode nicht auf die 90°–90°-Doppelstreuung beschränkt, sondern man überlegt sich leicht, daß sie bei beliebigen Streuwinkeln anwendbar ist.

Die üblicherweise verwendeten ebenen Targetfolien sind natürlich für solche Messungen ungeeignet, denn sie besitzen in den verschiedenen Azimutrichtungen ganz verschiedene wirksame Dicken. Das würde die Messungen verfälschen. Am besten verwendet man deshalb Gastargets[2,3]). Hierbei können die Gasdrucke leicht so niedrig gehalten werden, daß Vielfach- und Mehrfachstreuung keine Rolle spielen.—Bei derartigen Experimenten ist das Ringzählrohr ein ideales Nachweisinstrument. Es wurde an anderer Stelle[3]) beschrieben. Wegen seines toroidförmigen Zählvolumens integriert es über den vollen Azimutwinkelbereich $0 \ldots . 2\pi$, so daß man mit je einem Zählrohr für die nach links bzw. rechts gestreuten Teilchen auskommt. Auf diese Weise werden umständliche Zähleranordnungen vermieden.

[2]) J. Kessler und K. Ulmer, Physikal. Verhandlungen **10** (1959) 8.

[3]) J. Kessler, Z. Phys. **155** (1959) 350.

NUCLEAR INSTRUMENTS AND METHODS 10 (1961) 247–248; NORTH-HOLLAND PUBLISHING CO.

BOOK REVIEWS

Nuclear Propulsion (editor: M. W. Thring), Butterworths, London 1960 (50s.)

This volume contains a collection of sixteen articles by British scientists and industry men on the problems of nuclear propulsion, the subject being defined in a very broad sense. The first half of the book is devoted to the fundamentals of nuclear power generation, beginning with an introductory chapter on nuclear reactions followed by chapters on reactor physics, the thermodynamics of nuclear power systems and the various problems of reactor engineering: metallurgy, heat transfer, control and instrumentation. The chapters in the second half discuss the specific problems involved in the application of nuclear power to marine, air and space propulsion. The book ends with a chapter on life in sealed cabins.

With a few exceptions the chapters are well-written; as in most edited volumes there is, however, a certain amount of overlapping and repetition when chapters on nearby subjects are compared. There is very little detailed information to be found in the book on the few nuclear powered craft in actual operation: The American submarines and the Russian icebreaker Lenin. Also the chapters on space propulsion deal mainly with basic rocket theory with very little supporting data of existing rocket systems. This is of course mainly due to the classification of these projects, but it is to be regretted that some recent release of information came too late for inclusion.

As a whole the book gives a comprehensive survey of the technical and economical problems and possibilities of nuclear propulsion – one should perhaps add: from a British point of view – and it should be of interest as an introduction to this field to many categories of people: industry men as well as those working with basic nuclear research.

LARS HÖGBERG

Sector-Focused Cyclotrons. Proceedings of an Informal Conference, Sea Island, Georgia, February 2–4, 1959. National Academy of Sciences – National Research Council, Washington, D.C., 1959. Price U.S. $ 2.50.

Already in 1938, not long after the construction of the first cyclotron, a paper was published by L. H. Thomas pointing out the possibilities of using sector focusing magnets in cyclotrons. In an ordinary cyclotron the magnetic field strength is only a function of the radius, which must be decreasing to give a stable collected beam. But to compensate for the relativistic mass change, the field strength should vary in the opposite way. This could be achieved using Thomas ideas, according to which the magnet is divided into sectors with different field shapes. Thereby a field could be obtained with an effective mean value, which is an increasing function of the radius, but which could still give a collected beam.

However, these ideas seem to have been forgotten and instead, to reach relativistic energies, the method of frequency modulation was introduced just after World War II. One disadvantage here is the pulsed beam, which implies a low mean intensity and makes it difficult to do some experiments requiring a high beam quality and intensity. Therefore, during the last few years, some cyclotrons have been constructed based on the principles of sector focusing, and still more machines are under design.

This Conference brought together nearly all of the interested parties for an exchange of ideas, and the Proceedings therefore give a rather complete review of the field. It is a book with 291 pages presenting the forty-nine papers given at the Conference including the informal discussions held by the members. The Proceedings are arranged in six parts, corresponding to the different sessions. Of course, the main interest is devoted to the sector focusing, but also other cyclotron problems as e.g. the shielding, the means of focusing the external beam, and the instrumentation are dealt with. In the first session are described the methods to calculate the orbits for different field shapes, and not only the results are given but in some cases also the computer technique. As difficult as to figure out a suitable field shape is certainly to realize it by constructing a suitable magnet. Especially when the field strength should be variable to produce different energies, the problem has been solved with experimental methods using models. However, efforts have not only been made to design a usable magnet, but economical points of view have also been taken into account. In the following sessions, where the radio frequency system and the beam quality are discussed, is emphasized the importance of a high quality radio frequency system, which together with a precision made magnetic field are the most important factors, determining the beam quality. The Proceedings end with a table containing the main data of fifteen sector-focused cyclotrons, most of which are still under construction. This book gives a good review of the field, and is of great value to the expert it might certainly serve as an introduction. As a cyclotron is so complex, many details of interest there might also be of importance in other fields, especially where magnetic systems are used.

MATS OLSMATS

Penetration of Charged Particles in Matter, E. A. Uehling (Editor). Nuclear Science Series, Report Numer 29. National Academy of Science, National Research Council, publication 752, Washington D.C. $ 2.

This book presents the proceedings of the Gathlinburgh Conference of September 1958 on the Penetration of Charged Particles in Matter. It is evident that there has been a great deal of progress in this field on both theoretical and experimental methods. Some 25 different contributions which are divided into 6 different chapters are published in this volume. They deal with stopping power and ranges, charge changing collisions, atomic and molecular scattering, ionization in gases by high energy particles and microscopic and macroscopic energy loss distributions. At the end there is an Appendix by Fano, which contains some post-conference discussions on "Collective" Effects in Atoms and Extended Media. This topic had been subject to some disagreement between the experts during the conference. Fano's paper clarifies the situation and it seems that of the disagreement there is "very little, if any, matter of substance (which) remains unresolved".

TOR RAGNAR GERHOLM

Reports on Progress in Physics, Volume **13** (1960). Executive Editor: A. C. Stickland. Published by the Physical Society, London.

The 1960 volume of the Reports on Progress in Physics contains 10 different contributions. These are:

Optical Properties of Thin Films, by O.S. Heavens.

Group Theory in Solide State Physics, by D. F. Johnston.

Photoelectric Photometry, by H. J. J. Braddick.

Experimental Analysis of the Electronic Structure of Metals, by A. B. Pippard.

New Developments in Interference Spectroscopy, by P. Jacquinot.

Planetary Nebulae, by M. J. Seaton.

Band Structure Calculations in Solids, by L. Pincherle.

Orbital Electron Capture by the Nucleus, by R. Bouchez and P. Depommier.

Precision Measurement in Gamma Ray Spectroscopy by G. A. Bartholomew, J. W. Knowles and G. E. Lee-Whiting and

^{3}He Induced Reactions, by D. A. Bromley and E. Almquist.

It follows from this list of contents that the volume covers a wide variety of very different subjects. It is impossible to give a fair account of the various contributions. The reviewer feels forced to restrict himself to pass only the general comment that the quality of the contributions are all of the high standard which one is used to find in this excellent annually appearing series of review articles. The Reports serve two different purposes: they provide for the newcomers in the field a general and comprehensive introduction to current theories and experimental techniques and for the experts they are useful as reference books. One expects that in such review articles due credit should be given to those who have given the most important contributions to the development in the field covered by the article. In so far the reviewer is competent to judge there should be no reason for complains in this respect. The excellent article by Bartholomew, Knowles and Lee-Whiting, for example, deals in some detail with the very interesting Russian contributions to the development of high precision gamma ray spectrometers. Hitherto these Russian instruments have been but little known to the nuclear physicists in the West. TOR RAGNAR GERHOLM

Spotlight on Industry

This section appears each month and features various happenings of interest in the nuclear industrial world and objective information on products of the nuclear manufacturers. It is offered entirely as a service and all nuclear manufacturers are cordially invited to submit clearly objective and descriptive material on their endeavours and product developments for consideration for use in this section.

DIRECT READING INDUCTANCE AND CAPACITANCE METER

Solartron Laboratory Instruments Limited, Cox Lane, Chessington, Surrey, England

The Solartron L-C Meter MM 906 has been developed for quick, accurate component checks and in situ measurements of inductance and capacitance, including "strays". With minimum f.s.d. ranges of 0 to 3 μH and 0 to 3 pF, this is a unique instrument for optimising component and wiring layouts in circuit development. It provides a continuous monitor of L and C from 0 to 300 μH and 0 to 300 pF respectively, in five ranges with $\pm$ 3% accuracy. This accuracy is maintained with resistance loads of 20 kΩ shunt, 10Ω series on "Inductance" setting and 0.1 MΩ shunt on "Capacitance" setting. A "guard Voltage", sufficient to drive to 200 pF, enables the elimination of effects due to unwanted capacitances.

Valve interelectrode capacitances may be measured, giving clear accurate readings on the 4" scale.

AIR MONITOR TO DETECT RADIATION IN IODINE VAPORS

Nuclear Measurements Corp. 2460 N. Arlington Ave. Indianapolis 18, Indiana, U.S.A.

The first commercial air monitor to effectively detect radiation in air-borne iodine vapors is offered.

Called the AM-2S, it is designed primarily for protection of personnel working near reactors. It detects, measures, and records the amount of specific gamma activity within the energy range of 0.33 to 0.55 MeV, and warns of any alarm condition. In addition, the unit can be set for other gamma emitters for any energy range desired.

In operation, vapors are deposited on an activated carbon filter. The iodine activity is detected and recorded, and when a preset alarm level is reached, a built-in bell and light both signal the warning.

By employing optional count ratemeters and detectors, the AM-2S offers a wide choice of program possibilities. It can detect a specific gamma energy span and/or gross gamma and/or gross beta-gamma activity.

The monitor is mounted on a mobile cart. Dimensions are 16" deep $\times$ 36" high $\times$ 36" wide. Net weight is approximately 450 lbs.

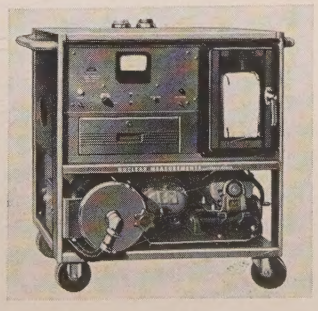

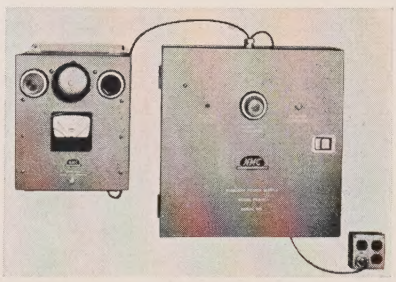

AUXILIARY POWER SUPPLY FOR GAMMA RADIATION AREA MONITOR

Nuclear Measurements Corp., 2460 N. Arlington Ave., Indianapolis 18, Indiana, U.S.A.

A new auxiliary power supply unit for use with its gamma radiation area monitor is announced. The monitors are used as an automatic alarm system in any area where gamma radiation is present from stored or processed fissionable materials.

Designated as Model PSA-11, the auxiliary supplies power to the GA-2 gamma monitor in the event of failure in the primary 110-volt source. It is said to provide power for a minimum of eight hours without recharging.

The auxiliary unit is a wet cell system with built-in battery charger. Once the primary power source is restored, it begins to recharge automatically.

Encased in a sealed industrial box, the PSA-11 is designed for wall mounting adjacent to the area monitor. Weight is 120 pounds, including batteries. Dimensions are 20½" square $\times$ 6½" deep.

DIGITAL VOLTMETER
(With print-out facilities)

Solartron Laboratory Instruments Limited, Cox Lane, Chessington, Surrey, England

D.C. Digital Voltmeter LM 902.2 was announced. D.C. voltages from 100 μV to 1.500 kV are presented as a 4 digit display in decimal form with polarity discrimination. Display is by means of optical projection and is free from the ambiguity common to other systems of digital presentation. Red and black backgrounds signify positive and negative inputs respectively.

Wide voltage measurements are covered in 5 ranges. The input impedance is 10 MΩ, except on the two lower ranges which have impedances of 1 MΩ and 100 kΩ. The long term accuracy is $\pm$ 0.1% of maximum reading on each range. Two additional voltage ranges of 100 V to 1 kV have input impedances of 100 MΩ and a measuring accuracy of $\pm$ 0.5%.

The read-out time is constant at 280 milliseconds irrespective of the voltage input, which may be "floated" up to 700 V with respect to earth.

A "check" position on the range switch permits zero setting and a calibration check. The internal Zener reference can be preset to its precise value and corrected if necessary against the built-in Weston standard cell.

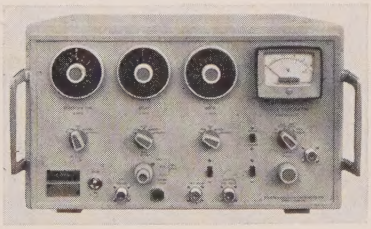

Under normal (AUTO) operation voltages are measured continuously, any variations causing the instrument to display a new reading. For maximum versatility of application, the LM 902.2 has an adjustable "dead zone", which can (within limits) make the instrument insensitive to small changes in voltage. Thus, it is possible to obtain jitter free readings in the presence of transients. 50 c/s ripple components that may be present on the voltage to be measured can be attenuated or rejected by switching in Short or Long time constants on the input circuit.

When switched to SAMPLE mode of operation a single voltage reading is taken, either by manual operation of a panel button or by remote electrical command. This reading will remain on display until a succeeding sample is taken.

Two 50-way sockets at the rear provide decimal coded digital information, polarity and print command signals suitable for feeding into a Venner TSA 65 Printer and an additional display unit.

ASTRACON IMAGE TUBE

Westinghouse Electric International Company, 40 Wall Street, New York 5, N.Y., U.S.A.

A new electronic tube has enabled Westinghouse scientists to photograph the faint tracks of cosmic rays as they move through a solid crystal.

The high-energy-particle camera used in performing the photography was described by A. E. Anderson, manager of the applied physics department of the Westinghouse research laboratories, Pittsburgh, Pennsylvania, at the Fifth International Congress on High-Speed Photography sponsored by the Society of Motion Picture and Television Engineers.

In the Westinghouse experiments, the brightening is accomplished by a new light amplifier tube called the Astracon. The tube is based upon a thin film system invented at the Westinghouse research laboratories several years ago, where it was recently brought to practical application.

The Astracon takes incoming photons and uses them to release electrons from a light-sensitive input surface. The emitted electrons are accelerated and guided successively onto a series of thin films. At each film, an incident electron ejects five or six additional electrons, which move on to the next film. After being multiplied in this way through several stages, the electrons strike a phosphor screen similar to that in the viewing end of a television picture tube. Here they re-emit about 10 000 photons of light (in a fourstage tube) for each photon that originally entered the tube.

The light that is generating along the path of a cosmic ray or other high-energy particle moving through the crystal is focused by a mirror system onto the input surface of an Astracon tube. The image produced by the tube then passes through a lens system which focuses it onto the input surface of a second Astracon tube. This second tube is triggered to operate only when a desired flash of light occurs in the crystal. Thus, it acts as a shutter that can be opened or closed in a small fraction of a second and also as an amplifier of light during the time it is turned on. The final image produced by the second Astracon tube then is directed onto a photographic film, which records the pictures of the path of the particle.

The dark current characteristics of the Astracon are more than adequate for nuclear track photography and other low-light-level applications.

The Astracon already has been used experimentally in astronomy for increasing the brightness of the images and spectra of distant stars. Additional applications are forecast for the tube. For example, it is expected to be useful in brightening X-ray images, thereby shortening exposure time and reducing the dosage normally encountered by the patient.

SAMARIUM DOPED CALCIUM FLUORIDE

Single Crystal Division, Semi-Elements Inc., Saxonburg Boulevard Saxonburg, Pa., U.S.A.

Samarium doped Calcium Fluoride is, at the present time, one of the best laser materials. This material requires only 1/500 the pumping power in comparison to ruby. The appearance of Samarium doped Calcium Fluoride is a transparent green material and currently Semi-Elements, Inc. is growing it in the desirable laser size of $\frac{3}{4}$" in diameter by 1" or more in length. Larger sizes would be grown on request.

In addition to Samarium doped Calcium Fluoride, Semi-Elements, Inc. is also producing Gadolinium doped Calcium Fluoride which is also available in the same size single crystal ingot. In addition to the laser uses of Calcium Fluoride, this material is also good for fluorescence studies as well as maser applications.

Semi-Elements, Inc. is also probing other likely laser materials. It is expected that Calcium Fluoride will be available in every rare earth material available.

THE CAMBRIDGE MICROSCAN X-RAY ANALYSER

Cambridge Instrument Company, Ltd., 18 Grosvenor Place, London, S.W. 1, England

The technique of X-ray microanalysis consists of focusing an electron beam, normally accelerated from 0 to 50 kV, on to a region of the specimen surface approximately 1 μ in diameter and rather less in depth and analysing spectroscopically the resulting X-rays excited from the specimen. So far, the technique has been used almost exclusively for research work on metallurgical problems although it also has applications in biological and other fields.

As well as static probe point-by-point quantitative microanalyses, the Cambridge instrument can also be used for scanning the surface of the specimen over an area up to $\frac{1}{2}$ mm $\times$ $\frac{1}{2}$ mm. The characteristic X-rays from any single element (with atomic number 12 or greater) can be selected by a crystal spectrometer and detected by a proportional counter. The signal from the counter modulates the brightness of a beam scanning a cathode-ray tube, in synchronism with the probe scanning the specimen, and forms an image corresponding with the area scanned and showing semi-quantitatively the distribution of the chosen element.

Some of the back scattered electrons from the surface of the specimen strike a scintillation counter, the signal from which modulates the beam of a second cathode-ray tube to form a reflected electron image of the region. This image is similar in its quality of contrast to an optical image photographed by oblique illumination and shows topographical details.

The magnification, for both images, can be controlled from 250 to 3000 $\times$ and the resolution is normally about 1 μ although this can, under good conditions, be reduced to $\frac{1}{2}$ μ for the electron image.

The accuracy for quantitative analysis is to $\pm$ 1 % which reduces, under favourable conditions, to 0.1 %. The minimum concentration that can be detected under good conditions is 0.1 % corresponding to a mass sensitivity of about 10^{-14} g.

Electron-probe supplies

E.H.T. supply; 4–50 kV D.C. negative. Stabilized to 1 part in 5000 (including ripple) over 15 minutes. Maximum output 250 μA.

Filament supply; 6 V D.C. stabilized to 1 %. Output variable from 1–3 A by rheostat. Insulated from earth to 50 kV.

Grid bias; 22 position variable resistor controlling the beam current over the range 1–250 μA at 50 kV.

Lens supplies; Two identical supplies current stabilized to 1 part in 10000 (including ripple) over 15 minutes. Output variable between 10 and 160 mA, feeding into 600 ohms.

Meters; E.H.T. potential, Beam current.

On control console: Probe current Objective lens current, Condenser lens current.

Electron-probe

Focus; Condenser and objective lenses giving up to about 500 : 1 demagnification of the electron source. Intermediate fluorescent screen.

Objective lens apertures; Normally 400 μ. Interchangeable with a 200 μ aperture for greater resolution.

Beam alignment; Provision for centring filament, gun unit, and condenser lens on the axis of the objective lens.

Probe diameter; Less than 1 μ.

Scanning area; Up to $\frac{1}{3}$ mm square at 20 kV.

Magnification; 250 $\times$ to 2000 $\times$ on two ranges (for 30 kV and 10 kV).

Resolution (electron image); Better than 1 μ.

Resolution (X-ray image); Approximately 1 μ.

Column exit ports; 6 provided, 3 of which are used.

Cool finger; Copper rod cooled by liquid nitrogen for reducing carbon contamination when necessary.

Specimen facilities

Specimen table; Rotatable, with position indicator lights. Holders for 1 specimen and 13 pure standards.

Specimen; Normal size $\frac{1}{4}$ inch diameter up to $\frac{1}{8}$ inch long. Larger sizes (not interchangeable through the air-lock) can be examined with less facilities for manipulation.

Specimen movements; Rotatable about the optical axis. Two orthogonal traverses $\pm$ 0.125 in.

Air-lock; Specimens in $\frac{1}{4}$ inch diameter holder and standards can be changed without destroying the vacuum for longer than about 45 seconds.

Optical microscope; 4 mm or 16 mm objective lenses selected under vacuum. Eyepiece 8 $\times$. Total magnification 88 $\times$ or 360 $\times$. 8 mm (22 $\times$) objective available if required.

Ratemeter

Counts rates; 3–100000 a second in 10 ranges.

Paralysis time; Normally 3 μs.

Input resolution; Approximately 2μs.

Integrating time constants; Varied in 6 steps at each of which mean probable error remains constant irrespective of count rate.

Other electronic units

E.H.T. supply unit for proportional and scintillation counters; 2200 V at 3 mA. Stabilized to 0.1 %. Ripple less than 0.03 V RMS. Output subdivided by two potentiometers to provide two identical supplies variable from 500 to 2000 V.

Main amplifier; General purpose linear A.C. amplifier with fixed constants. Head amplifier gain 150, main amplifier gain 1000 maximum. Stability as before.

Pulse monitor; General purpose oscilloscope.

Probe current indicator; Illuminated moving scale type.

Pen recorder; Potentiometric type. Chart speed $\frac{1}{2}$ inch a minute, response time 1.8 seconds for full scale deflection.

Dekatron scaler; 9 count ranges from 100–10^6 counts. 6 time settings from 100–10^5 seconds. Input resolution 5μs.

Services required

Electric supply; 200–250 V, 50–60 c/s, 3.6 kVA.

Water supply; 1 litre a minute at a maximum static pressure of 40 lbs/sq. in (2812 g/sq. cm).

Vacuum system

Pumps; 1 Edwards type ISC 150 rotary vacuum pump backing 1 Edwards type 203B oil diffusion pump (water-cooled).

Pumping times (during operation); After using air-lock—46 seconds. Total column—8 minutes.

Vacuum gauges; Edwards Pirani and Penning gauges. Ultimate vacuum pressure 10^{-5} mm Hg.

Vacuum reservoir; Will back the diffusion pump for periods up to 1 hour with the rotary pump switched off.

Electron image

Scintillation counter; Phosphor, and plastic light guide to photomultiplier.

X-ray image

X-ray spectrometer; Semi-focusing curved crystal vacuum spectrometer. 4 crystals interchangeable under vacuum. Bragg angle range 10°–65°. 0.00025 inch Melinex window.

Crystals; Lithium fluoride for wavelengths 0.7–3.5 Å. Elements 20–42 (Ca–Mo) on K radiations. Elements 50–92 (Sn–U) on L radiations.

Gypsum for wavelengths 2.7–10 Å., Elements 12–22 (Mg–Ti) on K radiations. Elements 33–56 (As–Ba) on L radiations.

Proportional counters; Sealed type Xenon—Ethyl formate filling with 0.005 inch Beryllium window.

interchangeable with

Flow type, Argon–Carbon dioxide filling with 0.00025 inch Melinex window.

Display unit

Cathode ray tubes; Double CRT display of electron and X-ray images with controls for spot, line, and raster. Controls for monitoring and superimposition are also provided on square faced flat tubes.

Line speeds; 50–200 lines a second approximately.

Slow scan; 1 line in 10–15 seconds in *X* or *Y* direction.

Frame speeds; 1 frame in 3 seconds-3 frames a second.

Raster size; 1–10 cm square on 10 cm square flat faces tubes.

Camera; "Wrayflex" 35 mm, f/2 lens.

Pulse analyser

Threshold coverage; 5–50 V manual control or auto sweep at 10 V a minute, 5–100 V manual control or auto sweep at 20 V a minute.

Threshold stability; 0.2 V.

Channel width; Narrow coverage of 0–10 V extending to 50 V for wide coverage. Accuracy ± 2%, stability ± 1%.

Resolving time; Less than 1 μs.

THE ISOTOPE INDEX COMPLETE GUIDE TO THE ISOTOPES

J. L. SOMMERVILLE, Editor

published by

SCIENTIFIC EQUIPMENT CO.

P.O. Box 19086–Indianapolis 19, Indiana, U.S.A.

(Volume V, September 1960)

CONTENTS

NEWS:

High Purity Isotopes 6

RADIOACTIVE ISOTOPES:

Labeled Compounds of 9
Carbon-14 10
Iodine-131 61
Phosphorus-32 64
Sulphur-35. 68
Tritium (H-3) 79
Other Radioactive Isotopes . . 86
Standard, Radiographic, and Therapeutic Sources. 97
Rock and Ore Standards . . . 104

STABLE ISOTOPES:

Labeled Compounds of Carbon-13 107
Deuterium (H-2) 108
Nitrogen-15 117
Other Stable Isotopes 119

THE ISOTOPE SUPPLIERS 130

USEFUL INFORMATION:

Definitions. 138
AEC Licensing Procedure . . . 139
General License Quantities. . . 140
Research Support Program . . 140
Generalized Decay Curve . . . 141
Table of Atomic Weights . . . 142

ADVERTISER'S INDEX

Price: Single copies $ 5.00 each. U.S. and Canada. Foreign $ 5.50 each. Sent postpaid.

SINGLE AND DOUBLE PULSE GENERATOR

Solartron Laboratory Instruments Limited, Cox Lane, Chessington, Surrey, England

The new, extremely versatile Solartron Decade Pulse Generator GO 1005 is typically suitable for accurate determination of transmission characteristics and transient response of amplifiers and networks, or testing the frequency and amplitude limits of electronic counters. This instrument provides positive or negative going, single or double rectangular pulses of up to 100 volts amplitude at repetition rates from 10 c/s to 1 Mc/s.

Three sets of concentric decade controls, with illuminated dials, permit coarse and fine adjustments of pulse duration, repetition rates and signal delay; with the aid of the built-in amplitude monitoring meter output requirements may be set up with ease and accuracy.

Signal delay time, relative to a 10 V prepulse output, is variable over the same range as the rectangular pulse duration viz. 250 mμsecs to 100 msecs)

In the double-pulse mode of operation the leading edge of the first rectangular pulse coincides with the prepulse and the leading edge of the second identical rectangular pulse occurs after the set signal delay.

A delayed-prepulse is also made available approx. 250 mμsecs after the prepulse, thus providing a trigger output which may be made to coincide exactly with the leading edge of the main rectangular pulse.

Incorporated are delay facilities and internal or external (up to 2 Mc/s) triggerings modes.